UNIVERSIDAD COMPLUTENSE DE MADRID

FACULTAD DE CIENCIAS FÍSICAS
Departamento de Astrofísica y Ciencias de la Atmósfera

STUDY OF HIGH-DENSITY MATERIAL IN CIRCUMNUCLEAR ENVIRONMENTS: SPECTROSCOPIAL ANALYSIS

MEMORIA PARA OPTAR AL GRADO DE DOCTOR

PRESENTADA POR

María Montero Castaño

Bajo la dirección del doctor
Paul T.P. Ho

Madrid, 2009

- **ISBN: 978-84-692-0060-5**

Universidad Complutense de Madrid
Facultad de Ciencias Físicas
Departamento de Astrofísica y Ciencias de la Atmósfera

ESTUDIO DEL MATERIAL DE ALTA DENSIDAD EN REGIONES CIRCUNNUCLEARES: ANÁLISIS ESPECTROSCÓPICO

Director:
Dr. Paul T.P. Ho
Harvard-Smithsonian Center for Astrophysics y
Academia Sinica Institute for Astronomy & Astrophysics

Memoria presentada por
D.ª María Montero Castaño
para aspirar al grado de
Doctor en Ciencias Físicas

2007

Resumen

De acuerdo con la normativa del Real Decreto 56/2005, que regula los estudios universitarios de postgrado de la Universidad Complutense, el original de esta memoria de investigación, escrita en su totalidad en lengua inglesa, se acompaña de un resumen en español donde se incluyen la introducción, los objetivos, las conclusiones y las aportaciones fundamentales de este trabajo.

Introducción

La evolución galáctica en su conjunto está íntimamente relacionada con los procesos que tienen lugar en los centros galácticos. Es por tanto que el conocimiento que nos aporta el estudio de las regiones nucleares contribuye a un mejor entendimiento de la evolución galáctica. Sin embargo, lo que hoy en día se conoce de estas regiones es todavía insuficiente, quedando muchas cuestiones importantes por resolver. Los centros galácticos se encuentran ocupados por gas, polvo y estrellas en grandes cantidades. Todos estos componentes interaccionan entre ellos, produciendo un escenario caótico y haciendo por tanto que el estudio de la dinámica y cinemática de estas regiones sea muy complicado. Además, estudios recientes sugieren que la presencia de un agujero negro supermasivo en los centros galácticos puede ser un suceso habitual (Mezger, Duschl & Zylka, 1996). En algunos casos los agujeros negros pueden encontrarse en estado latente, formando parte de lo que se ha llamado núcleos galácticos activos de baja luminosidad (LLAGNs en sus siglas en inglés), mientras que en otros casos la actividad nuclear es claramente detectable, es el caso de los núcleos galácticos activos (AGNs en sus siglas en inglés) (Mezger, Duschl & Zylka, 1996).

El primer problema que nos encontramos al estudiar los núcleos galácticos es la dificultad técnica para observar regiones envueltas en una gran cantidad de polvo. Por esta razón las observaciones en el rango del ultravioleta y en el óptico no son

factibles y surge la necesidad de encontrar otra zona del espectro inmune a la absorción producida por el polvo. Las longitudes de onda en la cuales se pueden observar los centros galácticos tienen que ser o bien lo suficientemente largas como para no ser afectadas por el polvo o lo suficientemente cortas como para atravesarlo (Armstrong & Barrett, 1985). Debido a esta circunstancia, el estudio de los centros galácticos ha debido acometerse en el rango del infrarrojo y de las ondas de radio. La radiación en el infrarrojo proviene del calentamiento de las nubes de polvo por parte de las estrellas recién formadas a las cuales aún rodean. Por contra, la radiación en el rango de las ondas de radio es producida por el gas presente en estas regiones. Debido a la gran cantidad de materia acumulada en los centros galácticos, el material allí localizado es muy denso, caliente y además turbulento (Hüttemeister et al., 1998). Para estudiar qué interacciones tienen lugar en estos parsecs centrales, el estudio del gas es especialmente útil, dado que nos permite estudiar la cinemática del material presente, el cual podría estar perdiendo momento angular y siendo arrastrado hacia el agujero negro central. Dadas las características previamente mencionadas sobre el material de los centros galácticos, el tipo de gas que se encuentra en estas regiones suele estar altamente excitado, por lo tanto, se detectan transiciones moleculares entre estados altamente excitados.

El centro de la Vía Láctea es la fuente con la cual se debe empezar todo estudio referente a los centros galácticos. La posición que ocupa el Sol en el Disco Galáctico no es la ideal para observar el centro de la Galaxia. Sin embargo, su proximidad (8 kpc, Reid (1993), $1''$ es equivalente a 0.038 pc) convierte el centro de la Vía Láctea en el único núcleo galáctico observable con la resolución suficiente como para poder distinguir las distintas estructuras allí localizadas hasta resoluciones de segundos de arco. A continuación se exponen algunas de las características principales del Centro Galáctico.

El Centro Galáctico

El Centro Galáctico está compuesto por el Bulbo Galáctico (con un radio de entre 0.3 y 3 kpc respecto al centro dinámico de la Vía Láctea), el Bulbo Nuclear (radio menor que 0.3 kpc) y la región ocupada por los complejos de nubes moleculares gigantes (GMCs en sus siglas en inglés) y la radiofuente Sgr A* (50 pc centrales) (Mezger, Duschl & Zylka, 1996).

El centro dinámico de la Galaxia está ocupado por Sgr A* (Balick & Brown, 1974), una radiofuente no térmica (ver figura 1.1 del capítulo de introducción de la versión en lengua inglesa, McGary et al. (2001)). Diversos estudios en el infrarrojo cercano, basados en la observación de las órbitas de las estrellas presentes en los parsecs centrales de la Vía Láctea, indican que el agujero negro central posee una

masa de aproxi-madamente 4×10^6 $M_\odot$ (Ghez et al., 2005; Schödel & Eckart, 2005). Alrededor de Sgr A* se detectan unos arcos (la mini-espiral o Sgr A Oeste) compuestos en su mayor parte por gas ionizado, claramente visibles en líneas de recombinación (Roberts & Goss, 1993; Shukla et al., 2004). La mini-espiral está formada por tres estructuras, el *arco occidental*, el *brazo septentrional* y la *barra alargada* (Roberts & Goss, 1993). El disco circunnuclear (DCN) es una estructura toroidal compuesta por gas neutro, tanto atómico como molecular (Genzel et al., 1985; Mezger et al., 1989), que rodea Sgr A* y la mini-espiral. El DCN tiene un radio interno de $\sim$ 1.5 pc (Jackson et al., 1993) y un radio externo más difuso, de alrededor de 5 pc, y rota alrededor de Sgr A* a una velocidad media de 100 km s^{-1} (Harris et al., 1985; Güsten et al., 1987; Jackson et al., 1993; Marshall et al., 1995; Christopher et al., 2005). A pesar de este movimiento rotacional uniforme, diversos estudios han demostrado que el DCN no es una estructura homogénea, sino que está formado por "glóbulos", pequeñas concentraciones de gas independientes unas de las otras que sin embargo siguen conjuntamente una misma rotación alrededor del agujero negro supermasivo central (Güsten et al., 1987; Wright et al., 2001; Shukla et al., 2004; Christopher et al., 2005). Dentro de la cavidad delimitada por el DCN, en su mayor parte libre de polvo, se ha encontrado también un cúmulo estelar. Este grupo de estrellas produce una radiación responsable de la ionización de la parte interna del DCN. Esta ionización es especialmente marcada en la parte occidental del DCN, en la cual esta estructura coincide con el *arco occidental* de la mini-espiral. A una distancia un poco mayor respecto a Sgr A* (entre 5 y 10 pc) se encuentra otro grupo de estructuras: dos GMCs (la *nube de 20 km s^{-1}* y la *nube de 50 km s^{-1}*, situadas al sur y el noreste del DCN, respectivamente); la *corriente occidental*, la *cresta molecular*, la *cresta septentrional* y dos nubes moleculares más pequeñas *SE1* y *SE2*. Pero no solamente los 10 pc centrales se encuentran ocupados por una gran cantidad de estructuras, sino que la densidad molecular es alta a lo largo de toda la zona molecular central (ZMC), la cual ocupa un radio de $\sim$ 200 pc (Morris & Serabyn, 1996).

En la ZMC se han encontrado conjuntos de nubes gaseosas. De estos conjuntos, los que se hallan a menor distancia del centro dinámico de la Vía Láctea (Sgr A, Sgr B, Sgr C y Sgr D) parecen formar un anillo circular, el anillo del Centro Galáctico (ACG) (Rodríguez-Fernández et al., 2006). Más allá de este anillo, es decir, a una distancia mayor del centro, el gas detectado no sigue órbitas circulares (Rodríguez-Fernández et al., 2006). Este distinto comportamiento puede ser debido al potencial producido por la barra de la Galaxia (Binney et al., 1991; Fux, 1999). Diferentes estudios y modelos sugieren que el material puede ser transportado de manera muy eficiente desde las partes externas hacia los núcleos de las galaxias mediante barras estelares (Matsuda & Nelson, 1977; Simkin, Su & Schwarz, 1980). La barra, al interaccionar con las órbitas estelares, produce una resonancia interna de Lindblad (RIL) (Telesco, Dressel & Wolstencroft, 1993). El gas sigue entonces órbitas x_1, paralelas a la barra, en la zona externa a la RIL y órbitas x_2 en la parte interna de

la RIL. Las órbitas x_2 son casi circulares y perpendiculares a la barra (Englmaier & Shlosman, 2000). Debido a los torques producidos por la barra, el material pierde momento angular y cae hacia el centro dinámico de la galaxia (Telesco, Dressel & Wolstencroft, 1993). En el lugar donde se produce la RIL se concentra gas en grandes proporciones, produciendo en algunos casos brotes de formación estelar. En el caso de la Vía Láctea el ACG se considera una RIL, donde se encuentra el 85-90% del gas total de la ZMC (Morris & Serabyn, 1996) (ver figura 1.2 en el capítulo de introducción de la versión en lengua inglesa). El destino final del gas arrastrado hasta la RIL es difícil de predecir, dado que dentro de la RIL hay órbitas estables. Por lo tanto el gas no tendría por qué ser acretado hacia el agujero negro central, sino que podría rotar a su alrededor.

Para poder estudiar qué sucede exactamente con el gas que se encuentra en el interior de la RIL, la única fuente a nuestra disposición es el Centro Galáctico. La resolución que proporciona la instrumentación actual permite observar el centro de la Vía Láctea hasta el extremo de poder distinguir diferentes estructuras en los parsecs centrales, aquéllas más susceptibles de interaccionar con Sgr A*.

Observaciones de líneas moleculares trazadoras de gas denso en el Centro Galáctico han demostrado que el DCN, además de estar formado por glóbulos, tiene diferentes inclinaciones en sus regiones septentrional y meridional, lo cual indica que ambas zonas pueden estar formadas por estructuras totalmente independientes (Harris et al., 1985; Güsten et al., 1987; Mezger et al., 1989; Jackson et al., 1993; Marr et al., 1993; Marshall et al., 1995; Wright et al., 2001; Shukla et al., 2004; Christopher et al., 2005). Además, el agujero negro supermasivo localizado en el centro de la Vía Láctea ha demostrado tener una luminosidad muy baja, que no se corresponde con la presencia de una masa de 4×10^6 $M_\odot$ en el centro dinámico. Diferentes teorías apuntan a un mecanismo de acrecimiento caracterizado por la pequeña cantidad total de masa acretada, al mismo tiempo que por la poca eficiencia del acrecimiento en sí (Quataert, 2003). Se plantean entonces muchas preguntas acerca de esta anomalía. Si el material es acretado a través de la mini-espiral, ¿de dónde procede ese material? ¿del DCN? ¿en su totalidad? ¿Pueden estar las GMCs, situadas más allá del DCN, interactuando con la mini-espiral sin ningún tipo de interferencia por parte del DCN? Todas estas preguntas no han sido contestadas todavía, por lo tanto el estudio del Centro Galáctico debe seguir adelante.

Por otro lado, para completar el estudio sobre núcleos galácticos es necesario ampliarlo a otras fuentes, dado que un solo objeto no puede en ningún caso proporcionar toda la información necesaria para aspirar a obtener conclusiones globales. Evidentemente, cualquier otro núcleo galáctico susceptible de ser observado se encuentra a una distancia mucho mayor que el Centro Galáctico. Sin embargo, al mismo tiempo, proporciona una visión complementaria, dado que al observar una región más extensa podemos comprobar diferentes estadios de la evolución nuclear, moviéndonos desde una distancia de cientos de parsecs del centro dinámico hasta

las decenas de parsecs centrales que son accesibles en el caso de la Vía Láctea. Con este propósito en mente, en este trabajo se ha acometido el estudio de la galaxia cercana IC 342 debido a sus características físicas, muy similares a las de Centro Galáctico y a su orientación en el cielo.

IC 342

IC 342 es un galaxia espiral de tipo Scd, muy cercana a la Vía Láctea (3.3 Mpc, Saha et al. (2002); Karachentsev (2005)). Posee una orientación ideal para su estudio, al estar prácticamente de frente (i = 25°, Lo et al. (1984)). A pesar de ello, existe el problema de que se encuentra muy cerca del Plano Galáctico, a apenas 10.6° del Ecuador. Por este motivo IC 342 no se ha observado de manera muy exhaustiva en el óptico, dado que no aparece como una fuente especialmente fuerte en ese rango, quizá por la extinción provocada por el polvo en la línea de visión. Sin embargo, numerosos estudios han demostrado que es una fuente excelente de emisión molecular (Downes et al., 1992).

Dada la distancia, la resolución que se puede alcanzar cuando se observa el Centro Galáctico no tiene comparación posible en el caso de IC 342, no obstante, se pueden trazar comparaciones con la Vía Láctea, habiéndose encontrado que las características físicas de la región nuclear de IC 342, la distribución del gas nuclear, encuentran sus equivalentes en la ZMC (Morris & Serabyn, 1996). Como en el caso del Centro Galáctico, IC 342 posee un anillo de gas molecular en interacción con una barra estelar (Ishizuki et al., 1990; Downes et al., 1992; Schulz et al., 2001). En el centro de IC 342 también se ha encontrado un cúmulo de estrellas (Böker et al., 1997), en una región en la que la presencia de gas es muy débil (Meier & Turner, 2005). La edad del cúmulo es ligeramente menor que en el caso del Centro Galáctico. También menor que su contrapartida en el Centro Galáctico es el agujero negro supermasivo que se cree está localizado en el centro dinámico de IC 342, 5×10^5 $M_\odot$ (Böker et al., 1999).

La barra en IC 342 tiene forma de S (mini-espiral) y está compuesta por material que se mueve hacia el centro de la galaxia, "cayendo" a lo largo de la barra (Turner & Hurt, 1992; Schinnerer et al., 2003). Cada brazo de la mini-espiral tiene un tamaño de 400 pc × 60 pc en CO(1-0) (Ishizuki et al., 1990). Los brazos avanzan hacia el centro hasta encontrarse con el anillo de gas, que tiene un radio de 80 pc. En las zonas donde los brazos que forman la barra y el anillo se encuentran, se acumulan grandes cantidades de gas en forma de GMCs, y se producen brotes de formación estelar (Böker et al., 1997). También se han encontrado GMCs en los brazos de la barra, en especial en el brazo septentrional. Las posiciones y nomenclatura de las diferentes GMCs del núcleo de IC 342 fueron definidas por Downes et al. (1992)

mediante observaciones en HCN(1-0). Todos los estudios posteriores han adoptado las mismas coordenadas (y nomenclatura).

Estudios en el infrarrojo cercano han mostrado que en la actualidad el cúmulo estelar nuclear no está sufriendo ningún proceso de formación estelar, por lo tanto la formación estelar en la región nuclear de IC 342 está dominada por los brotes que están teniendo lugar en el anillo gaseoso (Böker et al., 1997). A pesar de ello, el calentamiento de la cara interna del anillo gaseoso, resultante en la formación de regiones dominadas por fotones (PDRs en sus siglas en inglés), es debido a la acción del cúmulo estelar nuclear, dado que las estrellas que se están formando en el anillo son aún muy jóvenes ($\sim$ 5 Myr, Böker et al. (1997)) y la radiación ultravioleta que emiten es absorbida por el polvo de la nube materna que las rodea.

Por otro lado, Meier & Turner (2005) han descubierto que la distribución molecular en la región central de IC 342 es muy diferente dependiendo de la línea molecular estudiada (ver figura 1.5 en el capítulo de introducción de la versión en lengua inglesa). Argumentando que las condiciones de excitación y la densidad crítica para cada una de las líneas moleculares son muy similares, la única explicación posible es la no uniformidad de la distribución del gas molecular en la región central de IC 342. A pesar de ello, esquemáticamente la distribución del gas molecular en IC 342 es muy similar a la distribución en el Centro Galáctico (ver figura 1.6 en el capítulo de introducción de la versión en lengua inglesa), por lo tanto es natural intentar buscar similitudes entre las dos fuentes, las cuales nos pueden ayudar a bosquejar una imagen más completa de las características de los centros galácticos.

Objetivos

El objetivo principal de este trabajo de investigación es el estudio de la distribución del gas molecular, su cinemática y condiciones de excitación en las inmediaciones de un agujero negro supermasivo. Dadas las diferentes características del material presente en estas regiones, expuestas previamente, se ha acometido el estudio del gas molecular neutro denso, y más concretamente de las transiciones entre estados altamente excitados de varios trazadores moleculares, en las regiones centrales de dos núcleos galácticos: el Centro Galáctico y la región nuclear de IC 342.

En el caso del Centro Galáctico, observaciones de especies moleculares trazadoras de gas denso, en concreto HCN y HCO^+, han localizado la emisión procedente de estas especies confinada a lo largo del DCN (Güsten et al., 1987; Jackson et al., 1993; Marr et al., 1993; Marshall et al., 1995; Wright et al., 2001; Shukla et al., 2004; Christopher et al., 2005). Estos resultados también han demostrado que, a diferencia de lo que se pensaba en el pasado, el DCN es una estructura estable, no transitoria (Jackson et al., 1993; Shukla et al., 2004; Christopher et al., 2005). Éste es un tema en el cual es importante ahondar, dado que la estabilidad, o transitoriedad, del DCN es fundamental para entender la dinámica que gobierna el Centro Galáctico, y por extensión la evolución de la Vía Láctea.

Al mismo tiempo, observaciones en NH_3, una molécula trazadora de gas denso y caliente, han proporcionado nuevos datos sobre la distribución gaseosa en los 10 pc centrales (Coil & Ho, 1999, 2000; McGary et al., 2001; Herrnstein & Ho, 2002, 2005). La emisión procedente de las transiciones en los estados menos excitados, (1,1) y (2,2), se encuentra muy extendida, mientras que la procedente de transiciones en estados más excitados, (3,3) y (6,6), está más concentrada en torno a Sgr A*. NH_3(3,3) traza parte del DCN, pero la detección más importante se produce fuera del DCN. Por el contrario, NH_3(6,6), que traza gas a $\sim$ 412 K, ha sido localizada en el interior de la cavidad delimitada por el DCN (ver figura 1.3 en el capítulo de introducción de la versión en lengua inglesa). Es interesante resaltar que la zona oriental del DCN, desde la que (6,6) parece acercarse al agujero negro, se consideraba hasta entonces prácticamente desierta de gas molecular (Herrnstein & Ho, 2002). La "incursión" del NH_3(6,6) camino de Sgr A* no se corresponde espacialmente con los arcos de la mini-espiral, por lo tanto parece que ambas estructuras no están relacionadas. Al mismo tiempo, el estudio de los perfiles de la línea, muy anchos, indica que hay una alta probabilidad de que se esté produciendo una interacción con el agujero negro. En resumen, Herrnstein & Ho (2002) han localizado gas denso y caliente a una distancia de 1.5 pc de Sgr A*. Por consiguiente, el siguiente paso sería ampliar el estudio incluyendo otros trazadores de gas denso y caliente, con el fin de entender qué tipo de interacciones se están produciendo en la zona más interna de la Vía Láctea.

Con este propósito, el primer objetivo de este trabajo ha sido llevar a cabo observaciones en alta resolución de los 2 pc centrales de la Vía Láctea, a fin de estudiar tanto la distribución del gas en las inmediaciones de Sgr A*, como la dinámica y la cinemática que rigen las distintas estructuras presentes en la zona. Este trabajo se ha hecho mediante el estudio de dos moléculas, HCN y CS en dos transiciones, HCN(4-3) y CS(7-6), por medio del Submillimeter Array (SMA). Los resultados de este proyecto se presentan en el capítulo 2 de la versión en lengua inglesa.

HCN y CS son moléculas trazadoras de gas denso debido a sus altas densidades críticas ($n_{H_2} > 10^5\,cm^{-3}$). Diferentes estudios han detectado HCN en los parsecs centrales de la Galaxia (Güsten et al., 1987; Jackson et al., 1993; Marshall et al., 1995; Wright et al., 2001; Christopher et al., 2005) (ver figura 1.4 en el capítulo de introducción de la versión en lengua inglesa). Sin embargo, observaciones en alta resolución solamente habían sido posibles para la transición más baja de HCN, (1-0), dado que no existían intrumentos que poseyeran los receptores adecuados. Desgraciadamente, esta transición sufre absorción producida por las nubes frías situadas en la línea de visión (Güsten et al., 1987; Wright et al., 2001; Christopher et al., 2005). En cambio, las observaciones con antenas únicas de las transiciones más altas del HCN, han demostrado que éstas no son afectadas por la absorción (Jackson et al., 1993; Marshall et al., 1995). CS no ha sido observada anteriormente en los 2 pc centrales de la Galaxia, aunque sí ha sido detectada en la *nube de 50 km s*$^{-1}$. Transiciones altamente excitadas de ambas moléculas son ahora observables mediante el SMA, capaz de producir mapas de alta resolución. Como complemento al proyecto previamente mencionado, también se está llevando a cabo el estudio de la misma región de la Vía Láctea mediante la observación de otras dos transiciones diferentes, HCN(3-2) y HCO^+(3-2), haciendo uso una vez más del SMA. Este estudio se encuentra aún en su fase inicial, y como tal se presenta en el apéndice A de la versión en lengua inglesa. No existen estudios previos de estas dos transiciones en alta resolución en el Centro Galáctico, pero sí en transiciones entre estados menos excitados, tales como (1-0) (Marr et al., 1993; Wright et al., 2001; Christopher et al., 2005). Estos estudios han revelado que existe un exceso de HCN(1-0) con respecto a HCO^+(1-0) en el DCN, a pesar de que ambas transiciones, cuyas condiciones de excitación son similares, trazan las mismas regiones de la estructura toroidal. Sin embargo, esta diferencia en emisión no es aparente en nubes moleculares quiescentes del Disco Galáctico, donde el cociente entre ambas transiciones tiende a la unidad (Nyman, 1983; Vogel & Welch, 1983; Blake et al., 1987). Christopher et al. (2005) observaron que el cociente HCO^+/HCN es mayor en las regiones menos masivas, por lo tanto la relación entre ambas transiciones puede aportar nuevos datos sobre la distribución del material gaseoso en el DCN. El estudio de este cociente haciendo uso de transiciones entre estados más altamente excitados proporciona un resultado más fiable, debido a que HCO^+ es más susceptible de sufrir absorción en la línea de visión que HCN (Wright et al., 2001), pero tal problema disminuye al trabajar con transiciones entre estados más altamente excitados. Además, la identificación de las

regiones menos masivas del DCN y su relación con la mini-espiral puede proporcionar información sobre las interacciones sufridas por el DCN y el posible acrecimiento del material que forma el DCN por parte del agujero negro supermasivo.

Una vez realizado el estudio del Centro Galáctico mediante trazadores de gas denso, el siguiente objetivo de este trabajo de investigación ha sido ampliar el estudio mediante la observación de otra fuente, IC 342, que proporcione una visión complementaria de la distribución del material en las regiones más internas de las galaxias. La combinación de los resultados obtenidos mediante la observación de cada fuente ayuda a obtener un resultado más globalizador.

Este trabajo se ha llevado a cabo mediante la observación de dos transiciones del amoníaco, (3,3) y (6,6), en la región nuclear de IC 342 por medio del Very Large Array (VLA). Los resultados obtenidos son presentados en los capítulos 3 y 4 de la versión en lengua inglesa.

NH_3 ha demostrado su tremenda utilidad en los estudios del Centro Galáctico, por lo tanto su uso en el caso de IC 342 es lógico. El amoníaco ha sido detectado en IC 342 en varias ocasiones, tanto con antenas únicas como con interferómetros (Martin & Ho, 1979; Ho, Martin, & Ruf, 1982; Ho & Martin, 1983; Ho et al., 1990; Mauersberger et al., 2003). A pesar de ello, las transiciones que han proporcionado los datos más interesantes en el caso del Centro Galáctico, (3,3) y (6,6), todavía no habían sido observadas en alta resolución en IC 342. Gracias a la implementación de unos nuevos receptores en el VLA ambas líneas moleculares pueden ser observadas en la actualidad con la resolución necesaria para proporcionar resultados concluyentes. La detección de dos transiciones metaestables (J=K) de la molécula de NH_3 permite calcular la temperatura rotacional del gas. Cuando además ambas especies tienen los spins de los átomos de hidrógeno orientados de la misma manera (K=3n, n es un entero, spins paralelos, transiciones "orto"; K$\neq$3n, spins antiparalelos, transiciones "para", Ho & Townes (1983)) la temperatura rotacional se convierte en una buena aproximación de la temperatura cinética, debido a que las transiciones entre los estados solamente se pueden producir por medio de colisiones (Ho, Martin & Barrett, 1981; Walmsley & Ungerechts, 1983). En el caso de NH_3(3,3) y (6,6) se dan estas condiciones, estando ambas en el estado orto. Estudios llevados a cabo por Mauersberger et al. (2003) e Israel & Baas (2003) han demostrado que la distribución del gas molecular en la región nuclear de IC 342 se puede explicar mediante la existencia de dos componentes gaseosas a diferentes temperaturas, tal y como se ha visto en el caso del Centro Galáctico. Por lo tanto, la detección de ambas transiciones en la región nuclear de IC 342 no es solamente útil a la hora de estudiar la distribución del gas denso y caliente en esta zona, comprobando si, como en el caso del Centro Galáctico, el gas más caliente se encuentra situado más cerca del centro dinámico, sino que además el cálculo de la temperatura rotacional proporciona una nueva pieza en el rompecabezas que representa el estudio de los núcleos galácticos.

En resumen, este trabajo de investigación ha sido realizado con el propósito de ampliar nuestro conocimiento sobre los distintos procesos que tienen lugar en los núcleos galácticos, a través del estudio de la geometría, la cinemática y los diferentes estados de excitación del gas molecular localizado en los parsecs centrales de dos centros galácticos.

Conclusiones y Aportaciones Fundamentales

Este trabajo de investigación realizado ha proporcionado una visión más completa de la naturaleza de los núcleos galácticos, ayudando a una mejor comprensión de la interacciones que rigen estas regiones.

La observación de las transiciones HCN(4-3) y CS(7-6) en los 2 pc centrales del Centro Galáctico ha demostrado que la emisión detectada de ambas transiciones procede del DCN, donde se encuentra en forma de "glóbulos". La naturaleza de esta estructura toroidal es inhomogénea en términos de densidad, temperatura y excitación, y el gas que la compone se encuentra en forma de glóbulos. Estos glóbulos, a pesar de ser estructuras independientes y por tanto experimentar diferentes procesos, siguen un movimiento rotacional común alrededor del agujero negro central. La parte interna del DCN es ionizada por el cúmulo estelar al cual rodea, mientras que la parte externa del DCN no experimenta ningún proceso de ionización. El gas ionizado que compone la mini-espiral parece estar interaccionando con el DCN en algunas zonas, llegando a "rellenar" un hueco que se detecta en la emisión de ambas transiciones en la parte meridional del DCN. Al comparar la emisión producida por ambas transiciones con datos previamente publicados de otros estudios moleculares se ha comprobado que el gas que compone el DCN es más denso pero más frío que el gas que se ha observado dentro de la cavidad a la cual rodea el DCN. El DCN en sí es más denso y caliente en la región meridional que en la región septentrional. También se ha hallado una posible conexión entre el gas molecular neutro detectado en las inmediaciones de Sgr A*, el DCN y las GMCs externas. Esta conexión debe ser estudiada con más detalle, debido a que el gas molecular neutro que se aproxima al agujero negro no parece estar relacionado con la mini-espiral. Debido a la naturaleza inhomogénea del DCN, formado por glóbulos independientes, se ha estudiado la posible estabilidad de dichos glóbulos, y por tanto la longevidad del DCN. El estudio llevado a cabo ha demostrado que los glóbulos poseen la suficiente densidad como para ser estables frente a las fricciones producidas por la atracción gravitatoria del agujero negro supermasivo central. Además, el período de tiempo necesario para que incluso una cantidad mínima del material que forma el DCN sea acretado (calculado basado en la cantidad de material que compone la mini-espiral y su tiempo de caída hacia el centro dinámico), es mucho mayor que el período de rotación del DCN, por lo tanto los glóbulos pueden tener órbitas estables alrededor de Sgr A* sin ser completamente acretados. En resumen, el DCN, a pesar de estar formado por glóbulos de materia independientes, es una estructura estable.

El estudio de las transiciones del amoníaco (3,3) y (6,6) en la región nuclear de IC 342 ha demostrado en primer lugar que la distribución del gas más caliente (trazado por (6,6)) se encuentra más concentrada que el gas templado (trazado por (3,3)). El gas caliente se detecta en las inmediaciones del centro dinámico de IC 342 y en el anillo molecular, mientras que el gas templado está más extendido,

siendo incluso detectado en los brazos de la mini-espiral. NH_3(3,3) no se detecta en las proximidades del centro dinámico, al igual que sucede en el caso del Centro Galáctico, donde el gas caliente se encuentra más cercano al centro de la Galaxia que el gas maás frío. Por otro lado, la detección de ambas transiciones en regiones donde estudios en el infrarrojo cercano no han mostrado la inexistencia de formación estelar, indica que el amoníaco es un excelente trazador de regiones de alta densidad y alta temperatura, pero no de formación estelar. sin embargo, la detección de dos transiciones de NH_3 permite calcular la temperatura de rotación del gas en el núcleo de IC 342. La comparación del resultado obtenido, $T_{rot} = 120$ K, con estudios previos indica que la distribución del gas en el núcleo de IC 342 se puede describir en términos de dos componentes gaseosas, cada una de las cuales definida por una temperatura diferente. El estudio presentado en este trabajo de investigación permite detectar aquella componente gaseosa que posee la temperatura más alta. Diferentes estudios en el Centro Galáctico han mostrado una situación similar. Por último, se ha detectado emisión procedente de gas caliente mediante la detección de NH_3(6,6) en una región alejada del centro de IC 342. Tal detección no se ha producido en ningún otro trazador molecular, ni siquiera en NH_3(3,3), lo cual sugiere que se trata de un caso de absorción producida por nubes moleculares frías en la línea de visión.

En resumen, la detección de tres transiciones moleculares entre estados altamente excitados, tanto en el Centro Galáctico como en IC 342, ha demostrado la presencia de gas muy denso en las regiones nucleares de ambas fuentes. Además, se ha comprobado que, tanto en el caso del Centro Galáctico como en el de IC 342, el gas molecular denso más caliente se encuentra más cerca del centro dinámico que el gas más frío, el cual se halla rotando alrededor de este mismo centro. En el caso del Centro Galáctico, el gas más frío pero al mismo tiempo más denso, ha logrado formar una estructura estable a pesar de las fricciones causadas por la atracción gravitatoria producida por el agujero negro central. Esta estructura podría estar interaccionando con el gas más caliente (y menos denso) que parece estar aproximándose a Sgr A*. Debido a la mayor distacia a IC 342, un estudio similar no puede ser llevado a cabo en el caso de esta galaxia, dado que no se posee la resolución necesaria como para poder observar con tanta precisión los parsecs centrales. Sin embargo, ambas fuentes muestran una distribución del gas molecular similar, tanto en términos de temperatura como de densidad, al mismo tiempo que esta distribución se ajusta en ambos casos a un modelo de dos componentes gaseosas a distinta temperatura. Estas características comunes demuestran que el Centro Galáctico y la región nuclear de IC 342 están claramente relacionadas y juntas pueden aportar una mejor comprensión sobre los núcleos galácticos.

A continuación se enumeran someramente las conclusiones alcanzadas en este trabajo, clasificadas atendiendo al objeto de estudio.

El Centro Galáctico

- ⋆ Ha sido detectada la emisión procedente de dos transiciones entre estados altamente excitados producidas por dos trazadores moleculares de gas denso, HCN(4-3) y CS(7-6), a una distancia de menos de 2 pc del agujero negro supermasivo localizado en el centro de la Vía Láctea.

- ⋆ Ambas transiciones, HCN(4-3) y CS(7-6), se detectan con claridad en la zona meridional del DCN, mientras que en la zona septentrional la detección es mucho más débil, especialemente en el caso de CS(7-6).

- ⋆ La detección de los diferentes trazadores moleculares en distintas zonas del DCN sugiere que los niveles de excitación del gas en las zonas septentrional y meridional del DCN son distintos, siendo la zona septentrional mucho menos densa y más fría que la zona meridional.

- ⋆ La región sureste del DCN, llamada *extensión meridional*, es la zona más densa del DCN, mientras que el *lóbulo suroeste*, situado al oeste de la *extensión meridional* parece estar más caliente pero ser menos denso. Además, la *extensión meridional* parece estar cayendo hacia el agujero negro supermasivo central mediante órbitas espirales.

- ⋆ El gas de la cara interna del DCN se encuentra más excitado que el gas de la parte externa del DCN, probablemente debido a la radiación procedente del cúmulo estelar nuclear.

- ⋆ Una interacción entre la mini-espiral y el DCN parece estar teniendo lugar. Se observa el ensanchamiento de las líneas en las regiones donde coinciden espacialmente el DCN y la mini-espiral. Además, se detecta un hueco en la región septentrional del DCN que es atravesado por el brazo septentrional de la mini-espiral.

- ⋆ El DCN está formado por glóbulos de varios tamaños, desde $3''$ hasta $13''$.

- ⋆ Los glóbulos son lo suficientemente densos ($n_{H_2} > 1.4 \times 10^7$ cm^{-3}) como para soportar las fricciones producidas por la atracción gravitatoria debida al agujero negro supermasivo situado en el centro de la Galaxia. Al mismo tiempo, el período de tiempo calculado para que el material que compone el DCN caiga hacia el centro de la Vía Láctea es mayor que su período de rotación (9×10^6 yr frente a 8×10^4 yr, tasa de caída 1.5×10^{-2} M$_\odot$ yr^{-1}), por lo tanto el DCN es una estructura estable y no transitoria.

- ⋆ Los resultados sufren la falta de datos de los espaciados cortos, en especial en la zona meridional del DCN. Pero, a pesar de ello, la falta de emisión extensa no parece afectar de una manera muy grave el resultado final, con lo cual la emisión procedente del DCN está dominada por los glóbulos.

IC 342

- ⋆ Dos transiciones de NH_3, molécula trazadora de gas denso y caliente, han sido detectas en la región nuclear de la galaxia cercana IC 342.

- ⋆ La emisión procedente de la transición más alta se ha detectado concentrada en torno al centro dinámico de IC 342. Tres picos de emisión han sido detectados en NH_3(6,6): el *pico (6,6)*, el *pico continuo* y el *pico oeste*.

- ⋆ El *pico continuo* coincide con el pico de emisión del continuo a 1.3 cm y se encuentra lo suficientemente cerca del pico del continuo a 6 cm como para poder considerar que los tres están relacionados. Este pico de emisión no coincide con ninguna de las GMCs detectadas por otros trazadores moleculares. Se considera que el *pico continuo* es un pico de temperatura y la falta de coincidencia con trazadores de gas frío sugiere que las zonas contiguas al centro dinámico de IC 342 están ocupadas por gas muy caliente.

- ⋆ El *pico (6,6)* está en la misma posición que una GMC con brotes de formación estelar, la GMC C. La GMC C se encuentra en la región donde coinciden los brazos de la mini-espiral, formados por material que se traslada hacia el núcleo, y el anillo molecular. El *pico (6,6)* es un pico de temperatura y densidad columnar.

- ⋆ El *pico oeste* se encuentra aislado, situado en una región alejada al oeste del centro dinámico de IC 342. Este pico no ha sido observado antes ni en radiocontinuo ni el otras líneas moleculares. Podría estar compuesto por gas muy caliente, y la falta de detección en trazadores de gas frío podría ser achacada a la absorción en la línea de visión.

- ⋆ NH_3(3,3), que traza gas a $\sim$ 125 K, ha sido detectada en una zona más amplia que NH_3(6,6). Se han localizado tres picos de emisión: el *pico septentrional*, el *pico central* y el *pico meridional*.

- ⋆ El *pico central*, el cual es el pico más fuerte detectado en NH_3(3,3), coincide con la GMC C. A su vez, el *pico (6,6)* detectado en NH_3(6,6) también coincide con el *pico central*. La coincidencia espacial de ambos picos confirma que el *pico central* es un pico de temperatura y densidad columnar.

- ⋆ El *pico septentrional* está situado en el brazo septentrional de la barra estelar. Su posición coincide con la de la GMC D'. La GMC D' se encuentra en la vanguardia del brazo, una zona muy turbulenta. Parece estar formada por gas denso y caliente, pero las fricciones producidas por la barra podrían impedir la aparición de brotes de formación estelar.

- ⋆ El *pico meridional* coincide con la posición de la GMC A. No parece que se esté produciendo un brote de formación estelar en esta región. La GMC

A parece formada por pequeños glóbulos de gas, densos y calientes. El gas situado entre estos glóbulos es mucho más difuso, permitiendo que penetre la radiación ultravioleta proveniente del cúmulo estelar central.

- ⋆ La falta de detección de $NH_3(3,3)$ en el centro dinámico de IC 342 sugiere que el gas concentrado en esa región es muy caliente, pero no forzosamente más denso que en otras zonas, tal y como se ha observado en el caso del Centro Galáctico.

- ⋆ No se ha encontrado una contrapartida en $NH_3(3,3)$ al *pico oeste* detectado en $NH_3(6,6)$, probablemente debido a la absorción producida en la línea de visión por nubes frías.

- ⋆ La temperatura rotacional calculada usando las dos transiciones del amoníaco es $\sim$ 120 K, de la cual se puede inferir un valor para la temperatura cinética de $\sim$ 170 K. La distribución del gas molecular presente en la región nuclear de IC 342 parece ajustarse a un modelo de dos componentes gaseosas, cada una de ellas a una diferente temperatura.

La comparación entre el Centro Galáctico y la región nuclear de IC 342 demuestra que ambas fuentes son muy similares y se complementan a la perfección para proporcionar una visión más global de las características de los núcleos galácticos.

Universidad Complutense de Madrid
Facultad de Ciencias Físicas
Departamento de Astrofísica y Ciencias de la Atmósfera

STUDY OF HIGH-DENSITY MATERIAL IN CIRCUMNUCLEAR ENVIRONMENTS: SPECTROSCOPICAL ANALYSIS

Thesis Advisor:
Dr. Paul T.P. Ho
Harvard-Smithsonian Center for Astrophysics and
Academia Sinica Institute for Astronomy & Astrophysics

Thesis presented by
María Montero Castaño
in partial fulfillment of the requirements
for the degree of
Doctor in Philosophy
in the subject of Physics

2007

A Maribel y Pedro, mis padres
A Carlos y Ana, mis hermanos
A Rodrigo

Preface

This thesis is dedicated to the study of the molecular gas distribution, its kinematics and excitation conditions in the vicinity of a supermassive black hole. Only in the case of the Galactic center, the inner parsecs of a galactic nucleus can be observed with enough resolution to disentangle the different structures located in close proximity to the black hole. Therefore, the Milky Way is the first source to consider when undertaking this kind of studies. However, in order to better understand the intricacies of galactic nuclei, the study has to be expanded to accomodate more sources. Because of its similar characteristics to the Milky Way, as well as its orientation and location in the sky, IC 342 is the perfect source to combine with the Galactic center.

The appropiate way to study the gas present in the nuclear environment is through the observation of highly-excited, high-density, high-temperature molecular tracers, because of the characteristics of the nuclear ISM, dense, warm and highly excited.

Chapter 1 presents a background on the foremost results on the topic, remarking the importance of the study of molecular tracers in galactic nuclei and explaining the connection between the Galactic center and the nuclear region of IC 342.

Chapters 2, 3 and 4 present three lines of research, each of them independent and important on its own but closely related to the other two. The combination of the results obtained in the three chapters provides a much more complete picture of galactic nuclei.

Chapter 2 reports the latest results on the distribution of two high-density molecular tracers in the inner 2 pc of the Milky Way, HCN(4-3) and CS(7-6), using the Submillimeter Array (SMA). The gas distribution has proved to be asymmetrical along the circumnuclear disk (CND), with the southern part denser and warmer than the northern part of the CND. At the same time, the inner edge of the CND seems to be suffering excitation by the nuclear stellar cluster. Also, the nature of the CND is clumpy, with dense enough clumps to overcome the tidal shear produced by the proximity of the black hole. However, the gas could be undergoing an ac-

cretion process towards Sgr A*, and a correlation between the minispiral "feeding" the black hole and the CND has been found.

Chapter 3 presents the succesful detection of $NH_3(6,6)$, a high-density and high-temperature tracer, in the nuclear region of IC 342, using the Very Large Array (VLA). Strong emission has been detected towards the dynamical center of IC 342, where lower-temperature molecular tracers are absent, as well as at the location of a star formation region. Also, evidence of the presence of hot gas in an isolated area farther outside the dynamical center, where no previous neither molecular nor continuum emission detections have been reported, has been found. Absorption along the line of sight by foreground cool clouds could be the reason the isolated peak has remained undetected.

Chapter 4 is a follow-up of the research presented in chapter 3, reporting the detection of $NH_3(3,3)$ in the nuclear region of IC 342, also using the VLA. The emission from the lower transition line is more extended than the emission from $NH_3(6,6)$, and it is not found near the dynamical center of the galaxy. $NH_3(3,3)$ has been found at the locations of three Giant Molecular Clouds (GMCs), only one of them characterized by a strong burst of star formation, whereas the other two GMCs seem to be undergoing different processes. Combining the results from chapter 3 and 4, a high rotational temperature, ~ 120 K, has been calculated. The gas distribution in the nuclear region of IC 342 could be explained by the presence of two-temperature material.

Chapter 5 is a summary of the conclusions of the research presented in the previous chapters as well as a discussion of the future work that must be undertaken to further expand this study.

Finally, an appendix has been added. Appendix A reports a very promissing work in progress, the detection of HCN(3-2) and HCO^+(3-2) in the Galactic center, using the SMA. The preliminary results are interesting enough to deserve to be mentioned in this dissertation. However, more observations are needed, and consequently it is still early to report conclusive results.

Acknowledgments

First and foremost, I want to thank Dr. Paul Ho for giving me the incredible opportunity to conduct this research under his guidance. Thanks for always being available to hear me out and offer a helpful suggestion, a new idea, a new way to look at the data and for gently pushing me to be the best I can be, while being, at the same time, concerned about my welfare during this time. I am sure that I could never thank him enough for all his encouragement and support.

I also want to thank the professors and students at the Astrophysics Department of the Complutense University for the continuous support and guidance. Special thanks to Dr. Elisa de Castro Rubio, my academic advisor, for immediately replying to all my questions and for her patience. Also, thanks to Dr. Jaime Zamorano Calvo for all of his suggestions to improve this dissertation. My fellow graduate students at the department have proved to be great people and an excellent source of information when one works in a different continent than that where the grad school she attends is located.

The Harvard-Smithsonian Center for Astrophysics (CfA), where I have spent more than four years working on this dissertation, has been an incredible place to pursue my research, both personally and scientifically. Many people have greatly helped me, and it is only fair that I acknowledge them. I especially want to mention Qizhou Zhang for his many useful suggestions to improve this work and his patience to answer all my questions. Charlie Qi helped me with the Submillimeter Array (SMA) data reduction, trying to clarify the intricacies of MIR for me. Jun-Hui Zhao solved my doubts about the Galactic center and Nimesh Patel could always be counted on to answer any kind of question about the SMA. Thanks to the two SMA directors, Jim Moran, for pushing for the SMA board to take an especial interest in the Galactic center and Ray Blundell, for keeping the support to the subject. Robin Herrnstein, whose steps I have tried to follow, has been involved in all of my research projects and I want to thank her for her help from the very beginning. Also, all my fellow predoc and postdoc radioastronomers, with whom I have shared so many hours discussing reduction techniques, second-shifts and also laughs: Daisuke, Luis, Daniel, Ramiro, Peter, Junzi, Yang, Keping, Thushara, Sergio and Jeff.

Thanks so much to the predoc coffee-break bunch. Those Friday afternoon chats were perfect to unwind after a week of hard work and to realize that I was not the only one struggling to make sense of my data.

I am forever indebted to all my amazing friends at the CfA who are now spread out all over the world: Alicia, Aurora, Mari Paz, David, Manuel, Manami, Paula, Hans-Jakob, who could always be counted on to discuss work and life and who are really an inspiration to me.

A very special thank-you goes to the Academia Sinica Institute for Astronomy and Astrophysics (ASIAA) in Taiwan, where I spent the summer of 2007, finishing up this work. Everybody was incredibly nice, helpful and going out of their ways to make me feel welcome and accepted. They also provided a refreshing new point of view regarding my research. Thanks to Jennifer, Hiro, Vicent, Dani, Yi-Jung and Satoko, truly wonderful people who I hope to see again soon.

Thanks are also due to all the observers at the SMA and the Very Large Array (VLA) who have collected the data used in this dissertation. The research work presented in this dissertation would not have been possible without an Academia Sinica Institute of Astronomy and Astrophysics Fellowship and a Smithsonian Institution Visiting Student Grant.

Although not directly related with the research presented in this dissertation, I want to thank the wonderful people at the Laboratory for Space Astrophysics and Theoretical Physics (LAEFF). Thanks so much for the opportunity to spend those long months working at the LAEFF and for showing me what research was all about. I would specially like to thank Patxi, who introduced me to Paul and is ultimately responsible for me having followed this path.

All my old friends, the "crazy astronomers", the "not-so-crazy physicists" and the "normal" high-school friends have been wonderful and even though most of them have decided to take different paths in their lives, they have kept an interest in my research and well-being. I want to mention one of them in particular, Ricardo, who started the ball rolling. Thanks as well to my great friends from Berkeley, the I-House bunch, where I spent a whole year learning the ropes of scientific research in the U.S.

A very, very special thank-you to my family, my parents, Maribel and Pedro, and my siblings, Carlos and Ana. This dissertation would not have been possible without my incredibly encouraging family and I am forever grateful to them. Thank you for the support, for having faith and for always being there for me in every sense of the word.

Last, but far for least, thanks to Rodrigo, for so many things, but especially for his patience during these long four years, for so many transcontinental flights, for

the daily phone calls, for his support every step of the way, for just being himself.

Contents

List of Figures

List of Tables

Chapter 1

Introduction

Galactic evolution is intimately related to the processes taking place in the nuclear regions of the galaxies. However, nuclear galactic environments are extremely chaotic regions, not at all well understood to this day. The inner parsecs of galaxies are overpopulated by gas, dust and stellar clusters interacting with each other, proving the understanding of the dynamics and the kinematics of the nuclear regions to be a very challenging task to undertake. Moreover, recent theories believe most of the galaxies to harbor a supermassive black hole in their centers, quiescent in some cases (low-luminosity active galactic nuclei, LLAGNs) and active in other cases, when it is considered an active galactic nuclei (AGN) (Mezger, Duschl & Zylka, 1996). It is imperative that we comprehend the interactions undergoing in the nuclear region since that will help us understand the evolution of the galaxy as a whole. As an ultimate goal, the study of different galactic nuclei can be applied to our own Galaxy, still largely unknown.

The study of galactic nuclei has not been possible until the second half of the XX century. Because of the large amounts of dust concentrated in the inner regions of galaxies, the extinction is extremely important (~ 30 magnitudes for our own Galactic center, Armstrong & Barrett (1985)) and galactic nuclei remain unobservable in optical and UV wavelengths. Therefore, the only way to observe these sources is using wavelengths long enough to be unaffected by the dust or short enough to penetrate it (Armstrong & Barrett, 1985). The development of radio and IR telescopes has made these observations possible. The improvement in technology in the later years, better instruments, thus better resolution, has greatly helped the process since we are now able to penetrate further and further inside the nuclear regions of the galaxies.

The IR radiation in the galactic nuclei comes from dust heated by the recently formed stars still embedded in their dusty "maternal" cocoons. However, the most

extended emission does not come in the form of IR radiation, but of radio emission. Because of the very nature of the nuclear environments, filled with large quantities of material, the study of the neutral gas present in the region is an excellent choice to shed light on the dynamics of the nucleus. Furthermore, the mass accreted by the supermassive black hole comes from the surrounding gas. Therefore, molecular line surveys are powerful tools to deepen our understanding of the nuclear regions of galaxies. Indeed, the gas circulating in galactic nuclei have proved to be a very rich source of molecular emission (Meier et al., 2000; Schinnerer et al., 2003; Combes et al., 2004; Krips et al., 2005; Meier & Turner, 2005; Krips et al., 2007; Boone et al., 2007).

An obvious choice to start the study of galactic nuclei is our own Galactic center. At 8.0 $\pm$ 0.5 kpc (Reid, 1993), it is the nearest source for galactic nuclei studies. However, because of the location of the Earth in the Galactic plane, we can only observe it edge-on. This orientation is responsible for the extinction and confusion, since large amounts of dust and gas are located along the line of sight. Nonetheless, the advantage of the proximity ($1''$ corresponds to 0.038 pc) greatly surpasses the not-so-good orientation and many molecular line surveys have been conducted in the inner parsecs of the Galactic center, providing fundamental information on the whereabouts of the gas in the vicinity of a supermassive black hole, its kinematics, mass, excitation and other characteristics which can only be measured in great detail when studying our own Galactic center due to the excellent resolution that can only be achieved when observing nearby sources (Harris et al., 1985; Serabyn & Güsten, 1986; Serabyn et al., 1986; Güsten et al., 1987; Ho et al., 1991; Hüttemeister et al., 1993; Jackson et al., 1993; Marr et al., 1993; Marshall et al., 1995; Coil & Ho, 1999, 2000; Wright et al., 2001; McGary et al., 2001; Herrnstein & Ho, 2002; Shukla et al., 2004; Herrnstein & Ho, 2005; Christopher et al., 2005; Bradford et al., 2005).

The Galactic center

Mezger, Duschl & Zylka (1996) described the inner part of the Milky Way as a region composed of the Galactic bulge (radius $\sim$ 0.3 - 3 kpc from the dynamical center of the Milky Way), the nuclear bulge (radius $<$ 0.3 kpc) and the Sgr A radio and GMC complex (inner 50 pc). The interstellar medium (ISM) composing this region is very warm and turbulent. The density of the ISM is higher than in any other region of the Galaxy, with 10% of the total mass of the Milky Way compressed in the Galactic bulge. Furthermore, Hüttemeister et al. (1993) found that the gas distribution in the Galactic center was better fitted by a two-component kinetic temperature, with a $\sim$ 200 K component representing approximately 25% of the gas and the rest at $\sim$ 25 K.

A nonthermal radio source, Sgr A* (first discovered by Balick & Brown (1974)), is located in the dynamical center. Sgr A* is associated with a supermassive black hole. NIR studies, based on precise measurements of stellar orbits in the vicinity of Sgr A* by two independent research groups, have found the black hole to have $\sim 4 \times 10^6$ $M_\odot$(Ghez et al., 2005; Schödel & Eckart, 2005). Arcs of ionized gas (Sgr A West or the "minispiral"), clearly detected in recombination lines (Roberts & Goss, 1993; Shukla et al., 2004), are observed around the black hole. Surrounding both the black hole and the minispiral a torus of neutral gas and dust has been found (the circumnuclear disk, CND), with a sharp inner radius of $\sim$ 1.5 pc (Jackson et al., 1993) and a more diffuse outer radius of roughly 5 pc. The overall motion of the CND is rotation around Sgr A* (with a rotation velocity of $\sim$ 100 km S^{-1}, Harris et al. (1985); Güsten et al. (1987); Jackson et al. (1993); Marshall et al. (1995); Christopher et al. (2005)). The western arc of Sgr A West traces the inner edge of the CND. The ionization is produced by the stars of the nuclear cluster inside the cavity (Genzel et al., 1985), where a dramatical reduction of the dust is found (Becklin et al., 1982). The CND has a clumpy nature, as it has been observed in various interferometric studies (Güsten et al., 1987; Wright et al., 2001; Shukla et al., 2004; Christopher et al., 2005). Close by, filling the inner 10 pc, a group of structures have been detected: two Giant Molecular Clouds (GMCs) (the *20 km s^{-1} cloud* and the *50 km s^{-1} cloud*, located south and northeast of the CND, respectively); the *western streamer*, the *molecular ridge*, the *northern ridge* and two small clouds, *SE1* and *SE2* (figure 1.1, McGary et al. (2001)). Farther away, the complexity increases, in what has been named the central molecular zone (CMZ), a region with roughly $\sim$ 200 pc radius (Morris & Serabyn, 1996). At larger radii the density drops dramatically, thus the definition.

The study of the CMZ has shown the presence of numerous cloud complexes. The innermost of these complexes, located between l = - 0.5° and l = 1° (Sgr A, Sgr B, Sgr C and Sgr D complexes) appear to form a circular ring in a face-on view of the Galactic center, the Galactic center ring (GCR) (Rodríguez-Fernández et al., 2006). The molecular gas farther out is following non-circular orbits (Rodríguez-Fernández et al., 2006), likely because of the bar potential of the Milky Way (Binney et al., 1991; Fux, 1999). An explanation of the material distribution in spiral galaxies has been modeled introducing a large-scale stellar bar which produces an Inner Lindblad Resonance (ILR) because of the interplay between the bar and the stellar orbits (Telesco, Dressel & Wolstencroft, 1993). At large radii, outside of the ILR, the bar curves around the ILR, with the material following x_1 orbits aligned with the bar, which are observed as dust lanes in galaxies. Inside the IRL, the gas follows nearly circular x_2 orbits, perpendicular to the bar (Englmaier & Shlosman, 2000). The torques produced by the stellar bar slow the gas in the dust lanes, which loses angular momentum and drifts towards the nucleus (Telesco, Dressel & Wolstencroft, 1993). The infalling gas interacts with the ILR, increasing the amount of gas in that region of the ILR where bursts of star formation are likely to occur. Sakamoto et al.

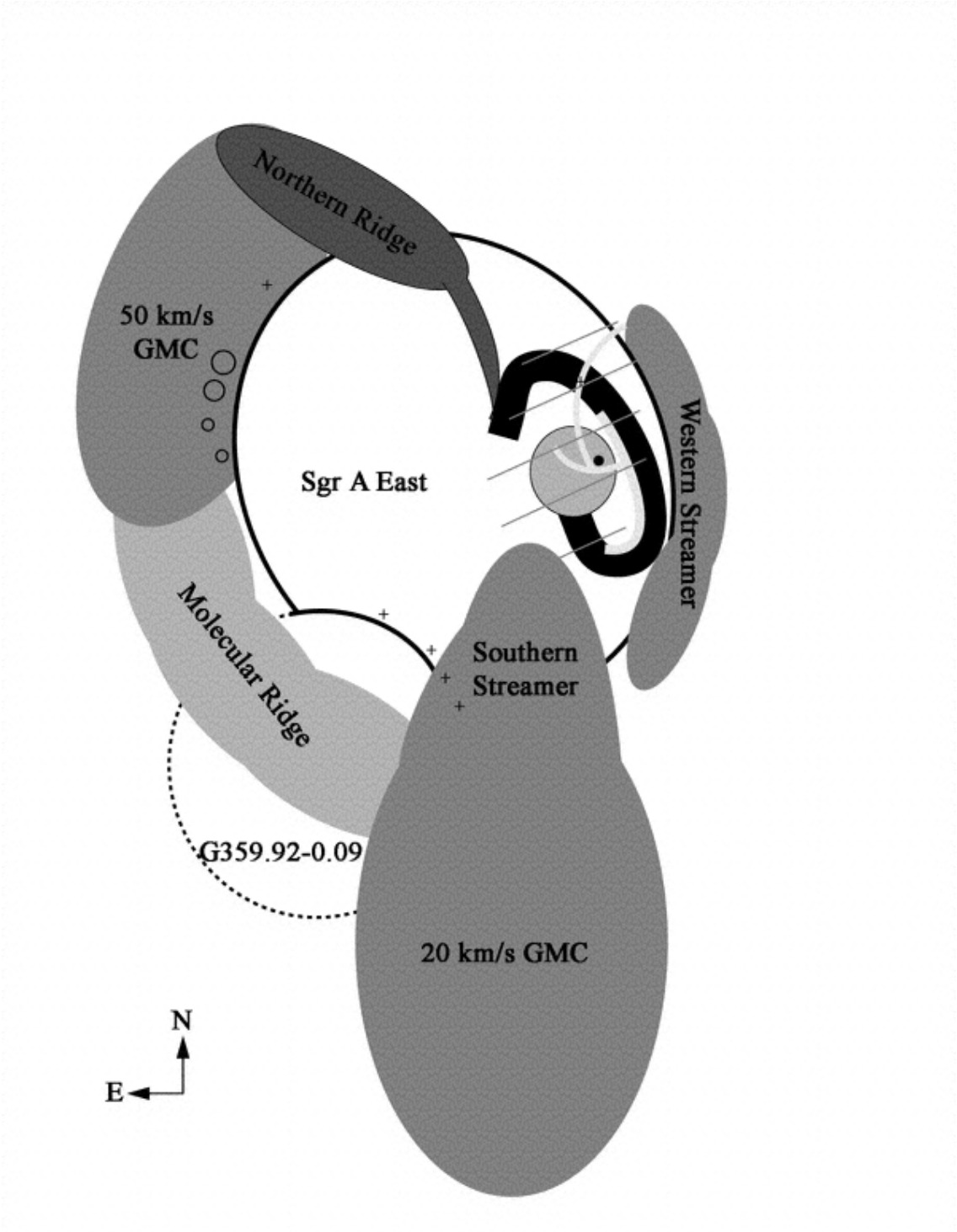

Figure 1.1: Schematic drawing of the central 10 pc of the Milky Way in the plane of the sky (Herrnstein & Ho, 2005). Sgr A* is marked by a black dot, the light grey arcs represent the minispiral and the CND is seen as an open black ring.

(1999) reported that barred galaxies have a larger amount of molecular gas in the central kiloparsec than unbarred galaxies, therefore, the bar seems to be an excellent tool to transport material towards the center. However, the effective inward flow of material towards the galactic nuclei, does not necessarily imply that such material will reach the very center, since the angular momentum still creates stable orbits inside the ILR. In the case of the Milky Way, the GCR can be interpreted as an ILR, whose mass represents $\sim$ 85-90% of the total molecular mass of the CMZ (Morris & Serabyn, 1996). Due to this scenario, a plausible representation of the gas distribution in the CMZ is presented in figure 1.2.

Because of the proximity of the Galactic center and the improved instrumentation, we are able to take this study to real depths, inside the GCR, since the high-resolution allow us to separate different features. We can then study what is the ultimate end of all the gas so efficiently dragged inwards by the large-scale bar, whether it is able to reach the supermassive black hole or it is "trapped" in orbits circling it. We can thus concentrate our study in the very central parsecs of the Milky Way, those occupied by the structures most likely to be interacting with the supermassive black hole.

The inner 5 pc of our Galaxy are composed of Sgr A*, the minispiral and the CND, and that is the region we would concentrate on. The origin of the CND is still unknown, but its clumpy nature and warped outline (Harris et al., 1985; Güsten et al., 1987; Mezger et al., 1989; Jackson et al., 1993; Marr et al., 1993; Marshall et al., 1995; Wright et al., 2001; Shukla et al., 2004; Christopher et al., 2005) are indications of a ring formed by independent structures, rotating together. At the same time, Sgr A* has been found to have a very low, sub-Eddington luminosity considering the presence of a $\sim 4 \times 10^6$ $M_\odot$ mass in its center ($\sim 10^{36}$ erg s^{-1}, Baganoff et al. (2001)). Why is Sgr A* so under-luminous? The accretion mechanism might be different than what we thought. Recent studies support accretion models with low mass accretion rates and low efficiency (Quataert, 2003). The accreting mass reaches the supermassive black hole through the minispiral, but, where does the minispiral takes the mass from? Is all the mass coming from the CND? Are the outside GMCs interacting directly with the minispiral without intervention of the CND? Many questions remain unsolved, thus the full understanding of the processes near the supermassive black hole is far from complete.

Previous molecular studies of the inner 5 pc of the Milky Way have detected high-density gas mostly along the CND (Güsten et al., 1987; Jackson et al., 1993; Marr et al., 1993; Marshall et al., 1995; Wright et al., 2001; Shukla et al., 2004; Christopher et al., 2005), nicely tracing the outline in various transitions of HCN and HCO^+. Recent HCN, HCO^+ results by Jackson et al. (1993); Shukla et al. (2004) and Christopher et al. (2005) suggest the CND to be a quite stable structure, while earlier results (Güsten et al., 1987; Dent et al., 1993) believed the CND to be a short lived transient feature. This is an important question we would like to address in

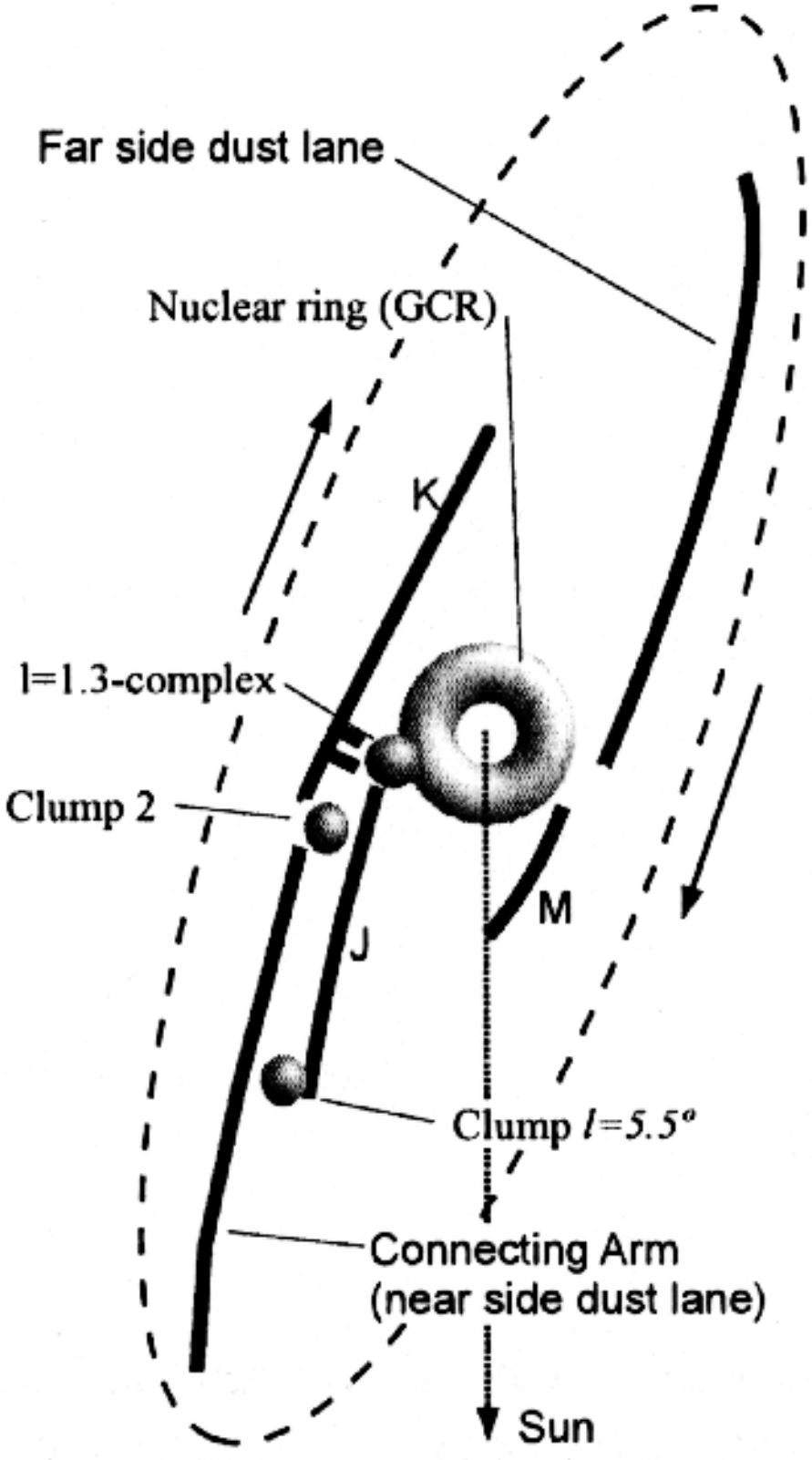

Figure 1.2: Schematic drawing of the Galactic center from Rodríguez-Fernández et al. (2006).

this work, since the stability or lack of of the CND changes the entire model of the Galactic center. Also, NH_3, a high-density and high-temperature molecular tracer, has provided a new vision of the Galactic center. Studies from Coil & Ho (1999, 2000); McGary et al. (2001) and Herrnstein & Ho (2002, 2005) of the inner 10 pc of the Galaxy have shown the gas to be extended in the case of the lower temperature transitions ((1,1) and (2,2), at 23 and 65 K, respectively) while higher temperature transitions are more concentrated towards Sgr A*. NH_3(3,3) traces parts of the CND, but it is strongly detected outside of it. However, the result reported on the highest-excitation transition studied, (6,6), tracing gas at $\sim$ 412 K, is even more stunning. NH_3(6,6) is found inside the inner cavity, which was previously predicted by Harris et al. (1985) (figure 1.3). In fact, the location where NH_3(6,6) has been detected approaching Sgr A*, the eastern side, was void of emission in other high density tracers (Herrnstein & Ho, 2002). Also, the distribution of NH_3(6,6) is not correlated to the minispiral one, which means that NH_3(6,6) is not associated with the arcs of ionized gas. The line profiles, very broad, indicate the possible interaction with the supermassive black hole. Therefore, hot and dense gas has been found within 1.5 pc of the supermassive black hole.

Consequently, the next step in the ladder of understanding the kinematics of the Galactic center should be to expand the study of high-density high-temperature molecular gas. With this goal in mind, we undertook the project of looking for highly-excited molecules in the Galactic center with high-resolution instruments. HCN and CS, due to their high critical density ($n_{H_2} > 10^5\,cm^{-3}$), are both high-density molecular tracers. HCN has already proved to be a successful tracer in the Galactic center (Güsten et al., 1987; Jackson et al., 1993; Marshall et al., 1995; Wright et al., 2001; Christopher et al., 2005). However, high-resolution results have only been instrumentally available in the lowest transition, (1-0), deeply affected by self-absorption because of the presence of foreground clouds of cold gas (Güsten et al., 1987; Wright et al., 2001; Christopher et al., 2005) (figure 1.4). Single-dish results in higher-excitation transitions have proved that the absorption is no longer a problem (Jackson et al., 1993; Marshall et al., 1995). CS has not been studied before in the inner parsecs of the Galaxy, but has been detected in the vicinity (more precisely towards the *50 km s^{-1} cloud*). With the development of the Submillimeter Array (SMA) suddenly we are able to study those high-density tracers at high-excitation levels. We have then proceeded to study two of these high-density high-excitation molecular tracers, HCN(4-3) and CS(7-6) in the inner 5 pc of the Milky Way. The results are reported in chapter 2. We are in the process of expanding these results with new SMA data, studying HCN(3-2) and HCO^+(3-2), molecular tracers closely correlated, which might help explain the mass distribution along the CND, since the ratio of HCO^+/HCN increases in low-mass regions (Christopher et al., 2005). The preliminary results are reported in appendix A.

In order to achieve a more comprehensive understanding of the intricacies of the

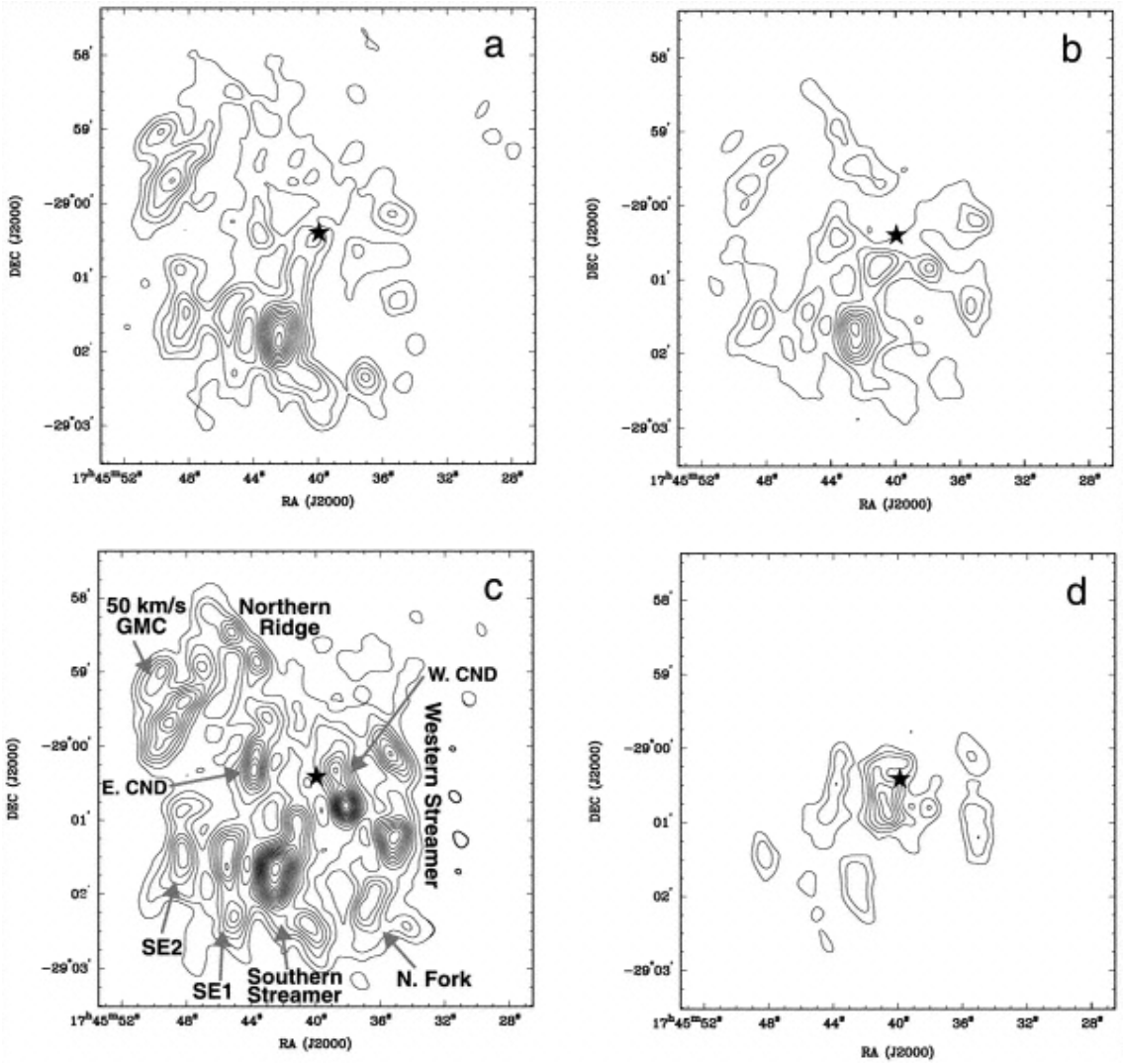

Figure 1.3: Integrated emission maps of *a)* $NH_3(1,1)$, *b)* $NH_3(2,2)$, *c)* $NH_3(3,3)$ and *d)* $NH_3(6,6)$ from Herrnstein & Ho (2005). Contours are in steps of 1.32 Jy beam^{-1} km s^{-1}in all four panels. Sgra A* is marked by a star.

dynamics in the nucleus of galaxies, we need to further expand our research to cover new sources. Fortunately, the Galactic center, although being the closest one, is not the only available galactic nucleus. Looking for a suitable source, with similar characteristics to the Milky Way, IC 342 has risen as the perfect companion for the Galaxy in this quest.

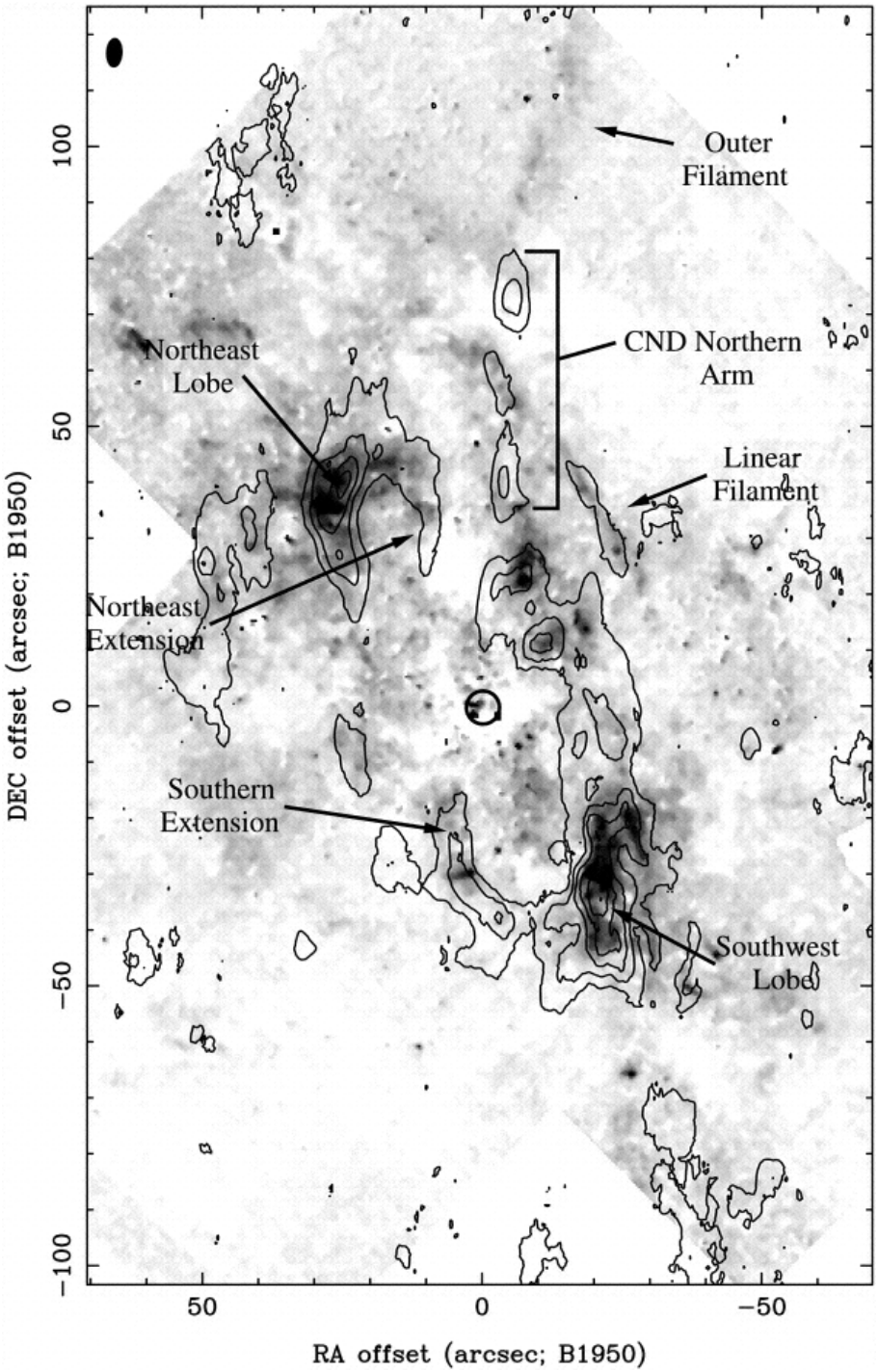

Figure 1.4: HCN(1-0) integrated intensity emission in the Galactic center from Christopher et al. (2005). Contour levels are in steps of 10.1 Jy beam^{-1} km s^{-1}from 5.1 Jy beam^{-1} km s^{-1}. Sgr A* is marked by a circle.

IC 342

IC 342 is a nearby (3.3 Mpc, Saha et al. (2002); Karachentsev (2005)) Scd spiral, just slightly further in the Hubble classification from the Milky Way (Crosthwaite et al., 2001). Because of its almost face-on orientation (i = 25°, Lo et al. (1984)), it has become an excellent source for the study of galactic nuclei. The location of IC 342 with respect to the Galactic plane is not ideal, since it is located barely 10.6° from the Galactic equator (Lo et al., 1984). This position could be responsible for extinction along the line of sight, since IC 342 does not appear as a strong optical source. However, IC 342 has been found to be a very rich source of molecular emission (Downes et al., 1992). Obviously, because of the distance, the dimensions we are considering are not the same for IC 342 and the Milky Way (1″ corresponds to 0.038 pc in the Galactic center, and to 16 pc in IC 342). Nonetheless, the molecular gas distribution in the center of IC 342 is similar to the distribution in the Galactic center, composed of GMCs and more diffuse gas, like in the CMZ (Morris & Serabyn, 1996). Like in the Milky Way, IC 342 has a molecular ring interacting with a large-scale bar (Ishizuki et al., 1990; Downes et al., 1992; Schulz et al., 2001). Also, a nuclear star cluster, located in the central region, void of gas (Meier & Turner, 2005), has been detected (Böker et al., 1997), although it is slightly older than the nuclear stellar cluster in the center of the Galaxy ($10^{6.8-7.8}$ and $10^{6.5}$ years, respectively, Böker et al. (1999)). The central black hole of IC 342 is expected not to be more massive than 5×10^5 $M_\odot$ (Böker et al., 1999).

The bar-like structure in the nuclear region of IC 342 has an S-shape (minispiral) and seems to be composed of infalling gas towards the very center (Turner & Hurt, 1992; Schinnerer et al., 2003). The bar, formed by a northern arm and a southern arm, each of them with a 400 pc× 60 pc size in CO(1-0) (Ishizuki et al., 1990), encounters a ring of neutral gas with a $\sim$ 80 pc radius. In the regions where the two arms and the ring interact, important concentrations of molecular gas (GMCs) with bursts of star formation have been found (Böker et al., 1997). Also, along the arms, especially the northern one, much better defined (Ishizuki et al., 1990), GMCs have been detected. High-resolution observations in HCN(1-0) by Downes et al. (1992) were the first to formally describe the GMCs and the positions reported in that paper have been adopted in later works. At the same time, the nuclear stellar cluster does not seem to be currently undergoing a process of star formation. Moreover, the star formation in the nuclear region of IC 342 seems to be dominated by the processes taking place in the molecular ring, and not the nuclear stellar cluster. However, the heating of the inner edge of the ring (Photon-Dominated Regions) is likely produced by the old stellar cluster since the newly formed stars ($\sim$ 5 Myr, Böker et al. (1997)) are still embedded in their cocoons of dust and gas and the UV radiation is absorbed. Meier & Turner (2005) found the molecular distribution of gas in the central region of IC 342 to be chemically varied. Different molecular tracers were strongly detected in different regions of the molecular ring or the arms (see figure

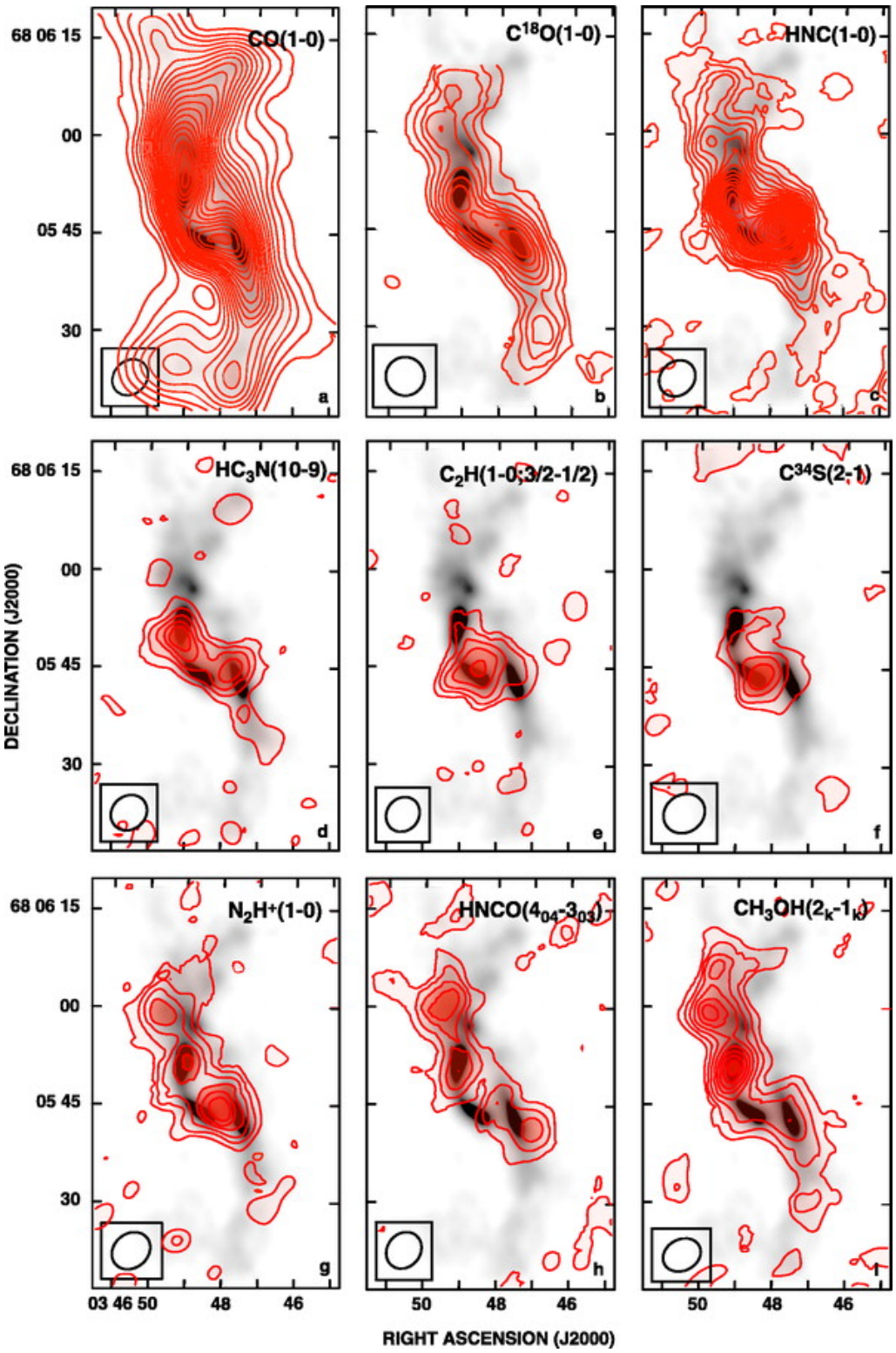

Figure 1.5: Integrated intensity of several molecular tracers in IC 342 by Meier & Turner (2005). Contour levels in steps of 2σ times the RMS intensity in each map, except for ^{12}CO(1-0), which is contoured in steps of 7.7 K km s^{-1}. The greyscale map is ^{12}CO(1-0) from Meier et al. (2000).

1.5). The chemical timescale and the differences in excitation and critical density were not responsible for the different gas distribution, since they were similar for all the molecular tracers studied (Meier & Turner, 2005). Therefore, the molecular gas distribution in the inner part of IC 342 is chemically differentiated. A schematic drawing of the molecular gas distribution in the nuclear region of IC 342 has been drawn by Meier & Turner (2005) (figure 1.6). The similarity of the gas distribution with the Galactic center is remarkable, barring size-wise differences. This result suggests that IC 342 might have a similar morphology than the Milky Way on a larger scale.

Because of the similarities in the gas distribution between the nuclear region of IC 342 and the Milky Way, it is easy to try to draw comparisons. As it was mentioned before, NH_3 have proved to be a key tool in the disentanglement of the dynamics of the Galactic center. For this reason, it is only obvious that similar attention should be paid in the case of IC 342. Previous studies have found various transitions of NH_3 to be strongly detected in IC 342 (Martin & Ho, 1979; Ho, Martin, & Ruf, 1982; Ho & Martin, 1983; Ho et al., 1990; Mauersberger et al., 2003). However, the highly-excited transitions that have produced the more interesting results in the case of the Galactic center have not been studied with high-resolution instruments. The improvement of the receivers in the Very Large Array (VLA) have made our work possible. We set out to detect NH_3(6,6) and (3,3) (chapters 3 and 4, respectively) in the nuclear region of IC 342. Because of the properties of the NH_3 molecule, the detection of two transitions allow us to calculate the rotational temperature. Better still, when the two transitions observed represent metastable "ortho" states of the NH_3 molecule (J=K and K=3n, n an integer) (see Ho & Townes (1983) for a more detailed explanation), the transitions between states can only be produced by collisions, therefore the rotational temperature is a good approximation to the kinetic temperature (Ho, Martin & Barrett, 1981; Walmsley & Ungerechts, 1983). As in the case of the Galactic center, a two-temperature component has proved to explain the gas distribution in the nuclear region of IC 342 (Mauersberger et al., 2003; Israel & Baas, 2003). Therefore, the detection and combination of NH_3(3,3) and (6,6) data can provide not only results on the distribution of high-density, high-temperature gas, and whether the warmer material is located more closely to the dynamical center, as it is the case of the Galactic center, but also shed some light on the temperature issue, thanks to a precise calculation of the temperature because of the characteristics of the NH_3 molecule.

In summary, the goal of this work is to better understand the processes taking place in the inner parsecs of galaxies, more precisely the geometry, kinematics and excitation conditions of the molecular gas concentrated in the vicinity of a super-massive black hole.

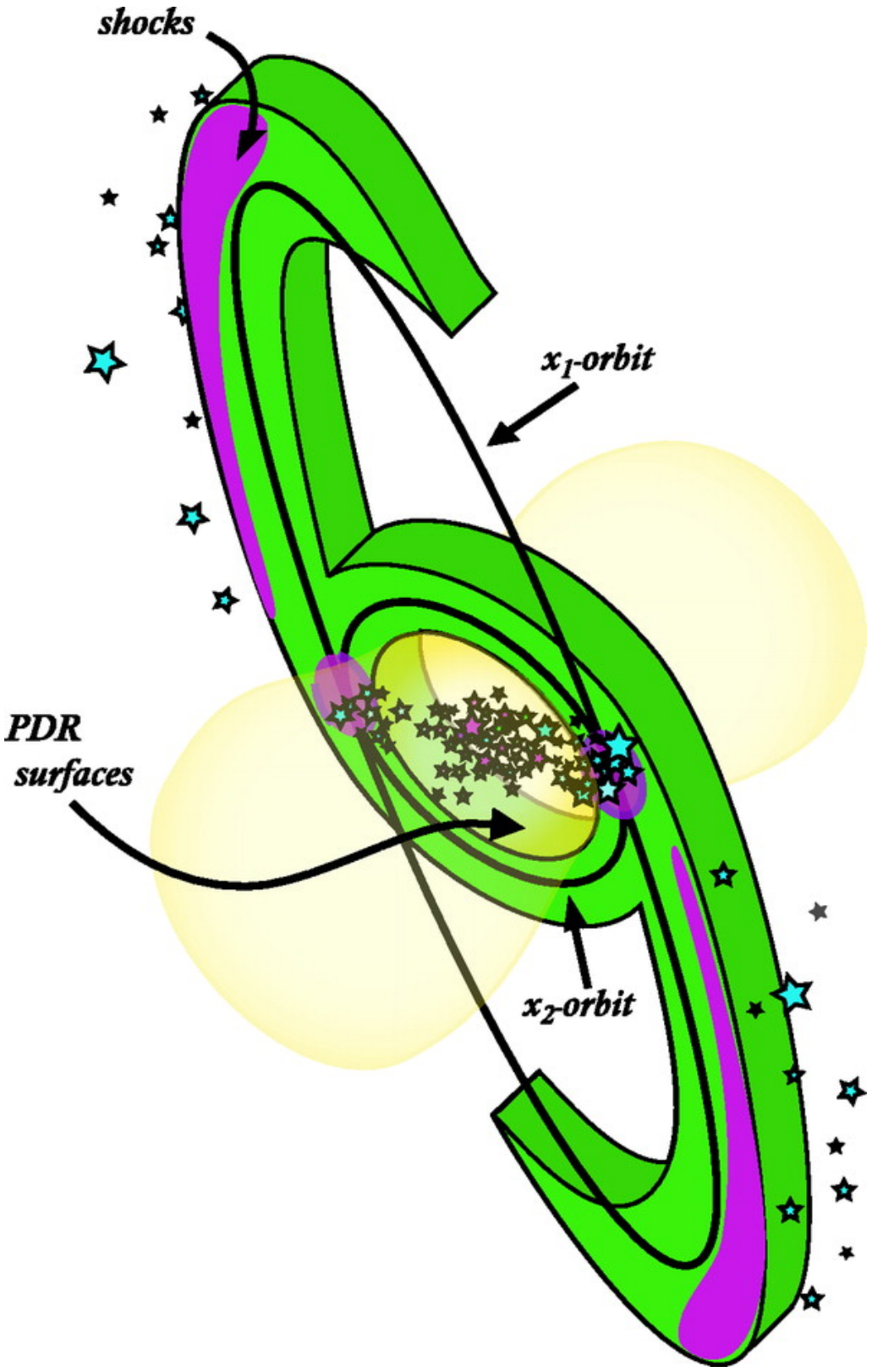

Figure 1.6: Schematic drawing of the nucleus of IC 342 from Meier & Turner (2005).

Chapter 2

Tracing the CND with high-density molecular tracers

2.1 Abstract

We present the first large-scale mosaic performed with the Submillimeter Array (SMA) in the Galactic center. We have produced a 25-pointing mosaic, covering a $\sim 2' \times 2'$ area around Sgr A*. We have detected emission from two high-density molecular tracers, HCN(4-3) and CS(7-6), the latter never before reported in this region. The data have an angular resolution of $4.6'' \times 3.1''$, and the spectral window coverage is from -180 km s^{-1} to 1490 km s^{-1} for HCN(4-3) and from -1605 km s^{-1} to 129 km s^{-1} for CS(7-6).

We detect both molecular tracers strongly in the southern part of the circumnuclear disk (CND), while they are weaker towards the northern part.

This result suggests that the southern part of the CND is denser than the northern part. Also, by comparing the HCN(4-3) results with HCN(1-0) results from Christopher et al. (2005) we can see that the northern and the southern parts of

the CND have different excitation levels, with the southern part warmer than the northern.

2.2 Introduction

The Galactic center, located at a 8 kpc distance (Reid, 1993) (1″ corresponds to 0.038 pc), is our unique laboratory to study the interactions between a supermassive black hole (4×10^6 $M_\odot$, Ghez et al. (2005); Schödel & Eckart (2005)) and its surrounding environment. This region is composed of a very dense and warm interstellar medium (ISM), mostly condensed in Giant Molecular Clouds (GMCs). These GMCs have different characteristics than those GMCs found in the Galactic disk. In the Galactic center, the GMCs are warmer, denser, and much more turbulent. The dynamical center of the Milky Way is occupied by a nonthermal compact radio source, the supermassive black hole Sgr A*. Surrounding this source, three arcs of ionized gas are present (the western arc, the northern arm and the extended bar, Roberts & Goss (1993)), forming the minispiral or Sgr A West. Both Sgr A* and the minispiral are surrounded by a ring-like structure, the circumnuclear disk (CND). The CND is composed of a mixture of neutral atomic and molecular gas and dust (Genzel et al., 1985; Mezger et al., 1989). The CND has an inner radius of ∼2 pc (Gatley et al., 1984; Genzel et al., 1985; Jackson et al., 1993; Christopher et al., 2005) and it extends until ∼ 5 pc (Harris et al., 1985; Genzel et al., 1985). It is tilted with respect to the Galactic plane (∼ 70°) and its main motion is rotation around Sgr A* (Gatley et al., 1984; Genzel et al., 1985; Lugten et al., 1986; Güsten et al., 1987). The inner cavity that the CND encloses is devoid of dust (Becklin et al., 1982), but it is occupied by ionized gas (minispiral) (Gatley et al., 1984), neutral molecular gas (Harris et al., 1985; Herrnstein & Ho, 2002) and a large amount of neutral atomic gas (Jackson et al., 1993). Also, inside the cavity, occupying the central parsec, stars in different evolutionary stages have been found (Paumard et al., 2006). The stars are rotating around Sgr A* and they could have been formed in-situ (Paumard et al., 2006) or spiraled inwards after formation (Gürkan & Rasio, 2005).

Güsten et al. (1987) have previously suggested the clumpiness of the CND, calculating a dynamical lifetime of 10^4 - 10^5 yr. However, later studies by Jackson et al. (1993), Shukla et al. (2004) and Christopher et al. (2005) suggest that the clumps have a higher density than previously calculated (∼ (3-4) × 10^7 cm^{-3}, Christopher et al. (2005)). The density of the clumps would allow them to overcome the tidal shear from Sgr A*, increasing the lifetime of the CND to 10^7 yr.

2.2.1 Molecular studies

The Galactic center has been studied numerous times in different molecular gas tracers. Coil & Ho (1999, 2000); McGary et al. (2001); Herrnstein & Ho (2002, 2005) studied the emission from four different ammonia rotation inversion transitions (NH_3(1,1), (2,2), (3,3) and (6,6)) using the Very Large Array (VLA). Ammonia is a moderately high-density ($\sim 10^4$ cm^{-3}), and high-temperature (23 to 412 K, (1,1) to (6,6) transitions) tracer. These studies showed that the colder gas (NH_3(1,1) and (2,2)) is highly extended in this region, showing no strong emission in the CND. However, NH_3(3,3) (energy above ground $\sim$ 125 K) is more concentrated towards the center, proving to be much more useful for tracing the CND, although still not found any closer to the supermassive black hole than the CND. NH_3(6,6), on the other hand (tracing material at $\sim$ 412 K), is found very close to Sgr A*, predominantly inside the CND, well within the inner cavity, while it is almost nonexistent further away. Therefore, very dense and warm gas is located in the inner 1.5 pc of the Galaxy.

Studies of other high-density tracers have also been carried out. In particular, HCN has proved to be a very useful molecular gas tracer in the Galactic center environment, providing important results regarding the structure of the CND. Güsten et al. (1987) studied HCN(1-0) emission using the Hat Creek Interferometer, achieving a 10″ resolution. The emission from this transition was detected along the CND, with the emission in the southern part stronger than the emission detected in the rest of the CND. Also, a gap was found in the eastern part of the CND. High-resolution results were also achieved by Wright et al. (2001) using the bigger Berkeley-Illinois-Maryland Array (BIMA). However, Wright et al. (2001) noted the self-absorption problem affecting HCN(1-0) (and HCO^+(1-0), which is closely correlated). This problem was also addressed by Christopher et al. (2005), who published their HCN(1-0) data from the Owens Valley Radio Observatory (OVRO) millimeter interferometer, with a 5″ resolution. In these latest results, the HCN emission is detected along the CND and also in various narrow structures outside of it, such as the linear filament. However, because of the self-absorption problem, the use of higher transitions was ever more pressing.

HCN(3-2) emission was detected by Jackson et al. (1993) using the IRAM 30-m telescope and by Marshall et al. (1995) using the 15-m James Clerk Maxwell Telescope (JCMT). In both cases, emission is detected along the CND, but it is remarkably stronger towards the south of the CND. The detection of HCN(4-3) emission (which traces material at $\sim$ 25 K, and has a critical density value of $\sim 10^8$ cm^{-3}; Choi et al. (2000); Takakuwa et al. (2007)) in the Galactic center region was also reported by Marshall et al. (1995) using the JCMT, achieving a 15″ resolution. The HCN(4-3) emission is also stronger towards the south of the CND, with very weak emission towards the north. Moreover, a dynamical model of a rotating torus de-

veloped by this group supported the idea that the northern and the southern parts of the CND are independent structures (each of them with a different inclination, e.g. a warped disk), following a common rotation pattern around Sgr A*. The self-absorption problem is much less evident for these higher-excitation transitions, suggesting that absorption is produced by lower excitation material along the line of sight.

In summary, the higher HCN lines, without the self-absorption problem, seem to be good tracers to study the geometry of the CND. However, higher-resolution results in these lines had not been available until now since the Submillimeter Array (SMA) is the first interferometer equipped with 350 GHz receivers.

CS has also been studied in the Galactic center in various transitions ((2-1), (3-2) and (5-4), Serabyn et al. (1989)) and strong CS(7-6) emission has been detected within 10 pc of Sgr A*, in the "50 km s^{-1} cloud" (Serabyn et al., 1992). However, no previous results on (7-6) have been reported in the CND. Our study images the distribution of CS(7-6) emission (which traces material at $\sim$ 49 K and has a critical density of $\sim 10^7$ cm^{-3}, Choi et al. (2000); Takakuwa et al. (2007)) in the central 4 pc of the Milky Way.

2.3 Observations

Observations of the HCN(4-3) (ν = 354.5054759 GHz) and CS(7-6) transitions (ν = 342.8830000 GHz) were made with the Submillimeter Array (Ho , Moran & Lo, 2004) in the compact configuration on 2005 July 1 and 7 and August 13 and in the subcompact configuration on 2007 May 5. We produced a 25-pointing mosaic (figure 2.1) covering a $\sim 2' \times 2'$ area, which encompasses Sgr A*, the mini-spiral and the CND. The central pointing was centered on $\alpha_{J2000.0} = 17^h45^m40.00^s$, $\delta_{J2000.0}$ = -29°00′26.60″, and the rest of the pointings were placed at half-beam spacings, effectively increasing the sensitivity of the mosaic (the primary beam for these frequencies is 36″). The data consisted of two 2 GHz bandwidths (upper sideband and lower sideband, USB and LSB, respectively) divided into 24 spectral windows, each of them composed of 128 channels with a velocity resolution of 0.7 km s^{-1}. HCN(4-3) was observed in the USB and CS(7-6) in the LSB. The velocity coverage for the USB was from -180 km s^{-1} to 1490 km s^{-1}, centered on the HCN(4-3) line at v_{LSR} = 0 km s^{-1} and from -1605 km s^{-1} to 129 km s^{-1} for the LSB, centered on the CS(7-6) line at v_{LSR} = 0 km s^{-1}. We averaged every 5 km s^{-1} since molecular lines in the vicinity of Sgr A* are very broad (FWHM $\approx$ 100 km s^{-1}; Harris et al. (1985)). Therefore the degraded velocity resolution was adequate to resolve the lines. The continuum subtraction was performed in the uv plane. The total

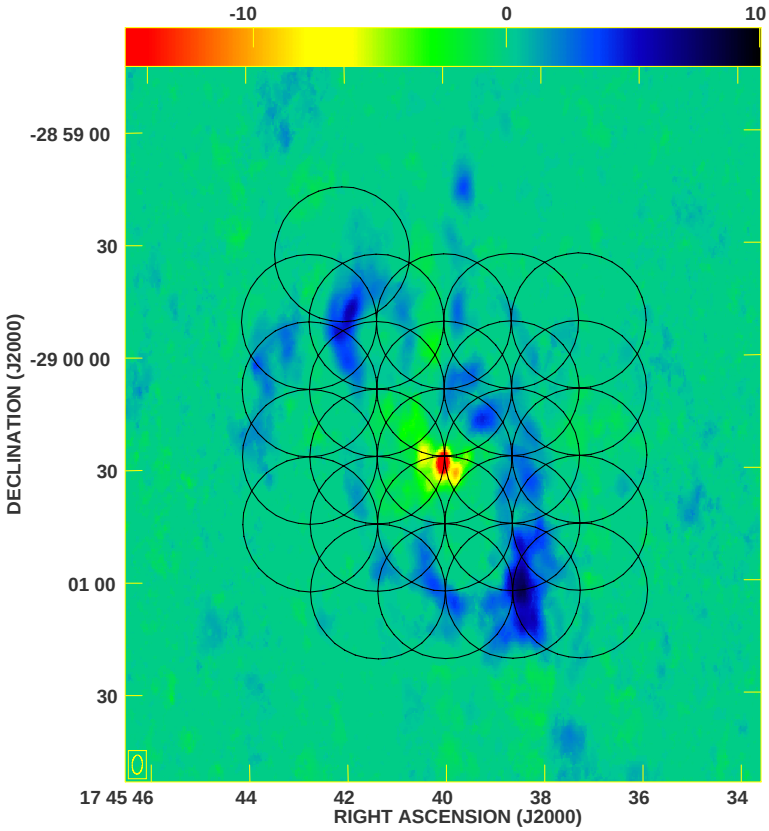

Figure 2.1: 25-pointing mosaic. The background image is HCN(1-0) from Christopher et al. (2005).

integration time per pointing was 30 minutes, but because of the distribution of the pointings, the actual time for the central 1.5′ covering the CND was 90 minutes. The phase calibrator was 1733-130 (NRAO 530), with a flux value of 0.84 Jy for the first two tracks and 0.79 Jy for the third and fourth tracks (the fourth track in the subcompact array). Also, during the fourth track we used 1751+096 as a phase calibrator as well, with a flux value of 1.75 Jy.

The data were calibrated using the MIR software package developed for the Owens Valley Radio Observatory (OVRO), which was modified for the SMA, and the imaging process was done using both the Multichannel Image Reconstruction Image Analysis and Display (MIRIAD) and the NRAO Astronomical Imaging Processing System (AIPS). To produce the dirty map we used the task invert in MIRIAD, with the systemp option to decrease the weight for visibilities with abnormally high system temperatures. Afterwards, we subtracted the continuum using line-free channels from both sides of the line for the HCN(4-3), and only one side for the CS(7-6), since the latter line was located close to the edge of the passband in order to be able to observe both molecular lines simultaneously. We cleaned the map using

the task mossdi2 also in MIRIAD, cleaning to a 1.5 σ level. The integrated intensity maps were produced using the MOMNT task in AIPS, with a minimum flux cutoff of 0.5 Jy and 0.3 Jy for the HCN(4-3) data and the CS(7-6) data, respectively. The flux cutoff was chosen based on the noise threshold, to suppress noise contribution, since if a straight summation was performed the contribution from the noise would build up and narrow line features would be lost. Natural weighting of the uv data produced an image with a synthesized beam of $4.6'' \times 3.0''$ with a position angle of 4.1° for the HCN(4-3) emission and $4.5'' \times 3.1''$ and a position angle of -4.4° for CS(7-6). The final RMS per channel is 0.3 Jy beam^{-1} and the overall achieved RMS sensitivity is 3.4 Jy beam^{-1} km s^{-1} (for HCN(4-3)) and 0.2 Jy beam^{-1} and 3.3 Jy beam^{-1} km s^{-1} (for CS(7-6), respectively).

The compact-north (for low declination sources) configuration of the SMA provides a maximum projected baseline distance of 91 m and a minimum of 11 m, while the subcompact configuration has a maximum projected baseline of 25 m and a minimum of 6 m. The combination of data from both configurations improves the detection of the extended emission (thanks to the subcompact configuration), since the short-spacings problem is less apparent, while providing a better resolution (because of the compact configuration). The data obtained using only the compact configuration show a better resolution, but the negative bowls seen in the maps indicate the loss of extended emission. By combining both configurations the problem is minimized. Eventually, the ultimate goal would be to combine these data with single-dish data.

2.4 HCN(4-3)

We detect the extended emission of HCN(4-3) within 2 pc of Sgr A* (figure 2.2). The southern part of the CND is clearly visible, tracing the southwest lobe and the southern extension (using the same nomenclature as Christopher et al. (2005)), while the emission from the northern part is more sparse and distributed.

Marshall et al. (1995) observed a similar distribution of HCN(4-3) emission using the James Clerk Maxwell Telescope (JCMT) ($15''$ spatial resolution), detecting the strongest emission to the south. Due to our higher resolution image, we can immediately appreciate that the emission is very clumpy around Sgr A*, i.e., the CND is composed of an array of blobs, in a necklace-like manner, especially towards the north, as was first noted by Güsten et al. (1987). We also compare the HCN(4-3) flux detected with the SMA to the single-dish flux detected with the JCMT. After smoothing the SMA resolution to match that of the JCMT, we find that the interferometer detects 61% of the emission detected with the single-dish over an

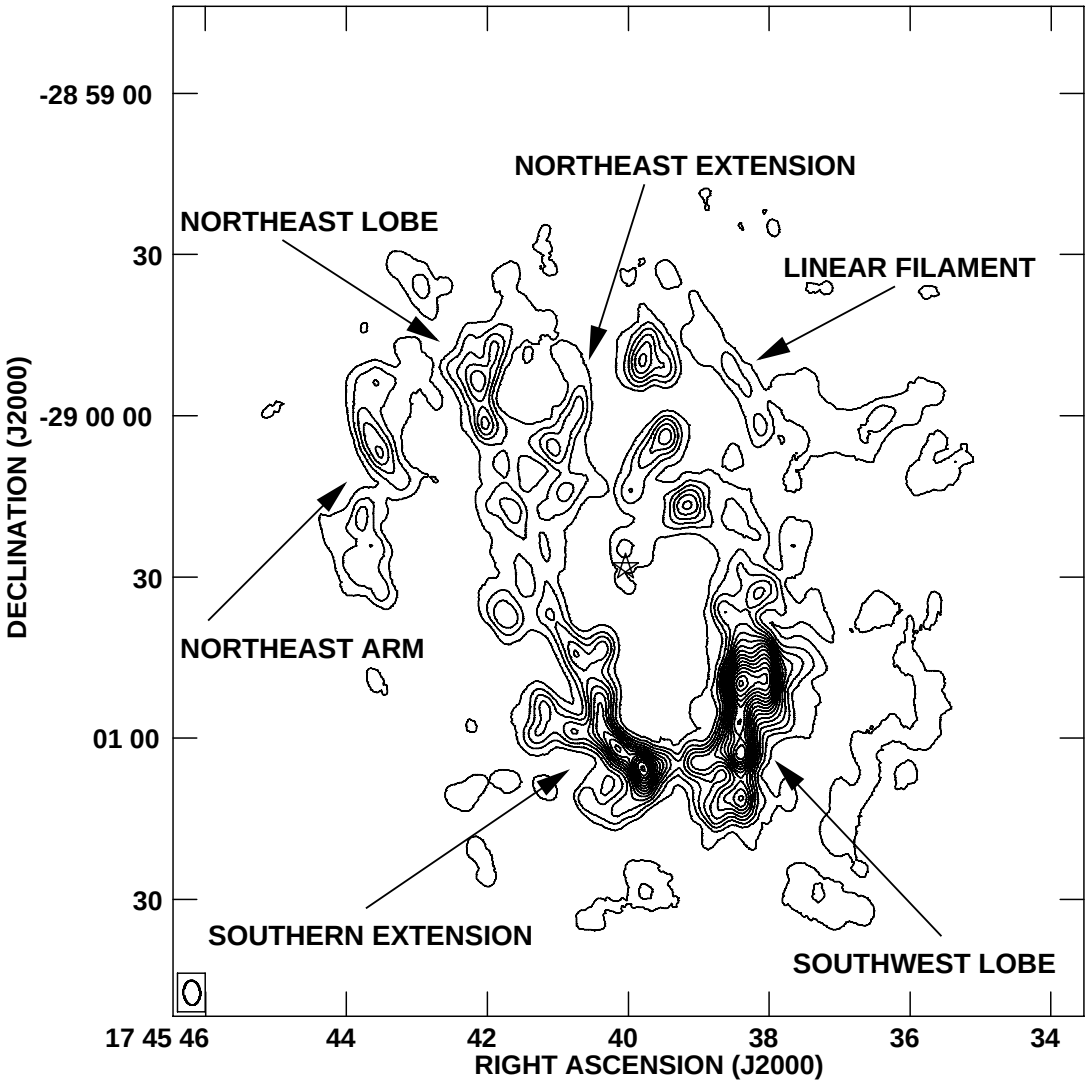

Figure 2.2: HCN(4-3) integrated intensity map. The contour levels are in steps of 6σ, from 3 to 93σ, but for the highest contour level, at 97σ (2.5×10^1 to 81.7×10^1 Jy beam^{-1} km s^{-1}). Sgr A* is marked with a star.

area that covers 10 JCMT beams. The missing flux would be spread over many SMA synthesized beams, which are approximately 16 times smaller in area than the JCMT beam (i.e. 161 SMA synthesized beams). The SMA data smoothed to the JCMT resolution (figure 2.3), however, show a very striking similarity to the JCMT emission map by Marshall et al. (1995) (figure 4 in the reference). This result suggests that the extended emission is a very low level contribution to the final result (21 Jy km s^{-1} per SMA synthesized beam), and most importantly that both the smoothed SMA and the JCMT emission maps are dominated by the clumps.

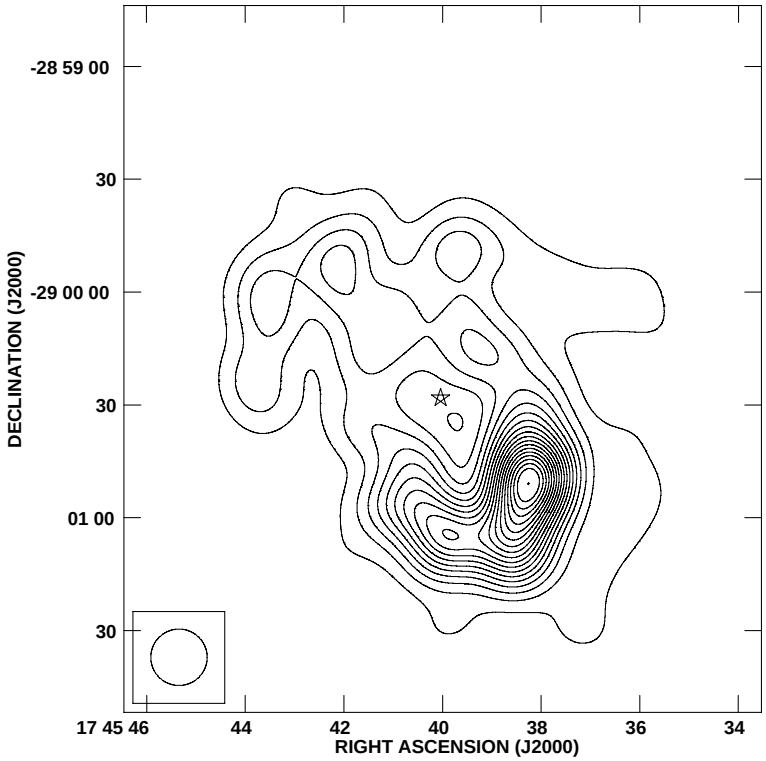

Figure 2.3: HCN(4-3) integrated intensity map smoothed to a 15″ resolution. The contour levels are in steps of 10σ, from 10 to 180σ, but the highest contour level, which is 194σ (2.7×10^1 to 5.2×10^3 Jy beam^{-1} km s^{-1}). Sgr A* is marked with a star.

It is widely accepted that the overall motion of the CND is rotation around Sgr A*, as we have previously mentioned. We plot the spectra at different peaks (clumps) along the CND to show the kinematics (Fig 2.4). Also, we plot the spectra at different "empty" locations close to peculiar-looking spectra to check whether the influence of negative bowls have affected the emission and, therefore, the final result. We observe that spectra A and Q show the largest velocity shifts, with spectrum A redshifted and spectrum Q blueshifted. Spectrum A peaks at $\sim$ 105 - 110 km s^{-1} and spectrum Q at $\sim$ -105 - -110 km s^{-1}, which agree with the values previously reported by Güsten et al. (1987); Jackson et al. (1993); Marshall et al. (1995) and Christopher et al. (2005). The rest of the features peak at intermediate velocities, in an orderly manner, consistent with a rotation pattern in the CND. With an average 110 km s^{-1} velocity and a 1.5 pc radius, if we consider the velocity to be purely rotational, the rotation period would be $\sim$ 8 $\times 10^4$ yr. But, there is much more information we can extract from the study of the spectra. In particular, there is a group of features worth observing closely. Firstly, spectrum H is slightly different from the rest. It does not seem to follow the rotation pattern and has a different linewidth, being narrower than the other spectra. These characteristics suggest that this feature may be the "70 km s^{-1} cloud", first reported by Güsten et al. (1987).

It seems to be near the CND, but has a non-negligible radial velocity component ($\sim$ 50 km s^{-1}, Jackson et al. (1993)), much larger than the rest of the clumps, whose predominant motion is rotation. Also, clump E shows a remarkably different spectrum, with two velocity components, roughly equal in intensity and an overall broader profile than nearby clumps. Clump E lies to the north of the minispiral northern arm (figure 2.5), believed to be interacting with the CND and creating a gap where the ionized gas is infalling towards Sgr A* (Wright et al., 2001) (in fact, Christopher et al. (2005) consider clump E part of the *CND northern arm*). Jackson et al. (1993) reported the detection of neutral gas also associated with the minispiral northern arm as far as 3 pc from the dynamical center of the Milky Way, consistent with a scenario of infalling gas through the CND gap. Clump G, located in close proximity to clump E, also shows a two-velocity component broad profile. Clump G is part of what Christopher et al. (2005) called the *linear filament*, a ridge of gas that appears to be connecting the *western streamer* and the CND (McGary et al., 2001), though it might be a projection effect. On the other hand, we observe a very peculiar (and broad) double-peak spectrum in clump N, which also seems to be in the path of the minispiral (figure 2.5). Serabyn & Lacy (1985) reported the western arc of the minispiral to have the same velocity field as the CND, therefore suggesting a connection between the molecular ring and Sgr A West. However, clump N might be also affected by a different process. When comparing spectrum M with spectrum N, we observe that both show two 'dips' at roughly the same velocities ($\sim$ -60 km s^{-1}, $\sim$ 10 km s^{-1}), even though spectrum M was taken a little farther from the apparent minispiral influence region. Also, spectrum L shows that there are strong negative bowls in the proximity of clump N because of the lack of short-spacings, so that these spectra are likely affected by this problem. We will go back to discuss this spectrum a little later.

Clump DD does show a very clear two-velocity component broad profile, and may be related to the interaction with the minispiral. Cloud DD is located at the end of the extended bar of Sgr A West (figure 2.5). We could be observing a similar behavior as the one detected for clump E. Also, absorption is likely not the answer for this feature due to its uniqueness among the nearby clumps. We would have expected the same profile to be shown by the rest of the adjacent clumps (such as C, D and AA), but that is not the case. We have not found strong negative bowls in the proximity of clump DD. Therefore the lack of short-spacings is probably not affecting the line profile for this clump.

It is important to remark (as Jackson et al. (1993) and Marshall et al. (1995) did previously) that we do detect emission in the eastern and northeastern parts of the CND, a section that is heavily affected by absorption by foreground cold clouds when using a lower transition line (Güsten et al., 1987). The emission peaks detected in this region (D and DD) are indeed strong, demonstrating that the higher temperature gas remains unaffected by the cold gas along the line of sight.

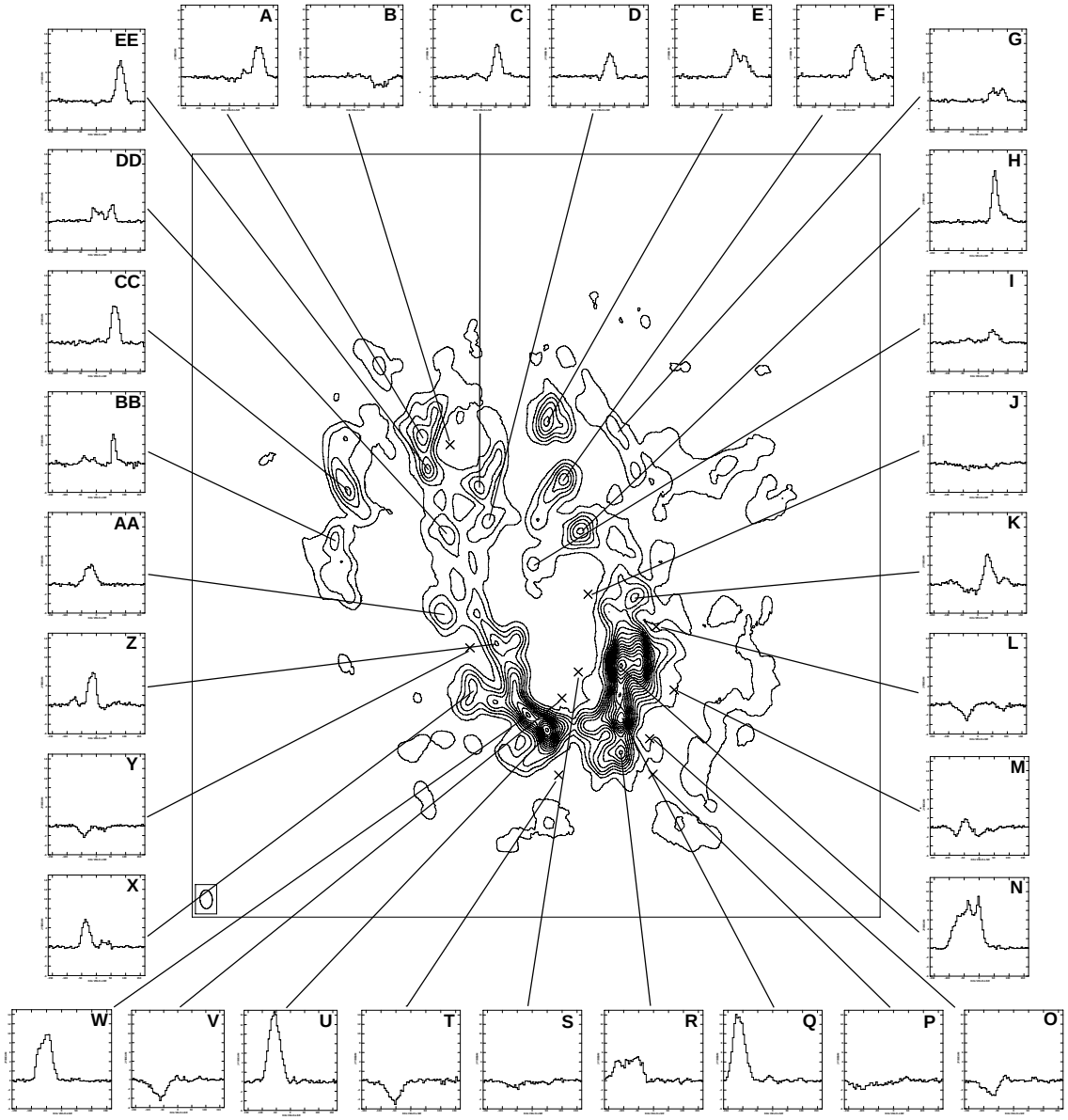

Figure 2.4: HCN(4-3) spectra measured at the positions of the different clumps.

Spectra BB and CC show very narrow profiles, especially spectrum BB. They are located outside of the main CND structure, in what we will call the *northeast arm*, therefore farther from the supermassive black hole. The greater distance from Sgr A* implies that the gravitational pull from the center will be less important, and the narrower linewidths may reflect a weaker interaction.

Spectra K shows a peculiar profile as well. Observing the profile of spectrum L, closely located, we infer that clump K is affected by the lack of short-spacings in the data. A similar behavior seems to be affecting clump Z, easily understood when

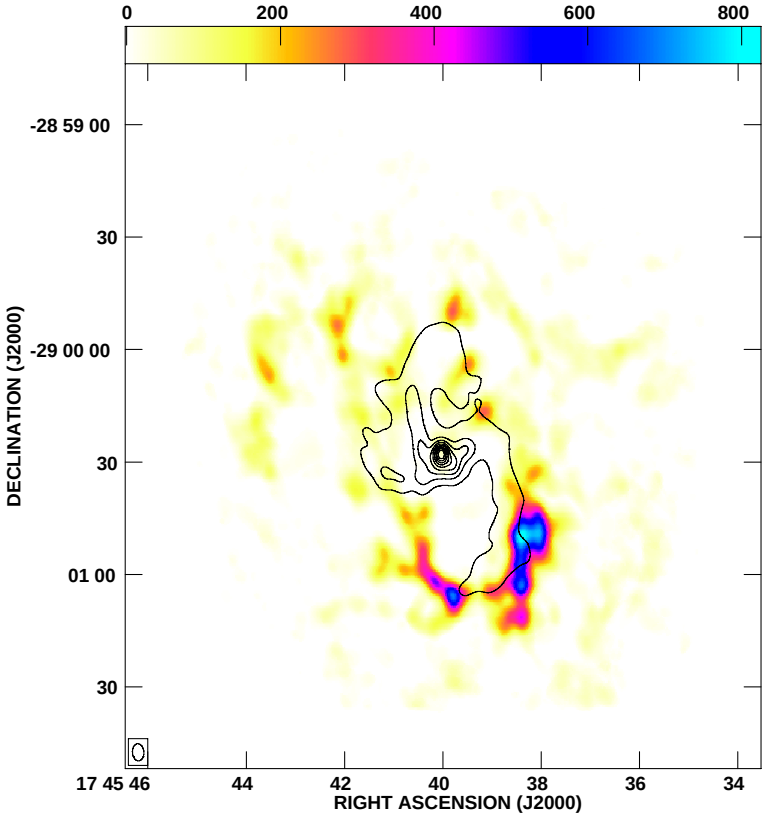

Figure 2.5: 6 cm continuum integrated intensity in contours (from Yusef-Zadeh & Morris (1987)). HCN(4-3) integrated intensity in false color-scale. Contour levels are in steps of 10% of the continuum emission peak, from 1×10^{-1} Jy beam^{-1} to 9×10^{-1} Jy beam^{-1}. The false color-scale is in Jy beam^{-1} km s^{-1}.

comparing to spectrum Y.

Clumps U, W and Q are likely also affected by the negative bowls (see spectra T, V and O), which are much stronger in the southern part of the CND, indicating that the loss of extended emission is more significant in that region than in the northern part, where only clump A seems to be affected.

Spectrum R seems to be especially affected by the short-spacings problem, resulting in a very broad but not very strong spectrum. In summary, HCN(4-3) has a lack of extended emission, especially remarkable in the southern part of the CND. However, such problem does not prevent the very strong detection of this molecular tracer along the CND and even further away, in the linear filament and the *northeast arm*.

Comparing our data with HCN(1-0) data from the Owens Valley Radio Observatory by Christopher et al. (2005) (figure 2.6, both maps convolved to the same

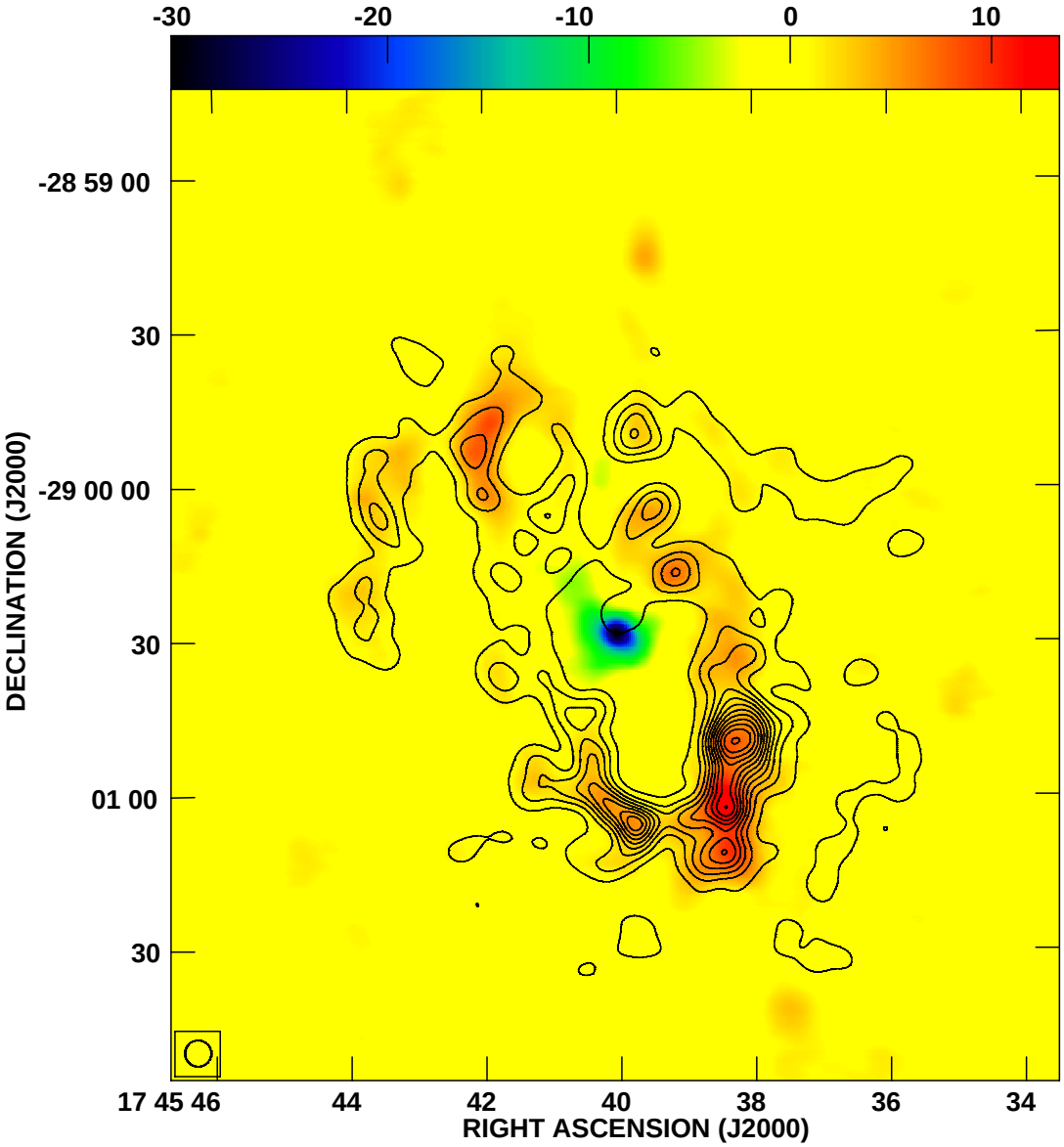

Figure 2.6: HCN(4-3) integrated intensity in contours. HCN(1-0) integrated intensity in false color-scale from Christopher et al. (2005). Contour levels are in steps of 6σ, from 3σ to 63σ, except for the highest contour level, at 70σ (5.9×10^1 to 13.7×10^1 Jy beam^{-1} km s^{-1}). The false-color scale is in Jy beam^{-1} km s^{-1}. Sgr A* is seen in absorption in HCN(1-0).

resolution and integrated over the same velocity range) we can see that both transitions coincide tracing the southern part of the CND, and even in some parts of the northern lobe of the CND, but HCN(1-0) is stronger to the north as compared to HCN(4-3). This result suggests that the northern and the southern parts of the CND have different excitation conditions, with the southern part warmer than the

northern part. The strongest peak in HCN(1-0) in the *southwest lobe* does not coincide with the strongest peak in HCN(4-3). It appears that the lower-excitation line is stronger towards the tip of the CND, where the most blueshifted material is detected, while HCN(4-3) is strongest north of that position, in what we have called clump N (figure 2.4). However, HCN(1-0) in the position of clump N is affected by self-absorption (Wright et al., 2001). Therefore, the difference in gas distribution could be due to this effect.

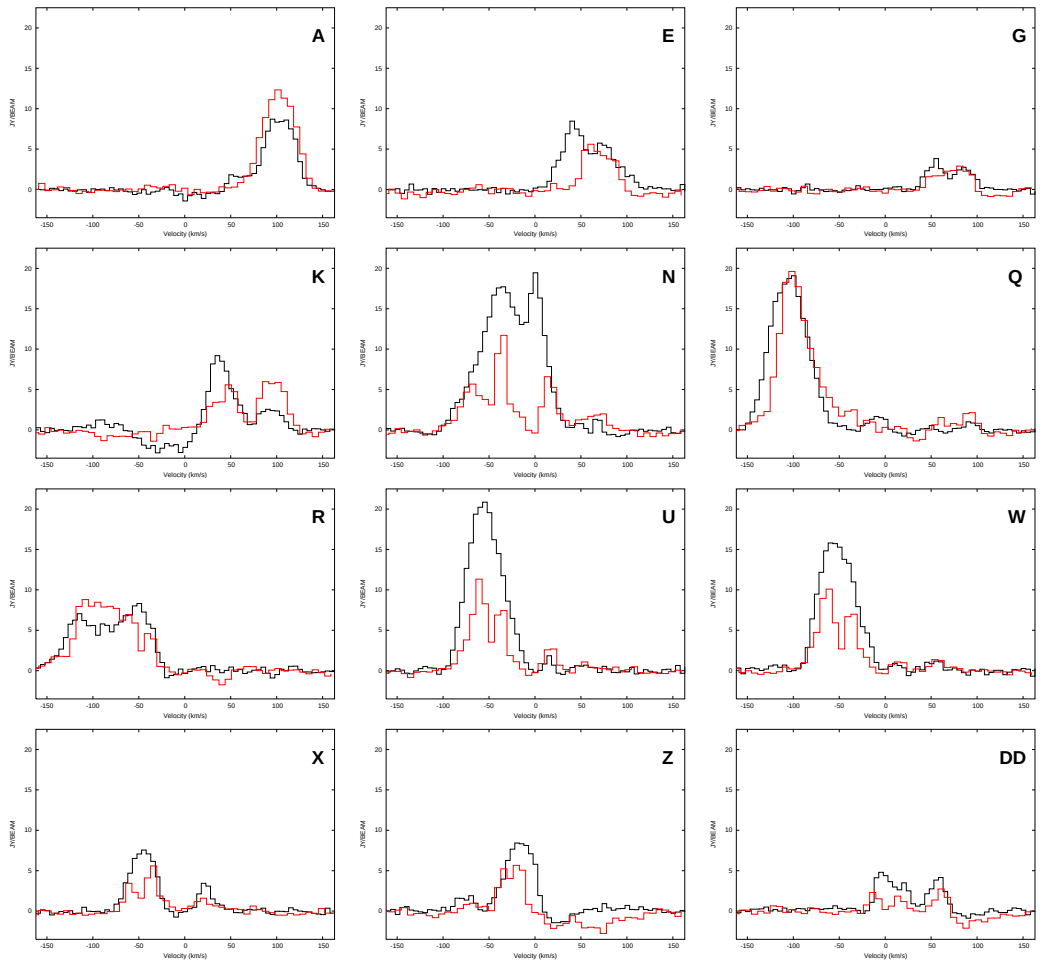

Figure 2.7: HCN(4-3) spectra (black contours) overplotted to HCN(1-0) spectra (red contours) from Christopher et al. (2005) at the locations of various clumps in figure 2.4 (HCN(1-0) scaled up by a factor of 10 to fit on the plot). HCN(4-3) and HCN(1-0) convolved to the same resolution.

We overplot the spectra at the locations of various clumps along the CND for HCN(4-3) and HCN(1-0) from Christopher et al. (2005) (figure 2.7, convolved to the same resolution). We confirm that HCN(1-0) suffers from strong self-absorption, a problem especially noticeable in clumps K, N, U, X and W. Clump N in both transitions seems affected, but HCN(1-0) suffers a much more dramatic "dip" than

HCN(4-3). The actual velocity at which the absorption affects the HCN(1-0) line (~ 0 km s^{-1}, produced by a well known cold cloud complex, the "local gas"; Güsten et al. (1987)) is slightly different from the velocity at which we find the dip in the HCN(4-3) spectrum. Also, the nearby clump K shows a similarly non-gaussian profile, but the rest of the clumps are mostly unaffected. Therefore, HCN(4-3) is likely not affected by absorption (and, if it is, not enough to explain the line profiles), but by the lack of short-spacings, a problem that can be solved by combining the interferometric data with single-dish data. HCN(1-0) could be missing extended emission as well, since the OVRO data have not been combined with single-dish data. Therefore, both transitions are likely affected by the short-spacings problem, but only in the case of (1-0) the self-absorption seems worrisome.

The ratio of both transitions (figure 2.8, where the HCN(1-0) contours have been overplotted to better explain the ratio) confirms that the southern part of the CND is more highly excited than the northern part. We have calculated the ratio using only the points with flux greater than or equal to 3σ, and in the case where the flux was lower, we have taken 3σ as the minimum value. The reasoning behind this treatment of the data was to assess the properties of the northern part of the CND. From figure 2.6 we can observe that the emission from HCN(4-3) in the northern lobe is fairly extended. Since no emission from HCN(1-0) was observed in that same location, the ratio cannot be calculated due to the clipping of the (1-0) map. Comparing the more excited molecular gas closer to the center with the less excited gas in the northern part of the CND would not have been possible. We have, however, not applied the same rule to the absorption features, leaving them blank, thus the void at the position of Sgr A*. The overplotting of the HCN(1-0) integrated emission map in figure 2.8 allows us to observe that, even though in some parts of the northern region of the CND the ratio is high, those correspond to the peripheral regions where the HCN(1-0) flux value has been artificially increased. Where both HCN(1-0) and HCN(4-3) have been detected, for example the *northeast lobe*, the value of the ratio is one of the lowest values along the CND. The ratio map therefore shows the *southern extension* as a whole, to be more excited that any other part of the CND. The large ratios in other parts of the CND, as in the *southwest lobe*, are interspersed among regions with smaller ratios, while the whole structure defined as the *southern extension* is seen at large ratios. Although all of the southern part of the CND is really affected by self-absorption (figure 2.7), this is an interesting result since it suggests that the *southern extension* is formed in its entirety by more excited gas than other parts of the CND. The question arises, then, why is the southeastern part of the CND more excited? What is the heating mechanism? Shocks? Radiation? We will address these questions later, once another important piece of information is presented. At the same time, the ratio map, especially in the northern part of the CND, suggests that the ratio increases as the gas approaches the center, i.e. the inner part of the CND is more excited than the outer part. Harris et al. (1985) suggested that the UV radiation from the nuclear cluster (which is located

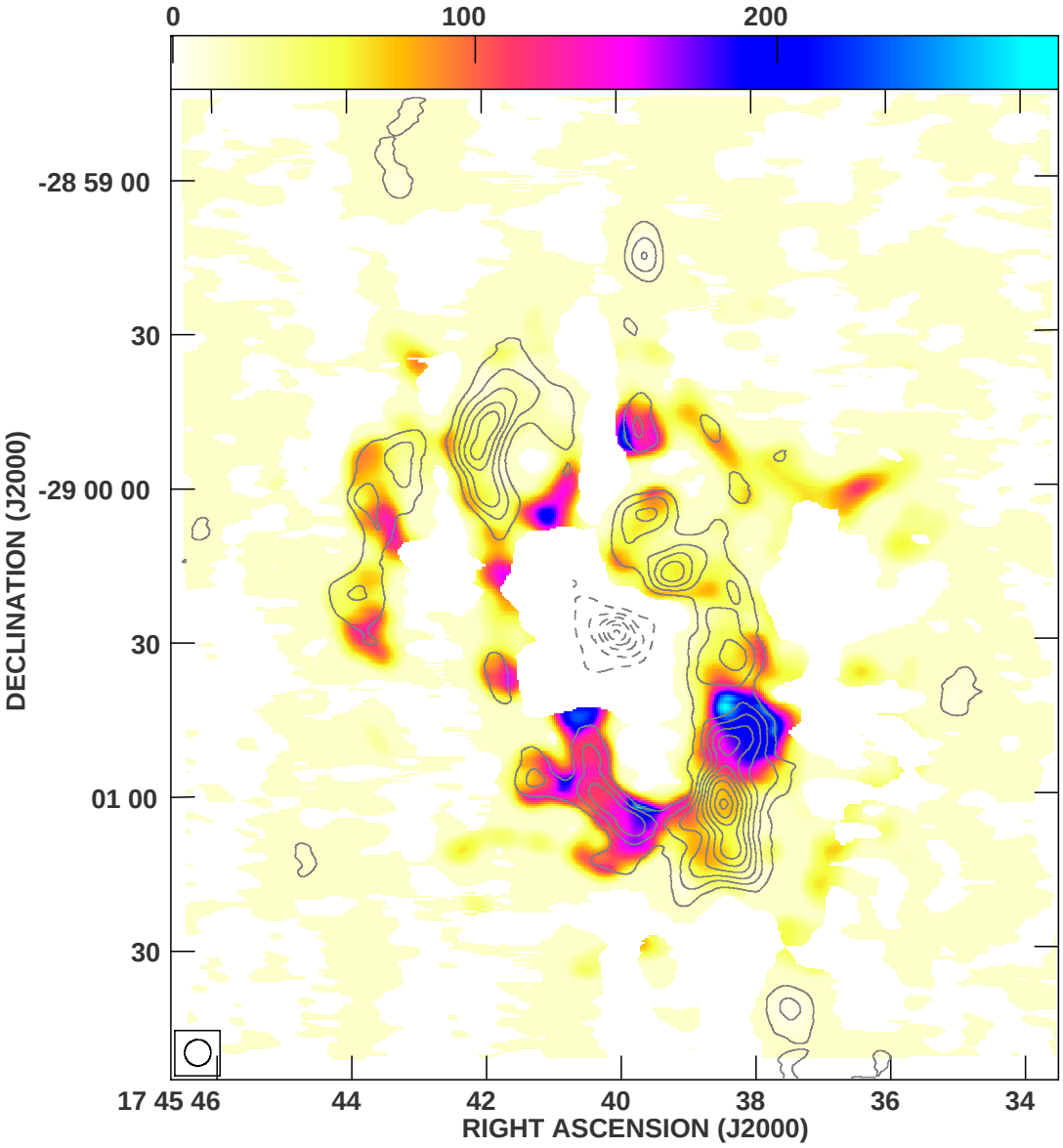

Figure 2.8: Ratio of HCN(4-3) and HCN(1-0) integrated intensities in color-scale. HCN(1-0) integrated intensity in contours. HCN(1-0) data from Christopher et al. (2005). Emission contour levels (solid lines) are in steps of 10σ, from -10σ to -60σ (-5 Jy beam^{-1} km s^{-1} to -30 Jy beam^{-1} km s^{-1}). Absorption contour levels (dashed lines) are in steps of 3σ, from 3σ to 24σ, except for the highest contour level, at 26σ (1.5 Jy beam^{-1} km s^{-1} to 13 Jy beam^{-1} km s^{-1}).

in a cavity void of dust, and therefore transparent to the UV radiation) could be responsible for the heating of the molecular gas composing the CND. The inner edge of the molecular ring would be heated by this radiation, but as the distance from the center increases, the radiation starts to be absorbed by the dust also composing

the ring and the outer parts of the CND would be less affected by this radiation. Finally, it is interesting to remark that the location of clump E, where we found a broad double-peak profile (figures 2.4 and 2.7) shows a large ratio value. This result suggests that clump E is suffering a higher level of excitation than the surrounding environment. The interaction with the northern arm of the minispiral may be a possible mechanism. A detailed kinematic study of the velocity distribution in the minispiral is needed to fully elucidate this situation, possibly.

When comparing the HCN(4-3) emission map with emission maps produced by NH_3 ((3,3) and (6,6), McGary et al. (2001) and Herrnstein & Ho (2002), respectively) we can gain a better understanding of the spatial distribution of the high-density molecular gas in the inner 2 pc of the Galactic center. NH_3 has a lower critical density (10^5 cm^{-3}) as compared to HCN, but traces gas at higher temperatures. Both NH_3(3,3) and (6,6) have remarkably different distributions in the central region of the Milky Way as shown by McGary et al. (2001) and Herrnstein & Ho (2002, 2005).

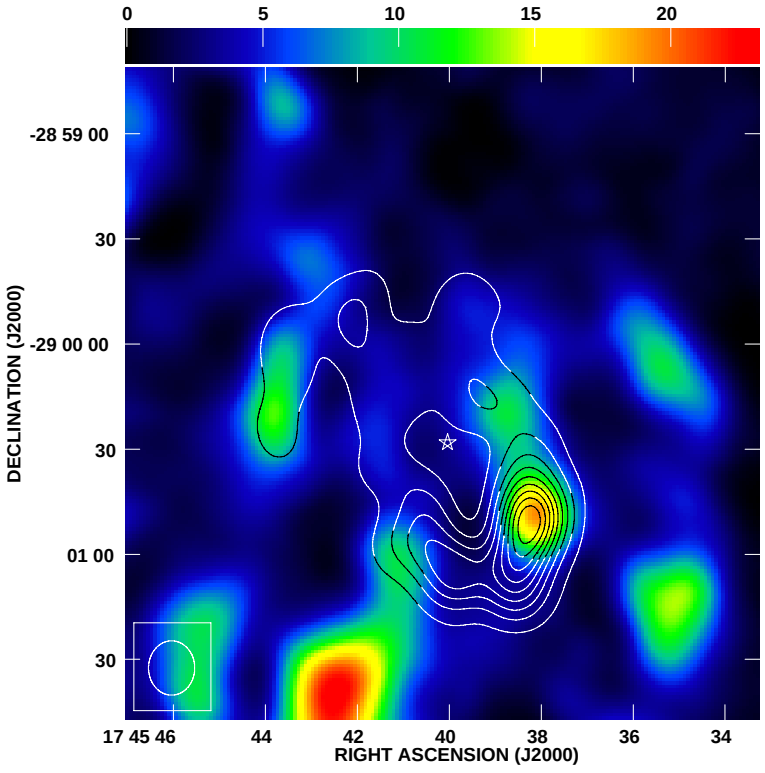

Figure 2.9: HCN(4-3) integrated intensity in contours. NH_3(3,3) integrated intensity in false color-scale from McGary et al. (2001). The HCN(4-3) image has been smoothed to match the resolution of the NH_3 image. Contour levels are are in steps of 10% of the intensity peak, from 1.8×10^2 to 16.2×10^2 Jy beam^{-1} km s^{-1}. The false color-scale is in Jy beam^{-1} km s^{-1}. Sgr A* is marked with a star.

A comparison of HCN(4-3) to NH_3(3,3) (figure 2.9; HCN(4-3) smoothed to match the NH_3(3,3) resolution) shows that the emission distributions from these two molecular lines are poorly correlated. However, both lines trace the western side of the CND and show the strongest peak along the CND at the same position on the *southwest lobe*. HCN(4-3) and NH_3(3,3) emission coincide in the *eastern arm* as well. It is worth noting that the *southern streamer* as traced by NH_3(3,3) (at $\alpha_{J2000.0} = 17^h45^m43^s$ and $\delta_{J2000.0}$ = -29°01′40″) seems to connect to the eastern side of the CND as traced by HCN(4-3). Herrnstein & Ho (2005) reported that no kinematic connection could be made between the *southern streamer* and the CND, but at the same time, it was clear that there was a change in the NH_3(3,3) emission when (at least in projection) it reached the CND. Therefore, the spatial alignment at the CND might only be a projection effect along the line of sight, but a physical connection could not be completely ruled out because of the resolution of the NH_3(3,3) data. We do indeed observe the same trend, the gas traced by both NH_3(3,3) and HCN(4-3) in the eastern part do not overlap, but it seems that the emission from NH_3(3,3) does become weaker in the vicinity of the CND. However, we need more information to proceed with a kinematic study and try to elucidate whether there is a connection between the *southern streamer* and the CND.

The comparison of HCN(4-3) and NH_3(6,6) (figure 2.10) shows a good correspondence in the eastern and northern parts of the CND, and even in the *northeast arm*. However, we can see that NH_3(6,6) is detected inside the central cavity of the CND, apparently approaching Sgr A*, while HCN(4-3) is only detected along the CND. This result suggests that the molecular gas that composes the CND is in general colder and maybe denser than the gas that is located inside of the cavity.

An interesting comparison can be made when overplotting the HCN(4-3)/HCN(1-0) ratio and the NH_3(6,6) integrated emission (figure 2.11). We observe that the southeastern part of the CND is located south of the strongest peak detected in NH_3(6,6). It looks like the material traced by NH_3(6,6) is "following" the path marked by the ratio towards Sgr A*. Since the large value of the ratio in the southeastern part of the CND indicates the presence of a larger amount of highly-excited material than of low-excited material, it means that the majority of the molecular gas in that region is warmer. Because NH_3(6,6) traces very warm gas and it penetrates from the eastern side of the CND towards the supermassive black hole, the southeastern side of the CND could be becoming warmer as it flows northwest, towards Sgr A*.

Interestingly enough, at the same location where the gas traced by NH_3(6,6) heads for Sgr A*, the value of the ratio changes radically, as if suddenly the level of excitation in the gas tracing the CND drops. At that location HCN(1-0) could be slightly affected by self-absorption (spectrum Z in figure 2.7), but the very low value of the ratio indicates that the amount of HCN(4-3) is also low, otherwise the ratio would have been large. The question remains as to why the material is

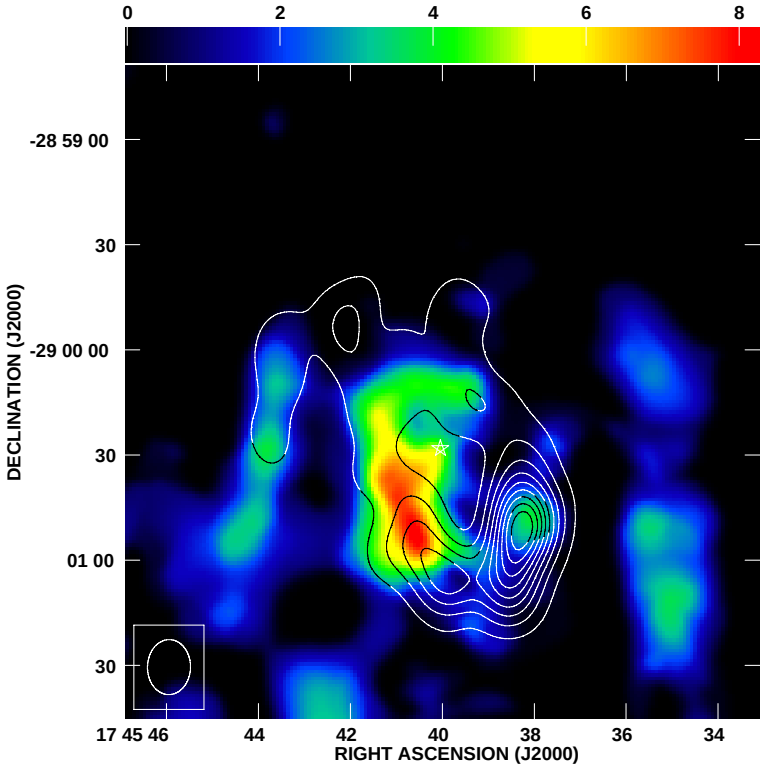

Figure 2.10: HCN(4-3) integrated intensity in contours. NH_3(6,6) integrated intensity in false color-scale from Herrnstein & Ho (2002). The HCN(4-3) image has been smoothed to match the resolution of the NH_3 image. Contour levels are in steps of 10% of the intensity peak, from 1.8×10^2 to 16.2×10^2 Jy beam^{-1} km s^{-1}. The false color-scale is in Jy beam^{-1} km s^{-1}. Sgr A* is marked with a star.

more highly excited precisely in the *southern extension*. When plotting the HCN(4-3)/HCN(1-0) ratio with the NH_3(3,3) integrated intensity map from McGary et al. (2001) (figure 2.12), we observe that the region where the *southern streamer* seems to reach the CND coincides with the location of the northernmost part of the high ratio, where NH_3(6,6) becomes stronger before heading northwest. Consequently, in terms of projection, there is a location in the southeastern part of the CND where the *southern streamer* traced by NH_3(3,3), the strongest peak in the NH_3(6,6) emission and the edge of the high-ratio area all coincide. Could it be that the material from the *southern streamer* is "pushing" the CND gas towards the supermassive black hole and at that same position the gas becomes so highly excited that HCN(4-3) is no longer excited enough, i.e., a higher HCN transition will be needed to trace the infalling gas? To prove this statement we would need to make a kinematic study of the different tracers in the southeastern part of the CND (HCN(4-3), NH_3(3,3) and (6,6)) and, in the future, expand the study to more highly-excited transitions of HCN.

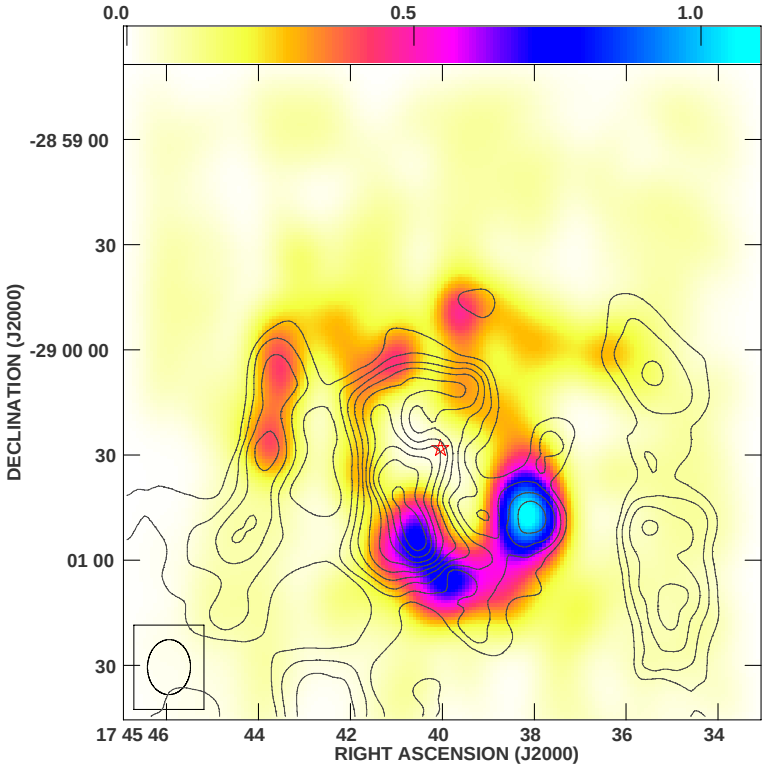

Figure 2.11: Ratio of HCN(4-3) and (1-0) integrated intensities in color-scale. NH_3(6,6) integrated intensity in contours from Herrnstein & Ho (2002). Contour levels are in steps of 10% of the intensity peak, from 8×10^{-1} to 74×10^{-1} Jy beam^{-1} km s^{-1}. Sgr A* is marked with a star.

2.5 CS(7-6)

In our experiment, we set up the correlator to sample the CS(7-6) line at the same time. Because of the locations of the two lines, CS(7-6) had to be placed at the edge of the passband, and the velocity coverage was not as broad for this line, from -150 to 128 km s^{-1}. As previously noted, this CS transition traces gas at even higher temperature than the observed HCN line but at a slightly lower density. We clearly detect and resolve the CS(7-6) emission in the southern part of the CND, but it is much weaker towards the northern part, although it is clearly detected in the *northeast arm* (figure 2.13). This result is consistent with the HCN results in suggesting that the northern and the southern parts of the CND have different excitation levels, since the warmer gas is absent from the north.

Comparing our results on CS(7-6) and HCN(4-3) (figure 2.14) we find that these two molecular lines correlate quite well with each other. The emission peaks coincide in the southern part of the CND, and even in the few places where CS(7-6) is found

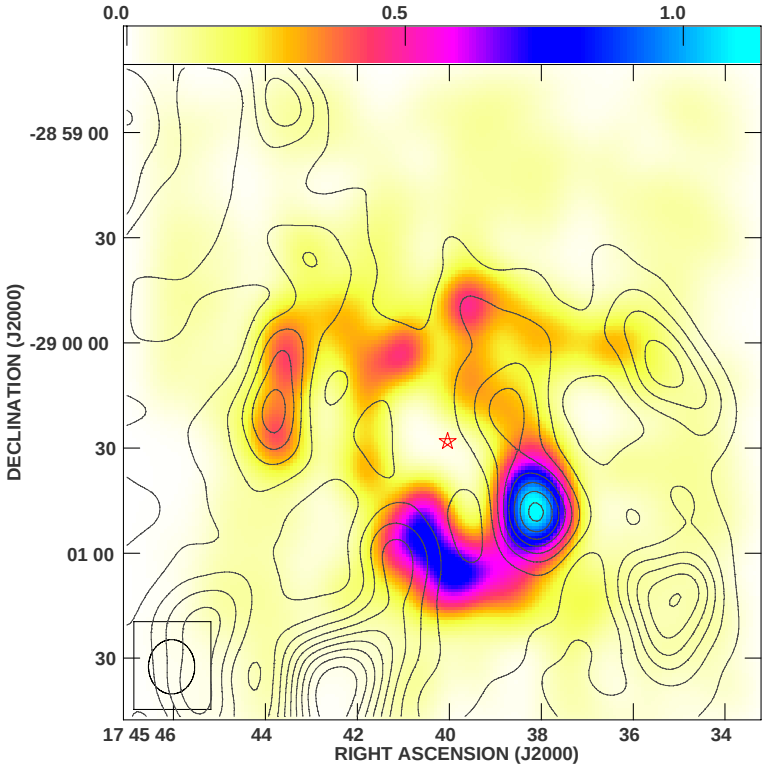

Figure 2.12: Ratio of HCN(4-3) and (1-0) integrated intensities in color-scale. NH_3(3,3) integrated intensity in contours from McGary et al. (2001). Contour levels are in steps of 10% of the intensity peak, from 8×10^{-1} to 74×10^{-1} Jy beam^{-1} km s^{-1}. Sgr A* is marked with a star.

in the northern part of the CND. Also, if we compare the spectra at the same positions (figures 2.4 and 2.15, CS(7-6) spectra plotted in the same velocity range as HCN(4-3) spectra, for the sake of comparison), we observe that both molecular lines have similar line profiles (FWHM $\approx$ 35 km s^{-1}), suggesting that these lines are tracing the same material. However, there are some differences between the two molecular tracers. First of all, we observe that HCN(4-3) is much stronger in the *southern extension* than CS(7-6). While both molecular tracers seem equally strong along the *southwest lobe*, even coinciding in the distribution of the gas, stronger in the northern part of the lobe, at the location of clump N, than in the southern part, CS(7-6) is obviously weaker in the *southern extension*. This result would suggest that the *southern extension* is composed by denser but colder gas than the *southwest lobe*. However, we noted in the previous section that the *southern extension* is highly excited. Also, because of the strong detection of NH_3(6,6) in the northern region of the *southern extension*, towards Sgr A*, we acknowledge the presence of warm material in the area. Therefore, the combination of the result drawn by the previous section and the picture presented by the weak emission of CS(7-6) in the *southern extension*, which traces warmer but less dense material than HCN(4-3), suggests

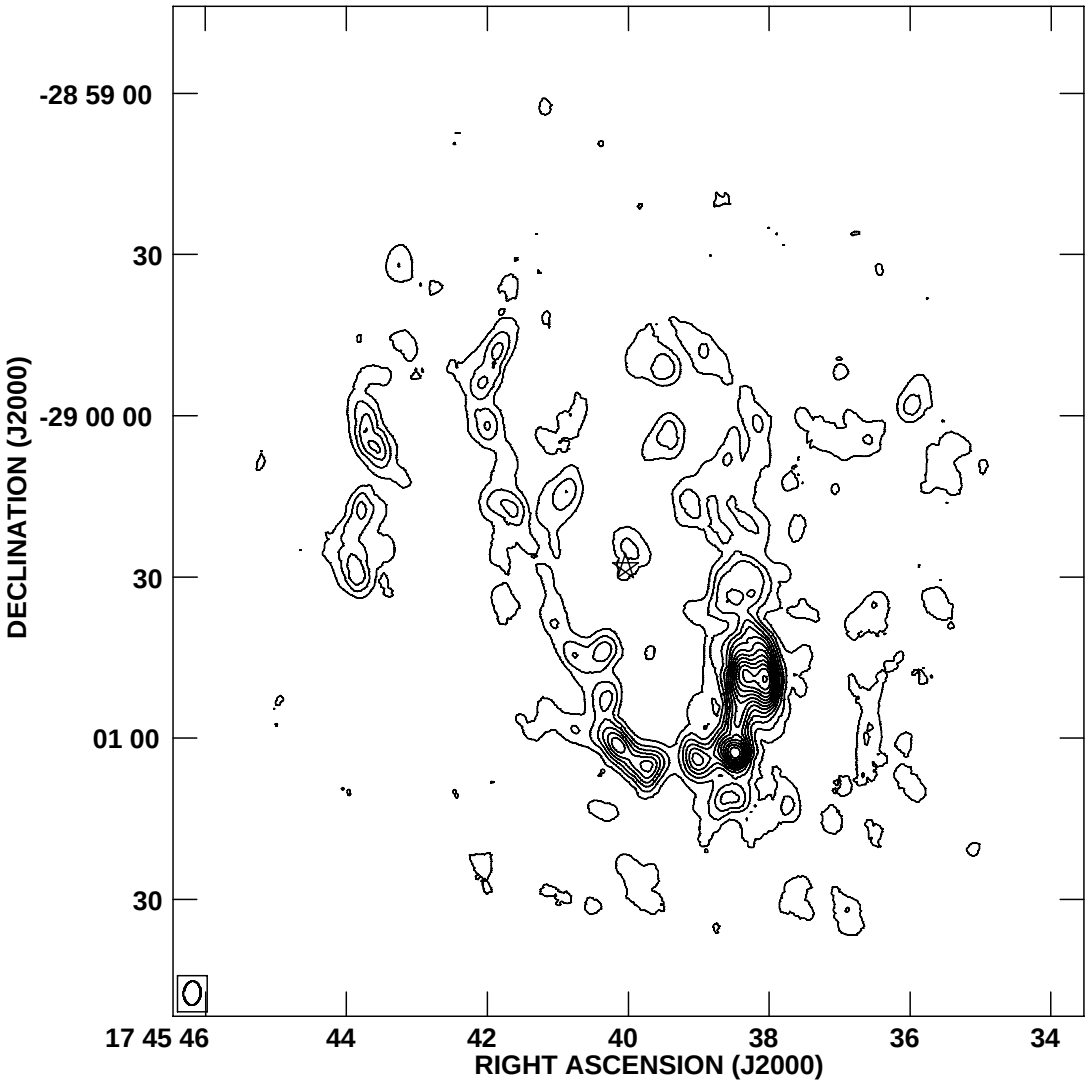

Figure 2.13: CS(7-6) integrated intensity emission map. Contour levels are in steps of 6σ, from 3σ to 69σ, except for the highest contour level, at 76σ ($1.0\times\ 10^1$ to $25.3\times\ 10^1$ Jy beam^{-1} km s^{-1}). Sgr A* is marked with a star.

a complicated morphology in the eastern part of the CND. The gas is denser and colder towards the south, and becomes much more diffuse and warmer heading north. This point will be discussed in detail later.

Another difference between the integrated emission from both molecular lines is that clump E in CS(7-6) does not show a double-peak profile, unlike its counterpart in HCN(4-3). The detection is much weaker, which could account for the lack of coincidence. Spectrum N shows a two-velocity component, consistent with the result in HCN(4-3). The line profile, however, is not as wide. Clump N in the case

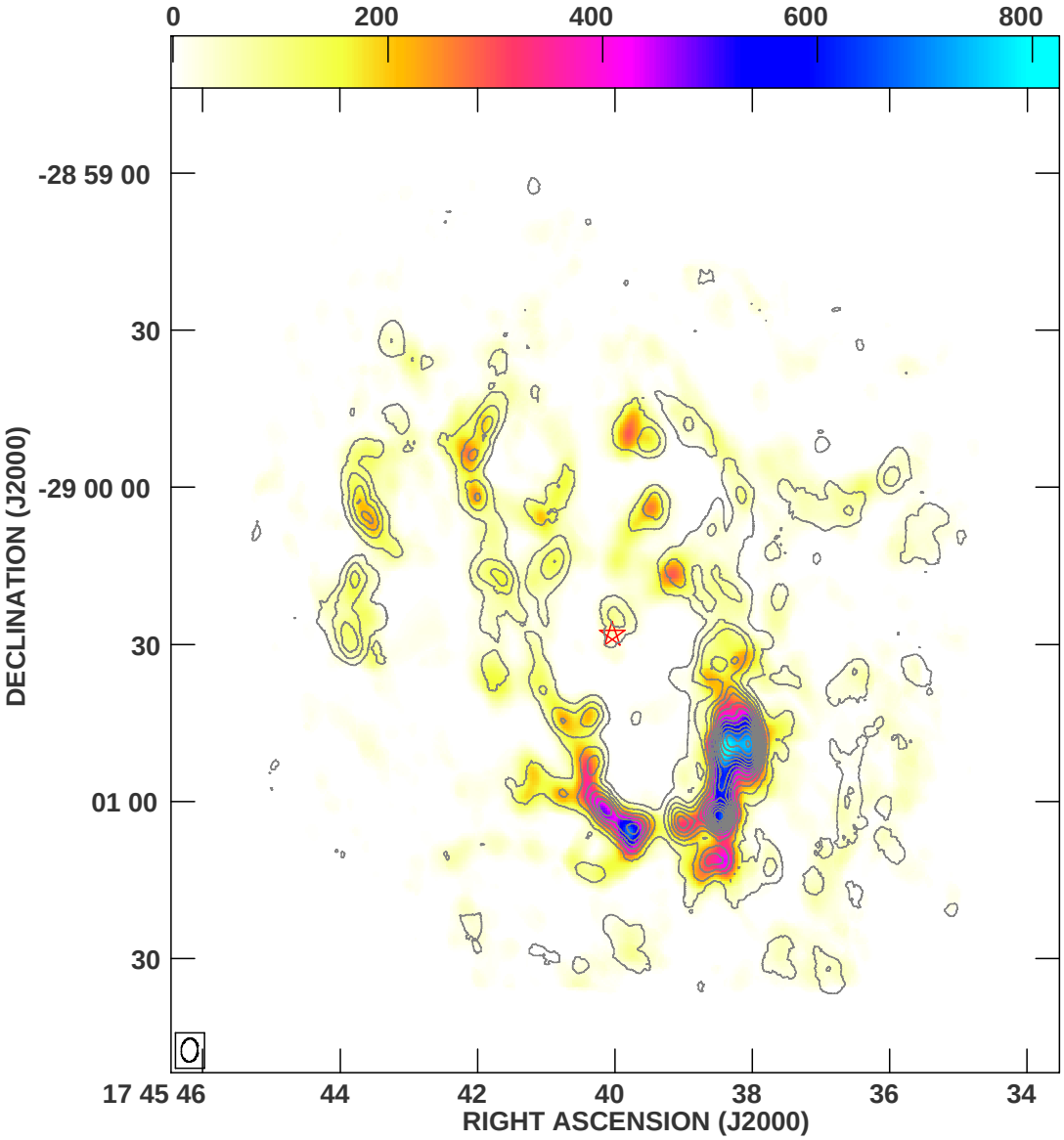

Figure 2.14: CS(7-6) integrated intensity in contours. HCN(4-3) integrated intensity in false color-scale. Contour levels are as in figure 2.13. The false color-scale is in Jy beam^{-1} km s^{-1}. Sgr A* is marked with a star.

of CS(7-6) is located a little further west than in the case of HCN(4-3). Since we have considered the interaction with the minispiral as likely affecting the profile of clump N in HCN(4-3), it could be that the greater distance from clump N in CS(7-6) to Sgr A West and a consequently weaker interaction is responsible for the narrower profile (compare figures 2.20 and 2.5). In order to check this conjecture, we extracted a spectrum closer to the inner side of the CND, 4.4″ east and 0.8″ south of clump N in CS(7-6) (at the location of clump N in HCN(4-3)) and overplotted the

two spectra (figure 2.16). The broadening in the profile of the spectrum closer to the minispiral is remarkable. We conclude that the interaction with the minispiral is likely affecting the line profile. At the same time, the absorption features detected in these spectra can be caused by the negative bowls. When we examine the spectra L and M, taken nearby, we see that the lack of short-spacings, may well affect the spectrum towards clump N.

Clump K presents a very surprising profile, unlike any other. It is clearly redshifted and very narrow, more so than the "70 km s^{-1} cloud", which is barely detected as clump H, but the negative bowls might be seriously affecting it if we pay attention to spectrum L, taken nearby. Nonetheless, the profile is very unexpected and it is probably worth a deeper study. The comparison of the spectrum in the same position in HCN(4-3) (figure 2.17) shows a similar profile. Is once again the presence of the minispiral affecting the line profiles in the *southwest lobe*? Both spectra seem to be suffering from absorption around 50 km s^{-1}, a situation especially noticeable in the HCN(4-3) spectrum. However, this absorption feature is not present anywhere else in the CND.

Clump DD produces a very remarkable spectrum, with two clearly separated peaks. The spectrum at the same position in HCN(4-3) shows this profile as well. There could be some interaction involved in this location as absorption does not seem to be responsible for the "dip" and the large negative bowls detected in the vicinity because of the lack of short-spacings are not so prominent. As we mentioned in the previous section, interaction with the extended bar of the minispiral is the most likely explanation of this broad profile.

Spectrum R shows a double peak profile and, observing the important negative bowls nearby (spectrum T) it is very likely that the short-spacings problem is the cause of this double-peak profile. This problem is probably also affecting clumps FF, U and W, if we compare with spectra T and V. Therefore, as in the case of HCN(4-3), the lack of short-spacings is affecting the data. However, because of the lack of single-dish observations of CS(7-6) in the Galactic center, we cannot calculate the amount of missing flux.

When we compare the CS(7-6) detected emission with the 6 cm continuum emission from Yusef-Zadeh & Morris (1987), we observe that the gap in the CND in the CS(7-6) emission towards the north coincides with the position of the northern arm of the minispiral, with clumps E and F delimiting the gap to the west and clump D to the east (figure 2.20).

The ratio between CS(7-6) and HCN(4-3) (calculated using only the pixels with flux $\geq 3\sigma$) is useful to better understand the distribution of the dense material (figure 2.19). We can observe that the ratio increases towards the inner edge of the CND, especially in the western part. Coincidentally, the western arc of the

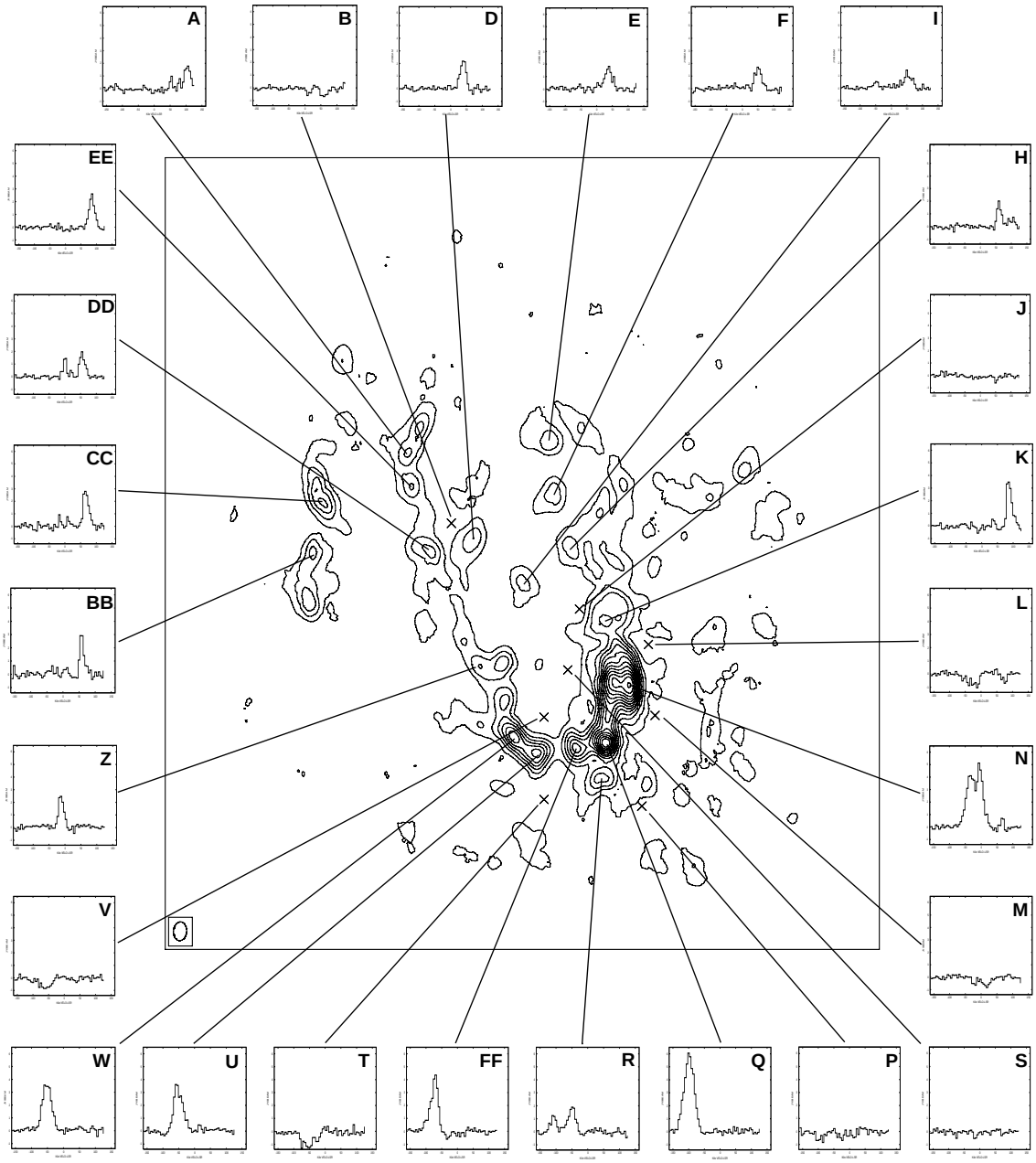

Figure 2.15: CS(7-6) spectra measured at the positions of the different clumps. The clumps have been named as in figure 2.4 (except clump FF) to facilitate the comparison between the two sets of spectra. Wherever the peak was not exactly at the same location the nearest peak has been used.

minispiral is observed in the same region (figure 2.20). Both CS(7-6) and HCN(4-3) have similarly high critical densities, with HCN(4-3) tracing slightly denser gas than CS(7-6), but the temperature traced by CS(7-6) is double the temperature traced by HCN(4-3) (49 K vs. 25 K). We could interpret the ratio distribution as

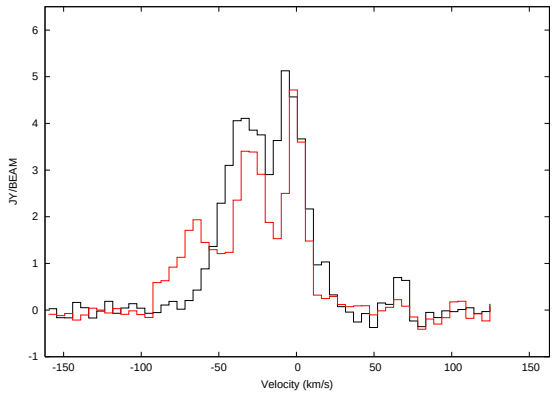

Figure 2.16: Comparison of the spectra at two locations in the *southwest lobe* in CS(7-6). Black contours represent the spectrum in clump N in figure 2.15, while red contours represent the spectrum in a position 4.4″ east and 0.8″ south of clump N (location of clump N in HCN(4-3), figure 2.4).

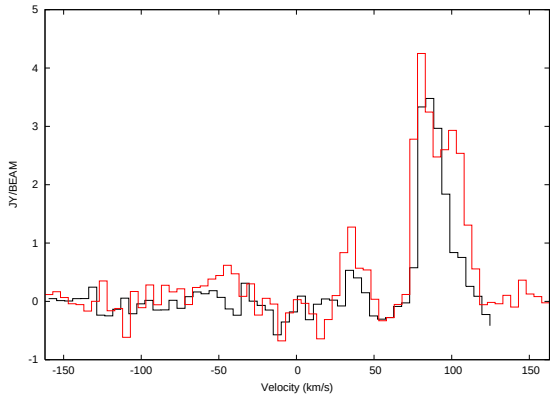

Figure 2.17: Comparison of the spectra at the location of clump K in figure 2.15, in the *southwest lobe*, in CS(7-6) and HCN(4-3). Black contours represent the spectrum at the location of clump K in CS(7-6), while red contours represent the spectrum in HCN(4-3).

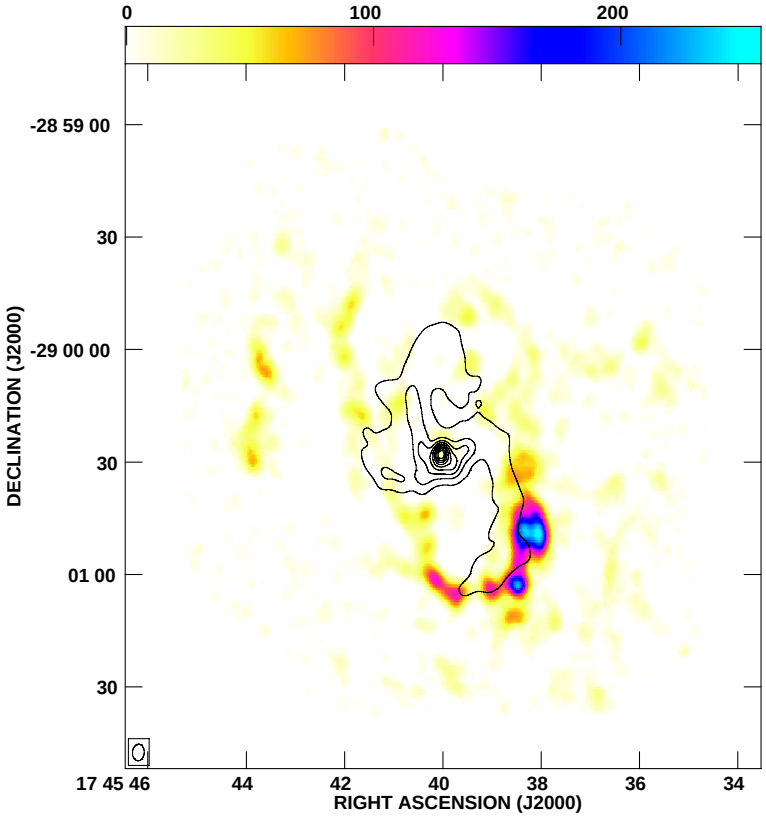

Figure 2.18: 6 cm continuum integrated intensity in contours (from (Yusef-Zadeh & Morris, 1987)). CS(7-6) integrated intensity in false color-scale. Contour levels are as in figure 2.5. The false color-scale is in Jy beam^{-1} km s^{-1}.

being ruled mostly by the temperature, although the density should also be a factor. Therefore the molecular gas in the inner side of the ring is likely warmer and could be less dense. As we mentioned before, the temperature increase can be due to the absorption of UV radiation emitted by the nuclear stellar cluster. High-ratio values found to the west, outside of the CND, can also be related to the presence of higher-temperature gas, as the *western streamer* is very clearly detected in NH_3(3,3) (tracing gas at $\sim$ 125 K).

The comparison of CS(7-6) and NH_3(3,3)) (figure 2.21, CS(7-6) smoothed to match the NH_3 resolution, NH_3(3,3) data from McGary et al. (2001)) shows that both molecular tracers coincide at the location of the strongest peak within the CND (as was also noted regarding HCN(4-3)) and the *northeast arm*. However, the coincidences stop there, with CS(7-6) and NH_3(3,3) having in general very different distributions in the region observed in both tracers. The NH_3(3,3) map by McGary et al. (2001) is much larger than the CS(7-6) map, and it is not represented here in its entirety. The correlation between the high-ratio values that we found previously west of the CND and the *western streamer* cannot be checked in this figure because

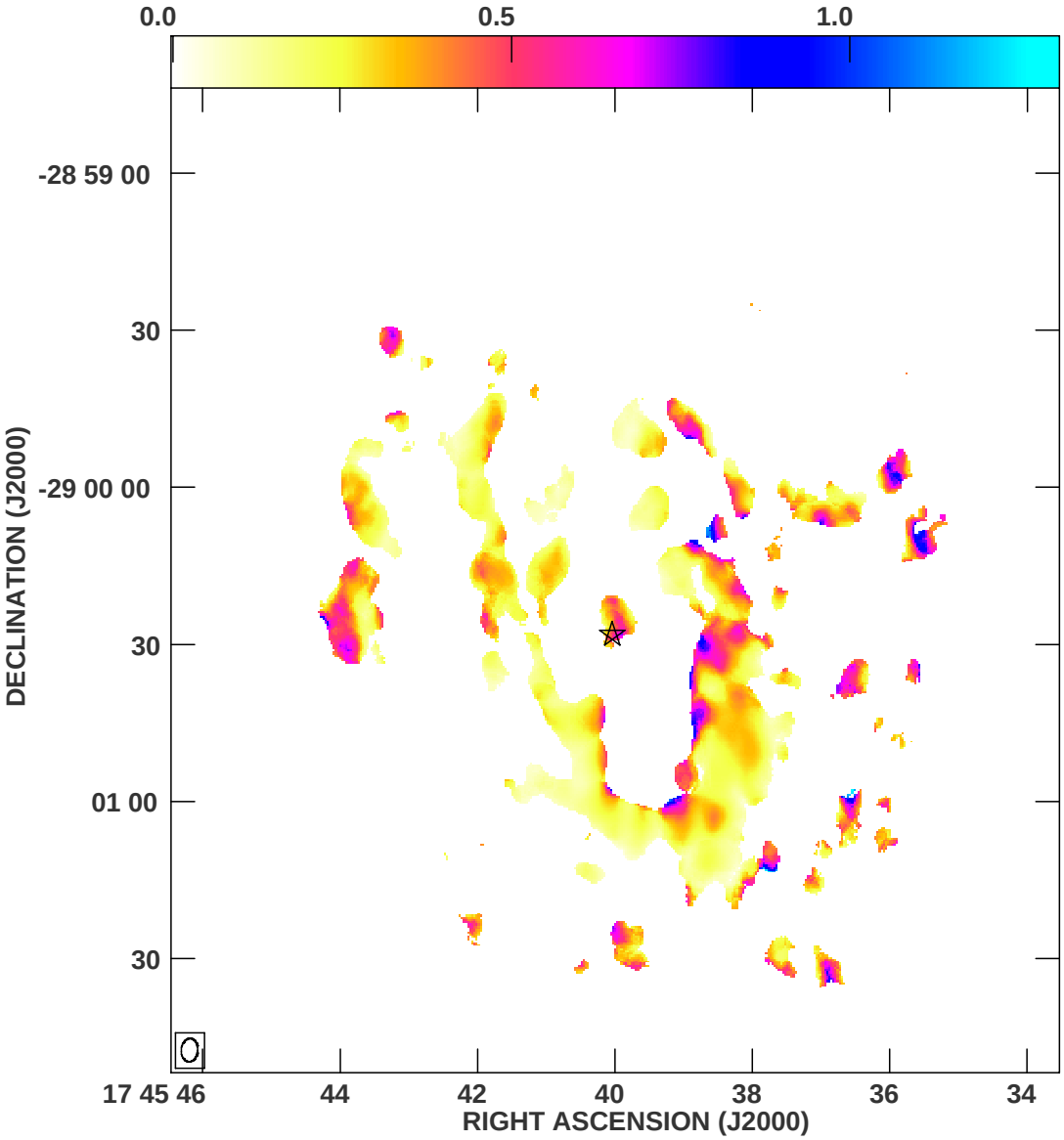

Figure 2.19: Ratio of CS(7-6) and HCN(4-3) integrated intensities. Sgr A* is marked with a star.

of the lower resolution of the NH_3(3,3) data, and the small clumps detected in CS(7-6) have been smoothed out.

When comparing CS(7-6) and NH_3(6,6) we observe that the eastern part of the CND and the *eastern arm* are the only regions where both molecular tracers overlap and are well correlated (figure 2.22). The comparison is similar to that obtained with HCN(4-3) and NH_3(6,6), except for the northern part of the CND, which is barely detected in CS(7-6). Once again, we note that NH_3(6,6) is detected inside the

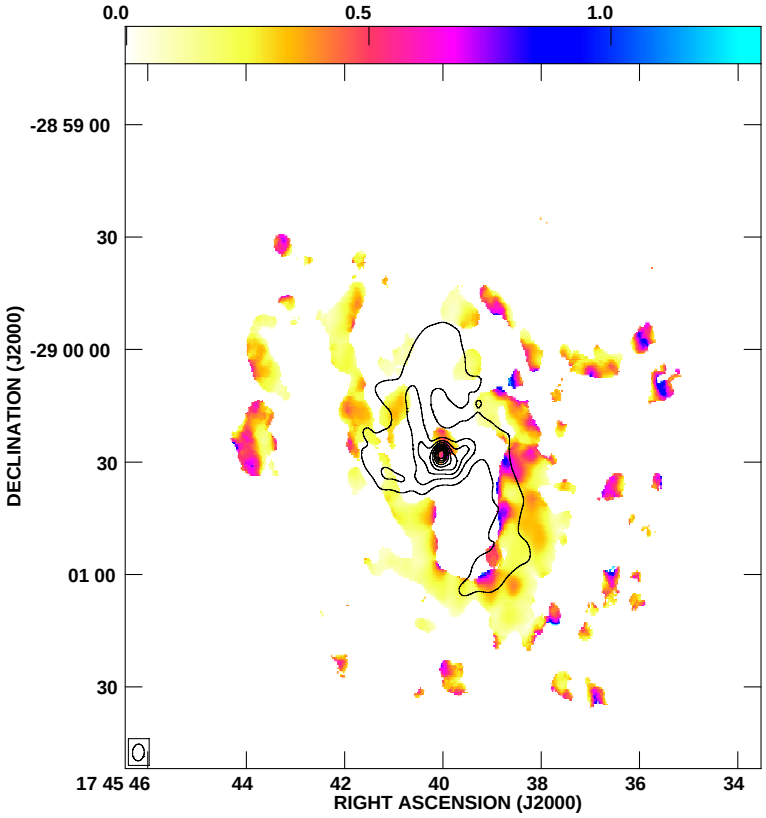

Figure 2.20: 6 cm continuum integrated intensity in contours (from Yusef-Zadeh & Morris (1987)). Ratio of CS(7-6) and HCN(4-3) in color-scale. Contour levels are as in figure 2.5.

central cavity, whereas CS(7-6) is limited to the CND. This result is consistent with the idea that the CND is better traced by higher-density and lower-temperature tracers since only a minimum part of the CND is traced by NH_3, while CS (and HCN) are detected along most of the structure.

Similarly to the way we proceeded in the previous section, we overplot the NH_3(6,6) map and the CS(7-6)/HCN(4-3) ratio (CS(7-6)/HCN(4-3) ratio convolved to the NH_3(6,6) resolution, figure 2.23). Unlike in the case of the HCN(4-3)/HCN(1-0) ratio map, the CS(7-6)/HCN(4-3) ratio does not correlate with the NH_3(6,6) emission. The highest ratio values, as mentioned before, are found in the western side of the CND, overlapping with the western arc of the minispiral (when higher-resolution is utilized since the NH_3(6,6) resolution is not sufficient to observe such details). If the CS(7-6)/HCN(4-3) ratio is tracing the region with the highest temperature-lowest density combination, then the western part of the CND is either warmer or less dense or both. Since NH_3(6,6) is detected more strongly in the eastern part of the CND, it indicates the presence of high-temperature gas in this region of the CND. Therefore, the western part of the CND may be less dense than

the eastern part, and the high-ratio could be in this case a sign of lower density instead of higher temperature. Naturally, a kinematic study would be necessary to characterize the relationship between the material traced by NH_3(6,6) and CS(7-6) and HCN(4-3). The Galactic center has been defined as a two-temperature component region (Hüttemeister et al., 1993; Herrnstein & Ho, 2005). Therefore, the material detected by the high-temperature tracers might be unrelated to the material observed in high-density but lower-temperature tracers, thus the need for a kinematic study. At the same time, the lack of strong HCN(1-0) emission in the *southern extension*, tracing the same material as HCN(4-3) (figures 2.6 and 2.8), but characterized by a lower temperature and critical density, indicate a higher temperature and density than in the *southwest lobe*. Furthermore, if a transition defined by a lower temperature and critical density, such as HCN(1-0), coincides in its spatial distribution in the southern part of the CND with a transition characterized by a higher-temperature but also lower critical density, CS(7-6) (both of them compared to HCN(4-3)), the *southern extension* will be then denser than the southwestern part of the CND.

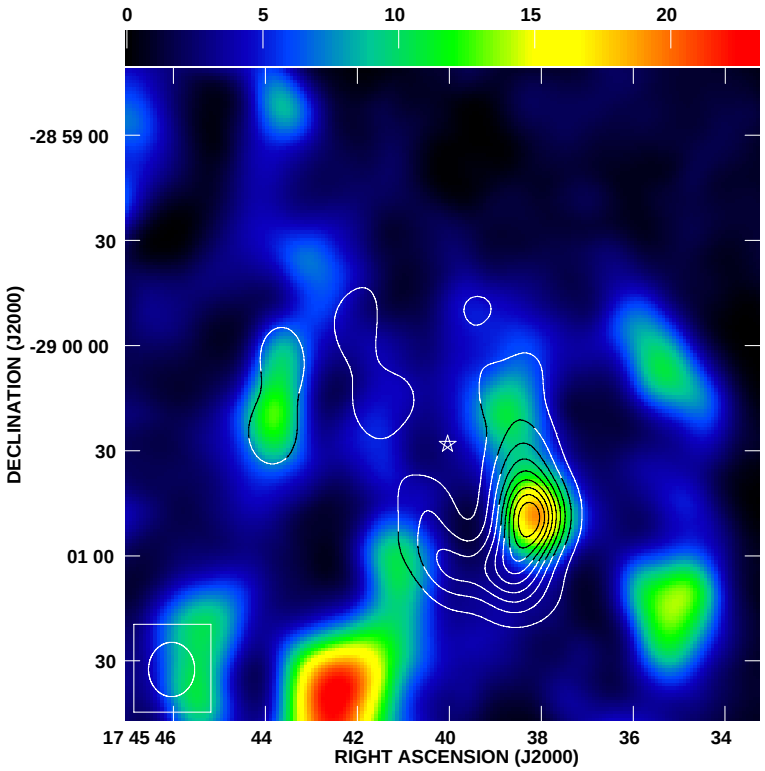

Figure 2.21: CS(7-6) integrated intensity in contours. NH_3(3,3) integrated intensity in false color-scale from McGary et al. (2001). The CS(7-6) image has been smoothed to match the resolution of the NH_3(3,3) image. Contour levels are in steps of 10% of the intensity peak, from 5.1×10^1 to 45.9×10^1 Jy beam^{-1} km s^{-1}. The false color-scale is in Jy beam^{-1} km s^{-1}. Sgr A* is marked with a star.

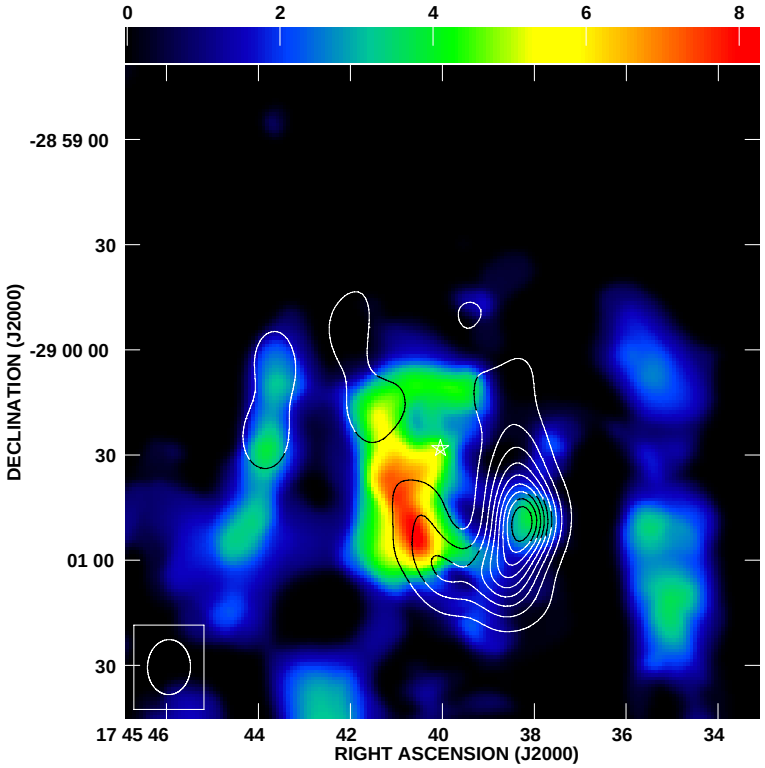

Figure 2.22: CS(7-6) integrated intensity in contours. NH_3(6,6) integrated intensity in false color-scale from Herrnstein & Ho (2002). The CS(7-6) image has been smoothed to match the resolution of the NH_3(6,6) image. Contour levels are in steps of 10% of the intensity peak, from 5.0× 10^1 to 45.0× 10^1 Jy beam^{-1} km s^{-1}. The false color-scale is in Jy beam^{-1} km s^{-1}. Sgr A* is marked with a star.

2.6 Mass estimates

In the previous section we noted the clumpy nature of the CND. As mentioned, Jackson et al. (1993); Shukla et al. (2004) and Christopher et al. (2005) found that the different clumps (or cores) within the CND were dense enough to overcome the tidal shear produced by the central supermassive black hole and therefore the CND might be a more stable structure than previously thought (Güsten et al., 1987). For our results, we use the Virial calculation to estimate the required masses and densities for a clump to be stable against tidal shear. We consider then, the clumps to be gravitationally bound against the motions of the gas in the clump, with uniform density and where the optical depths do not play a significant role in line-broadening (Rohlfs & Wilson, 2000).

$$M \;=\; 250 \left(\frac{\Delta v_{1/2}}{km\ s^{-1}} \right)^2 \left(\frac{R}{pc} \right) (M_\odot), \tag{2.1}$$

where $\Delta v_{1/2}$ is the FWHM velocity linewidth and R is the radius of the clump.

The results are displayed in tables 2.1 and 2.2. Table 2.1 shows the masses measured for the clumps marked in figure 2.2 and table 2.2 displays the results for the clumps in figure 2.13.

The virial masses calculated by Christopher et al. (2005) range from 2×10^3 to 89×10^3 $M_\odot$, while the results obtained by Shukla et al. (2004) are slightly smaller (3×10^3 to 45×10^3 $M_\odot$). Our measurements are similar, although a little bit higher than these previous results (4×10^3 to 595×10^3 $M_\odot$). We have not calculated the masses for all the clumps due to some difficult non-gaussian profiles (like clump R), that prevented us from being able to calculate a linewidth. The mean virial density of the clump, assuming spherical symmetry, can be calculated with:

$$\overline{\rho} \;=\; \frac{3M}{4\pi R^3} \tag{2.2}$$

Therefore, the internal virial density of the clump is:

$$n_{H_2} \;=\; \frac{3M}{4\pi R^3 m_{H_2}} \tag{2.3}$$

The critical density for a clump to survive the tidal shear from a 4×10^6 $M_\odot$ black hole is calculated using the model from Vollmer & Duschl (2000), which assumes the mass distribution in the inner region of the Milky Way to be described by a spherically symmetric approximation:

$$M \;=\; 4 \;\times\; 10^6 + 1.6 \;\times\; 10^6 (\frac{R}{pc})^{1.25} (M_\odot), \tag{2.4}$$

where R is the radius from the center of the Galaxy.

The critical density for a clump to be tidally stable is then:

$$n_{H_2} \;=\; 2.87 \;\times\; 10^7 [(\frac{R}{pc})^{-3} + 0.4 (\frac{R}{pc})^{-1.75}] (cm^{-3}) \tag{2.5}$$

For a 1.5 pc distance, using equation 2.5, we can calculate the critical density to be 1.4×10^7 cm^{-3}. Therefore, we can conclude that the clumps we have detected

using both HCN(4-3) and CS(7-6) are tidally stable, as it can been seen in tables 2.1 and 2.2.

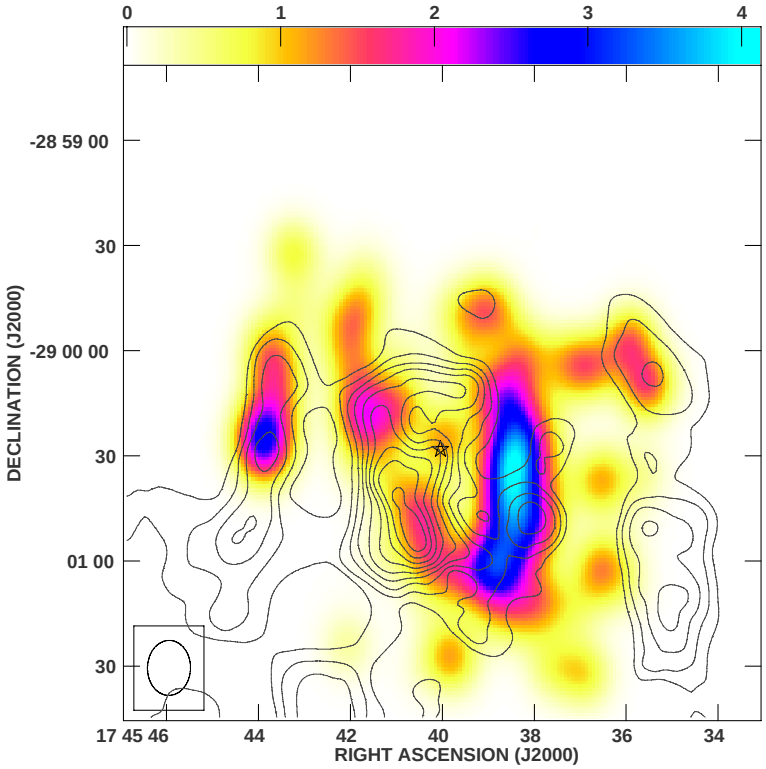

Figure 2.23: Ratio of CS(7-6) and HCN(4-3) integrated intensities in color-scale. NH_3(6,6) integrated intensity in contours from Herrnstein & Ho (2002). Contour levels are in steps of 10% of the intensity peak, from 8×10^{-1} to 74×10^{-1} Jy beam^{-1} km s^{-1}. Sgr A* is marked with a star.

Sanders (1998) reported that the total ionized gas of the minispiral is 10^2 $M_\odot$, and Jackson et al. (1993) measured a neutral gas mass in the northern arm of the minispiral of 3×10^2 $M_\odot$. We can then approximate the minispiral to be composed by a total mass of $\sim 4 \times 10^2$ $M_\odot$. At the same time, kinematic models by Sanders (1998), using an infalling gas velocity of half the rotation velocity (mentioned previously as 110 km s^{-1}), were able to explain the majority of the characteristics of the minispiral. Therefore, the infalling time should be $\sim 3 \times 10^4$ yr. Inflow models support the idea of the minispiral as being formed by a cloud that lost angular momentum, probably due to cloud-to-cloud collisions and then fell towards the center. While infalling, the UV radiation from the nuclear stellar cluster dissociated the molecular gas and later ionized the neutral atomic gas (Jackson et al., 1993). Consequently, if the material composing Sgr A West comes directly from the CND, which has a total molecular mass of 1.3×10^6 $M_\odot$ (calculated with the HCN(4-3) results), and the current mass of the minispiral takes 3×10^4 yr to reach the center, if a mere 10% of the CND is stripped off and becomes part of the minispiral (as Christopher

et al. (2005) considered), the lifetime of the CND is $\sim 9 \times 10^6$ yr, much longer that its rotation period (8×10^4 yr). Therefore, the CND is not a transient structure, since the amount of time needed for the CND to disappear "swallowed" by the inner cavity is longer than the amount of time needed to circle it. However, Herrnstein & Ho (2002) found the molecular gas approaching Sgr A*, as traced by $NH_3(6,6)$, not to follow the minispiral path. Consequently, the previous lifetime value can be an overestimation, since not all the molecular gas approaching the dynamical center of the Milky Way is contained in the minispiral. Finally, recent studies by Marrone et al. (2007) showed the accretion rate of Sgr A* to be between 2×10^{-9} and 2×10^{-7} $M_\odot$ yr^{-1}. If the infalling rate is 1.5×10^{-2} (considering for now only the material confined in Sgr A West), there is clearly a surplus of material inside the cavity that it is not accreting into the black hole. The remaining material could be undergoing star formation processes. Krabbe et al. (1991) reported that 10^3 - 10^4 $M_\odot$ in the inner cavity became stars around 10^6 years ago. With the infalling rate that we are considering, an accumulation of 10^4 $M_\odot$ will take $\sim 7 \times 10^5$ yr (and even less if we consider the material traced by $NH_3(6,6)$). Therefore, the material infalling towards Sgr A* could be forming stars in the inner cavity, and not only accreting into the black hole.

Table 2.1: Calculated masses for some of the detected peaks in HCN(4-3) marked in figure 2.4 in the Galactic center.

Clump	R (pc)	Δv (km s^{-1})	Virial Mass (10^3 $M_\odot$)	Virial density (10^7 cm^{-3})
A	0.139	38.5	51.39	9.3
C	0.087	28.5	17.63	13.0
E	0.098	55.0	74.16	38.1
F	0.092	40.0	36.85	22.9
H	0.074	21.5	8.57	10.2
I	0.103	36.0	33.31	14.8
K	0.110	29.0	23.18	8.4
N	0.253	97.0	594.88	17.7
Q	0.161	51.0	104.90	11.7
U	0.110	47.0	60.42	22.2
W	0.112	53.5	7.44	27.4
X	0.111	36.5	37.21	13.0
Z	0.146	49.0	87.64	13.6
AA	0.145	49.5	89.02	2.9
BB	0.088	17.0	6.35	4.5
CC	0.126	31.5	31.40	7.5
EE	0.083	30.0	6.25	5.3

Table 2.2: Calculated masses for some of the detected peaks in CS(7-6) marked in figure 2.15 in the Galactic center.

Clump	R (pc)	Δv (km s^{-1})	Virial Mass (10^3 M$_\odot$)	Virial density (10^7 cm^{-3})
A	0.066	23.5	9.16	15.1
D	0.113	22.5	14.32	4.8
E	0.080	31.0	19.34	17.9
F	0.093	29.0	19.51	11.7
I	0.083	30.0	18.66	15.8
H	0.064	15.9	4.09	7.5
K	0.151	20.6	16.09	2.2
N	0.183	52.5	126.05	9.9
Q	0.090	38.5	33.51	21.8
U	0.119	33.5	33.28	9.6
W	0.076	35.5	24.17	25.8
Z	0.099	20.0	9.93	4.9
BB	0.083	14.5	4.36	3.7
CC	0.135	21.5	15.58	3.1
EE	0.054	19.8	5.28	16.2
FF	0.077	22.5	9.75	10.3

2.7 Summary

We have successfully detected HCN(4-3) and CS(7-6) emission within 2 pc of Sgr A*, effectively tracing the CND. Both high-density molecular tracers are much more abundant in the southern part of the CND. Our results indicate that the northern and the southern parts of the CND have different excitation levels, as well as different densities, with the southern part of the CND warmer and denser than the northern part. Also, comparing our results with those from other high-density, high-temperature molecular tracers, we conclude that the molecular gas forming the CND is denser and colder than the molecular gas inside the inner cavity. More precisely, the southeastern part of the CND is denser than the southwestern part. However, the southeastern part seems to become more diffuse as the material heads northwest, approaching the supermassive black hole, as detected by NH_3(6,6). Also, we have observed that the inner edge of the CND seems more highly-excited that the outer part of the ring, as traced by the ratio of HCN(4-3)/HCN(1-0). Most likely the nuclear stellar cluster is responsible for the excitation of the inner side of the CND.

The emission from both molecular tracers, HCN(4-3) and CS(7-6), appears in clumps, forming a 'necklace-like' structure around CND. The clumps have various

sizes, from $\sim 3''$ to $\sim 13''$. In the case of HCN(4-3), the emission detected from these clumps amounts to 61% of the single-dish flux detected by Marshall et al. (1995). The lack of short-spacings seem to be affecting our results, more so in the southern part of the CND.

However, when smoothing our data to match the resolution of the JCMT results from Marshall et al. (1995), we can easily note the remarkable similarity between the smoothed (to a $15''$ resolution) HCN(4-3) emission map and the HCN(4-3) integrated emission map from Marshall et al. (1995). This result suggests that the extended emission does not greatly contribute to the final result and the molecular gas is mostly concentrated in clumps.

We have detected a correlation between the minispiral and the CND. Line-broadening has been detected in the spectra of the clumps that spatially coincide with the arcs of the minispiral. We have observed this phenomenon in the eastern, western and northern parts of the CND. The western arc of the minispiral and the inner western part of the CND seem to overlap. Also, we have observed that the eastern end of the extended bar of the minispiral spatially coincides, at least in projection, with the location of a clump characterized by a broad spectrum. A similar situation has been observed regarding the northern part of the CND and the northern arm of the minispiral, where line-broadening has also been found in the spectra of the clumps seemingly located at the very end of the northern arm. Furthermore, we have detected a gap in the northern region of the CND, which the northern arm of Sgr A West appears to be traversing.

All these different results suggest that the CND and the minispiral may be physically related. Sgr A West could be gas which has been stripped from the CND. While more detailed kinematics are needed, we detect the influence of the minispiral on the western inner part, the northern part and the eastern part of the CND, where we can see line-broadening in the vicinity of Sgr A West.

Also, we have demonstrated that the study of a higher HCN transition minimizes the self-absorption problem observed in lower transitions (Güsten et al., 1987; Wright et al., 2001; Christopher et al., 2005), therefore providing a much more conclusive result.

Finally, we confirm the stability of the CND based on the density of the clumps, which is large enough for the clumps to overcome the tidal shear produced by the supermassive black hole. Furthermore, the lifetime value of the CND is far longer than the rotation value. This result supports the conclusions of Jackson et al. (1993); Shukla et al. (2004) and Christopher et al. (2005), agreeing that the CND is not a transient structure.

Chapter 3

Hot molecular gas in the nuclear region of IC 342

Hot molecular gas in the nuclear region of IC 342, María Montero-Castaño, Robeson M. Herrnstein and Paul T.P. Ho. *The Astrophysical Journal*, 2006, Vol. 646, Issue 2, pp. 919-928.

3.1 Abstract

We present the first interferometric detection of extragalactic $NH_3(6,6)$ emission in the nearby galaxy IC 342 made using the VLA[1]. The data have a resolution of $7.8'' \times 5.0''$ and trace hot ($T \sim 412\,K$) and dense ($> 10^4\,cm^{-3}$) molecular gas. We have covered a $170'' \times 300''$ area, and detect two very strong line emission peaks, likely associated with the two strongest star formation regions of the central part of the galaxy. We compare these emission peaks to CO (1-0) and (2-1) emission data, which are the most abundant CO transitions and trace spatially extended emission. The $NH_3(6,6)$ emission is also compared to emission data from three high-density, nitrogen-bearing tracers: HNC(1-0), HC_3N(10-9) and N_2H^+(1-0). Our

results suggest that the molecular mass in the nuclear region of IC 342 has at least two different components, a dense and cold component and a less dense and hotter component.

3.2 Introduction

IC 342, a late-type spiral galaxy (Scd), is one of the closest galaxies to the Milky Way, located only ~ 3.3 Mpc away (Saha et al., 2002; Karachentsev, 2005) ($1''$ corresponds to 16 pc). The physical properties of its molecular clouds, its infrared luminosity, and the presence of a nuclear stellar cluster (Hüttemeister et al., 1995; Schulz et al., 2001) make IC 342 similar to the Milky Way in many ways. Because of its proximity to the Galactic equator, IC 342 is a faint optical source. However, it is a very rich source of molecular emission, and has been studied in numerous molecular tracers. Furthermore, IC 342 is nearly face-on, minimizing line broadening due to galactic rotation, thereby maximizing line intensity. This orientation makes IC 342 useful for Milky Way-like studies.

IC 342 has a high concentration of molecular gas within the inner 1 kpc, especially within 250 pc of the nucleus (corrected for a 3.3 Mpc distance; Israel & Baas (2003)). Inflow along a large-scale stellar bar (Schinnerer et al., 2003) has been proposed to explain the large quantity of gas in the nucleus. An S-shaped bar in the molecular gas (the "minispiral"), has been clearly detected in the nuclear region in CO(1-0) (Helfer et al., 2003) as well as in NIR observations (Böker et al., 1997). The minispiral is oriented in the north-south direction, and it is apparently unrelated to the spiral arms located further out in the disk (Lo et al., 1984). The two arms of the minispiral meet in a ring composed of dense gas (Ishizuki et al., 1990; Meier & Turner, 2001). This ring, $\sim 4''$ in radius, surrounds a central stellar cluster that occupies the central 80 pc of the galaxy (Turner & Hurt, 1992; Böker et al., 1997). The central stellar cluster is nonaxisymmetric, with a north-south elongation, which is believed to be caused by the presence of a nuclear stellar bar with a major axis diameter of $\sim 13''$ (Böker et al., 1997). The nuclear bar creates the ringlike structure at $4''$, an Inner Lindblad Resonance (ILR) (Böker et al., 1997). Inside the ring, the abundance decreases for all the molecular tracers studied to date (Meier & Turner, 2005).

Current star formation activity in the nucleus of IC 342 is dominated by two bright HII regions $\sim 4''$ west and east of the nuclear cluster. These star formation regions are ~ 5 Myr old. The central cluster, which is composed of young and massive supergiants, does not show evidence for current star formation (Böker et al., 1997).

High-resolution HCN(1-0) studies by Downes et al. (1992) have shown the presence of five giant molecular clouds (GMCs) in IC 342 (GMCs A, B, C, D, and E). These GMCs have sizes from 20 to 40 pc, masses of $\sim 10^6$ $M_\odot$ and average molecular densities of $\sim 10^4\,cm^{-3}$ (Schulz et al., 2001). Each GMC appears to be composed of multiple small, dense clouds (Meier & Turner, 2001), which have densities of $\sim 10^6\,cm^{-3}$ (Schulz et al., 2001). Downes et al. (1992) have shown that the distribution of GMCs extends close to the nucleus (within a distance of 183 pc, corrected for a 3.3 Mpc distance) and well inside the tidal limit. The region occupied by these GMCs includes both the arms of the minispiral and the ring.

GMCs A, B and C are located in the central ring, whereas GMCs D and E are in the northern arm and southern arm of the minispiral, respectively. GMCs B and C are situated where the arms of the minispiral meet the ring, and may be related to the young star formation regions found there (the two HII regions mentioned above). High-resolution studies of $C^{18}O$ by Meier & Turner (2001) show that GMC B is the warmest GMC in the central region. GMC A is the closest to the nucleus, but it does not show strong star formation. GMC D also does not show strong star formation, although it is located alongside the northern arm where Turner & Hurt (1992) detected large quantities of molecular gas with inward motions. GMC N, as noted by Meier & Turner (2005), is located close to GMCs A and B, in the molecular ring. It has only been detected in nitrogen-bearing molecules.

The GMCs are very warm, with a temperature of 50 to 70 K measured using HCN(1-0) (Downes et al. (1992)). However, more recent CO(2-1) observations by Meier et al. (2000) have shown that most of the gas within the GMCs has a temperature of only 10-20 K. This cool gas is surrounded by much hotter Photon Dominated Regions (PDRs) with temperatures that reach 50 K. The ionization of the PDRs may be produced by the central nuclear cluster, rather than by the HII regions close to GMCs B and C (Meier & Turner, 2005).

The GMCs associated with the nucleus of IC 342 have been the subject of numerous molecular line studies. However, few observations have been made in the rotation inversion transitions of NH_3. NH_3 is a good probe of the physical conditions in molecular clouds for many reasons. The large number of transitions concentrated around ~ 1.3 cm means that multiple ammonia lines can be detected with the same receiver on the same telescope, thereby circumventing cross calibration problems. Moreover, measuring two emission lines allows us to calculate the rotational temperature of the gas (Ho & Martin, 1983). Also, due to its high dipole moment, a density of $\sim 10^4\,cm^{-3}$ is necessary to excite NH_3, making it an excellent high-density gas tracer.

The first detection of extragalactic NH_3 emission was made in IC 342 by Martin & Ho (1979) using the 100m Effelsberg telescope of the Max-Plank-Institut für Radioastronomie. Numerous studies, both with interferometers and single-dish an-

tennas, have been carried out since then in IC 342 (Ho, Martin, & Ruf, 1982; Ho & Martin, 1983; Martin & Ho, 1986; Ho et al., 1990; Mauersberger et al., 2003), as well as in other galaxies (Henkel et al., 2000; Weißet al., 2001; Takano et al., 2002; Beuther et al., 2005; Ott et al., 2005). However, the only previous study of NH_3(6,6) in IC 342 was made by Mauersberger et al. (2003) using the 100m Effelsberg telescope. This study detected the presence of warm gas (>150 K) in the center of IC 342. In particular, they found a high abundance of NH_3(6,6) ($N_{66} = 3.2 \times 10^{12}$ cm^{-2}), which has an excitation energy above ground of 412 K. This study also suggested the presence of multiple components with different temperatures within the beam. However, due to the large beam [38″ for NH_3(6,6)] for these single-dish data, the multiple components could not be separated.

We have conducted a study of NH_3(6,6) using the VLA in order to resolve the structure of the hot dense gas in the nucleus of IC 342. Our interferometric observations produce a much smaller beam ($7.8'' \times 5.0''$), allowing us to separate the emission from different structures present in the nucleus of IC 342. In addition to studying the molecular structure of the IC 342 nuclear region, we also relate our data to the center of the Milky Way. As previously mentioned, IC 342 is a perfect candidate for Milky Way-like studies. Interferometric observations of NH_3(6,6) at the Galactic center. have shown that there is a large concentration of high density hot gas surrounding Sgr A* (Herrnstein & Ho, 2002, 2005). Therefore, the study of the nuclear region of IC 342 is not only important in itself, but it also provides an excellent opportunity to investigate the same processes that take place in our own Galactic center.

3.3 Observations

Observations of NH_3(6,6) (ν = 25.056025 GHz) were made with the NRAO Very Large Array (VLA[5]) in the D configuration on 2003 February 15 and 16. The pointing was centered on $\alpha_{J2000.0} = 03^h46^m48.7^s$, $\delta_{J2000.0} = 68°05'46.7''$. The data consisted of a 25 MHz bandwidth divided into 15 spectral channels with a velocity resolution of 9.3 km s^{-1}. The velocity coverage was from -30 km s^{-1} to +110 km s^{-1}, centered on $v_{LSR} = 40$ km s^{-1}. Channels 1, 14 and 15 were removed from the data because of low sensitivity due to the roll off in the passband response. Channels 2 and 3 were used for continuum subtraction, which was performed in the uv plane, thus resulting in an effective velocity coverage from 0 km s^{-1} to 90 km s^{-1}. The fact that the continuum subtraction has been performed using channels from only one side of the line does not affect the final result since the bandpass was calibrated by observing 0319+415 (3C84).

The data were calibrated using the NRAO Astronomical Imaging Processing System (AIPS). The total on-source integration time was ∼7 hours. The flux calibrator was 0137+331 (3C48) with an assumed flux of 0.99 Jy at 1.3 cm. The phase calibrator was 0228+673, with a measured flux of 1.04 ± 0.01 Jy. We performed phase-only self-calibration to correct for atmospheric fluctuations on short time-scales. The self-calibration was done on the broadband continuum data (the average of the inner 75% of the 25 MHz window), and the results were applied to the line data. Final deconvolution was performed using IMAGR. The overall improvement in RMS noise due to self-calibration was about a factor of 2. The final RMS noise per channel is 0.3 mJy beam^{-1}and the overall achieved RMS sensitivity is 3.6 mJy beam^{-1} km s^{-1}. Natural weighting of the uv data produced an image with a synthesized beam of $7.8'' \times 5.0''$ with a position angle of 64°. The integrated intensity map was produced using the MOMNT task with a minimum flux cutoff of 0.4 mJy. The absolute positional accuracy is limited by phase noise, and is on the order of 1″.

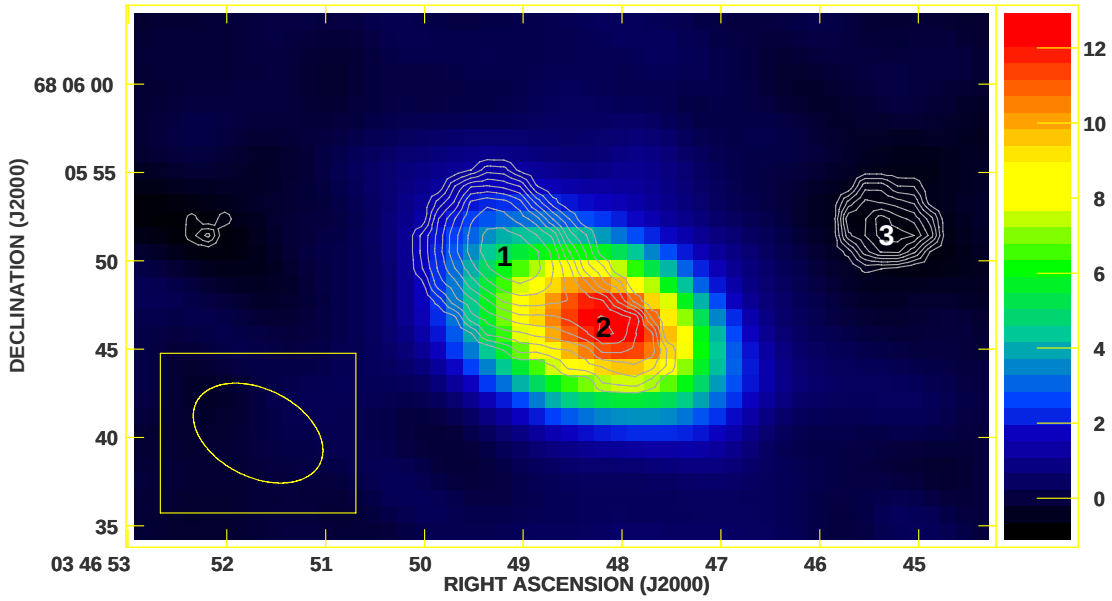

Figure 3.1: NH_3(6,6) integrated intensity map. The contours represent the line emission, while the false-color scale indicates the continuum emission at 1.3 cm. Peak 1 represents the *(6,6) peak*, peak 2 the *continuum peak* and peak 3 the *west peak*. The contour levels are in steps of 10% of the intensity peak, from 5.5 mJy beam km s^{-1} to 49.5 mJy beam km s^{-1}. The RMS is 3.6 mJy beam km s^{-1}, therefore the contour levels in the map are in steps of $\sim 1.5\,\sigma$, from $1.5\,\sigma$ to $13.7\,\sigma$. The false-color scale is in mJy beam^{-1}.

3.4 Results

We detect and resolve the extended NH_3(6,6) emission from IC 342 (figure 3.1). Three line emission peaks are clearly visible in our results, marked by numbers 1-3 on figure 3.1. Peaks 1 and 2 appear to be embedded in a single, extended molecular structure. The third peak, which has not been previously observed in any molecular tracer, is isolated. Comparing the line emission map with the continuum map (in contours and false colors, respectively, in figure 3.1), we find that peak 2 corresponds to the continuum emission peak, which marks the location of a strong heating source as well as the nucleus of IC 342 (Downes et al., 1992). Throughout this paper, peak 1 will be referred to as the *(6,6) peak*, peak 2 as the *continuum peak*, and peak 3 as the *west peak*.

We compared our NH_3(6,6) flux with the single-dish data from Mauersberger et al. (2003). Because the beam size for the 100m Effelsberg telescope is 38", all three of our NH_3(6,6) peaks are well within the Effelsberg beam. From Mauersberger et al. (2003), the single-dish flux is 4.5×10^{-3} Jy beam^{-1}, while the sum of the fluxes detected for the three NH_3*(6,6) peak*s presented in this paper is 4.6×10^{-3} Jy beam^{-1}. Therefore, there is no missing flux, and all emission detected in the single-dish data must originate in clouds with size scales smaller than $\sim 8''$.

Because the relative locations of the NH_3(6,6) emission peaks and the GMCs may provide a clue to the behavior of material near the nucleus of IC 342, we overlay the positions of the 6 GMCs on our NH_3(6,6) map (GMCs A, B, C, D, E and N in figure 3.2). We plot the spectra at the positions of our three peaks and the 6 GMCs. For comparison, we also plot spectra taken from three random, emission-free positions (figure 3.3).

In order to investigate the physical conditions in the NH_3(6,6) clouds that we observe, we also compare our NH_3(6,6) map to HC_3N(10-9), HNC(1-0), and N_2H^+(1-0) (Meier & Turner, 2005) (Figs. 3.4, 3.5 and 3.6, respectively), CO(2-1) (Schinnerer et al., 2003) (figure 3.7) and CO(1-0) (Helfer et al., 2003) (figure 3.8). We have chosen these five molecular lines for different reasons. HNC, HC_3N and N_2H^+ have proved to be high-density tracers. Moreover, these molecules are nitrogen bearing like NH_3. Comparing the results from HC_3N, HNC and N_2H^+ with NH_3, we can determine whether GMC N is also an emission peak in NH_3.

CO is second only to H_2 in terms of abundance in the interstellar medium. However, H_2 cannot be directly studied because of the lack of a dipole moment. We compare our NH_3(6,6) data to CO(2-1) and (1-0), which, because of their low excitation requirements, are the molecular tracers that detect more extended emission in IC 342. Most of the CO(1-0) emission comes from the extended ridges of the minispiral, but not directly from the GMCs embeded in it (Downes et al., 1992).

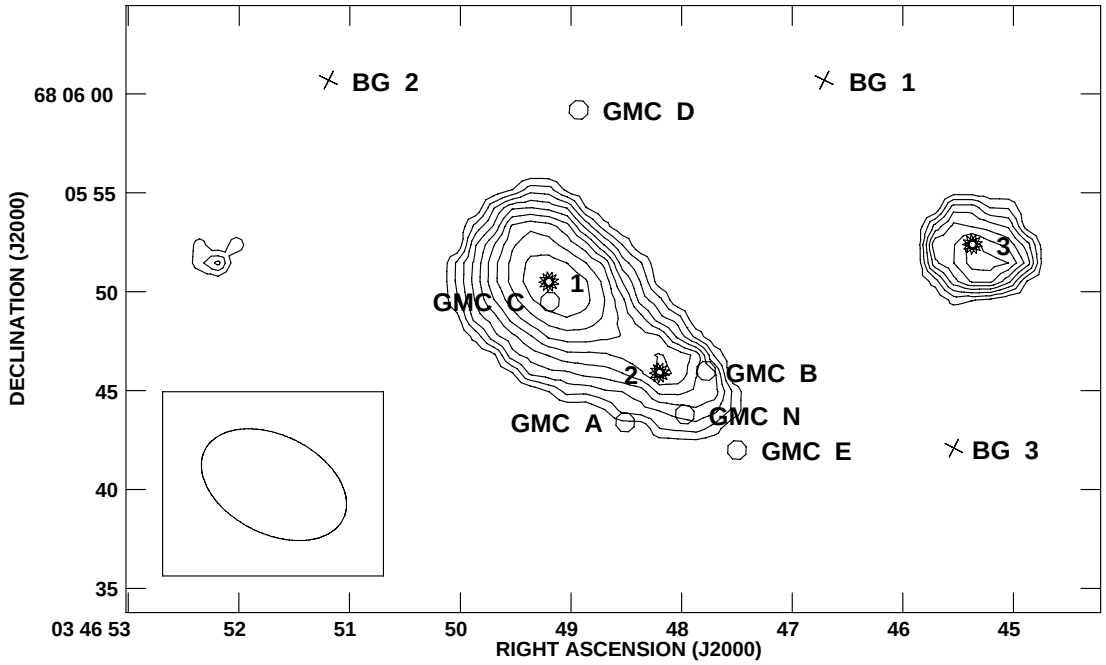

Figure 3.2: NH_3(6,6) integrated intensity map. We have marked the positions of the three NH_3(6,6) detected peaks as well as those of the 6 GMCs as described by Downes et al. (1992) and Meier & Turner (2005). The 6 GMCs are marked with circles, the *(6,6) peak* (peak 1), the *continuum peak* (peak 2) and the *west peak* (peak 3) are marked with stars and numbers. We have also marked three random background positions whose spectra we have plotted (figure 3.3) for comparison reasons. The background points are marked with crosses and labeled 'BG1', 'BG2' and 'BG3'.

In contrast, CO(2-1), at twice the excitation above ground, is detected in warmer gas than CO(1-0). As mentioned before, Meier et al. (2000) have found most of the gas inside the GMCs to be colder than the gas outside of them, since the GMCs are surrounded by PDRs. Thus, it is not surprising that the warmer CO(2-1) is detected in the thin outer layers of the GMCs where they are heated from outside by UV photons (Turner et al., 1993). Therefore, the comparison with NH_3(6,6) could provide some clue as to the kind of gas traced by this highly excited transition. We expect to find NH_3(6,6) concentrated in the areas where CO(1-0) is weaker and inside the GMCs traced by CO(2-1). A gas distribution of this sort would reflect the fact that NH_3 is optically thin, while CO is optically thick, and that the gas distribution depends on density. Therefore, even though the hotter CO has been detected outside of the GMCs instead of inside, we expect the optically thin and dense NH_3 to be found well inside the GMCs.

Because the different molecular lines have been measured using different telescopes, we have resampled the maps with the same size pixels, in order to allow a proper registration for direct comparison. We did not convolve the maps, choosing

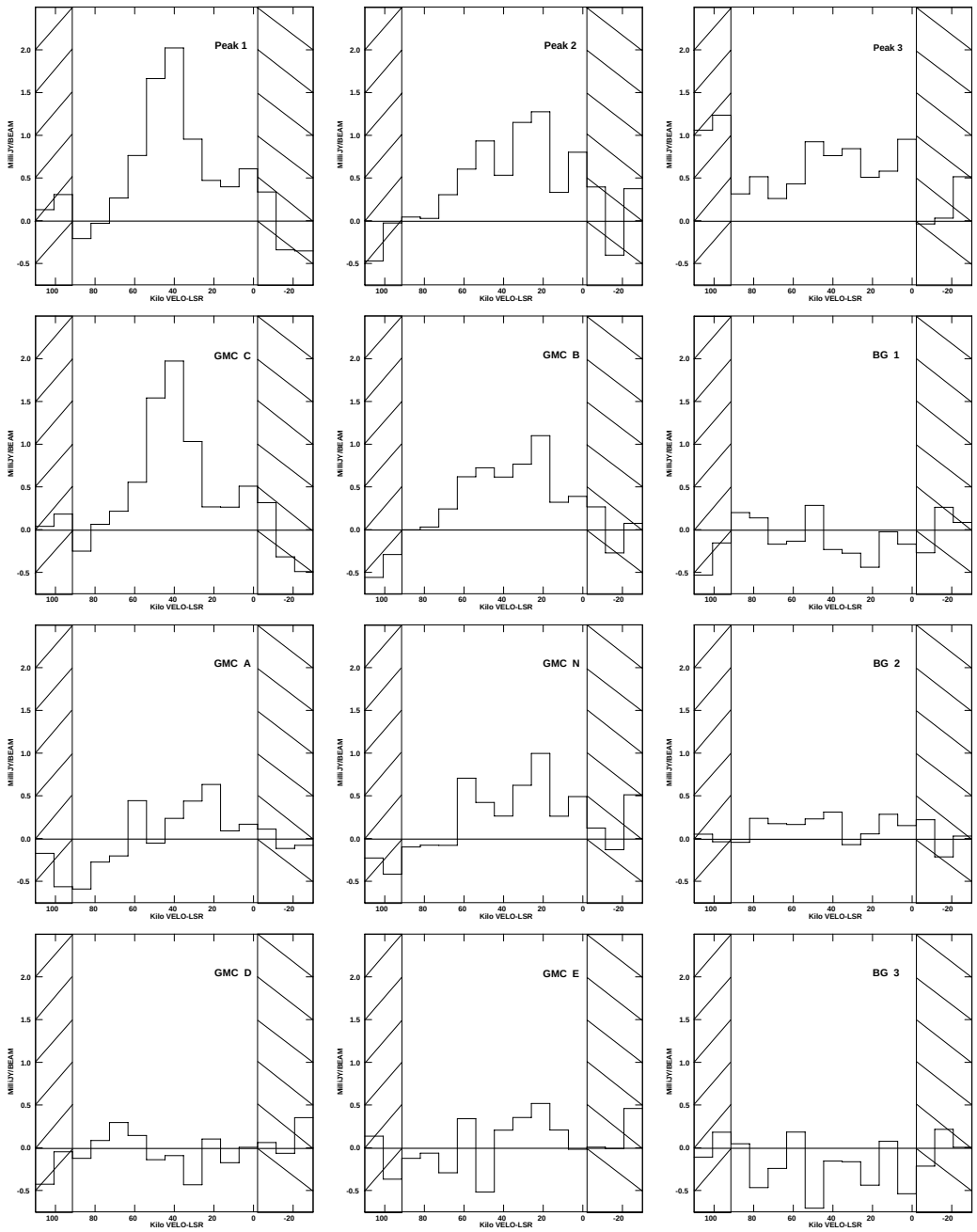

Figure 3.3: Spectra measured at the positions of the 6 GMCs (GMCs A, B, C, D, E and N), the three peaks detected in $NH_3(6,6)$ (peaks 1,2 and 3 from figure 3.2) and three random background positions (BG1, BG2 and BG3). The shaded areas represent the channels we have either removed because their noise level is too high (channels 1, 14 and 15), which correspond to velocities from -30 to -20 km s^{-1} and from -90 to +110 km s^{-1}, or used for continuum subtraction (channels 2 and 3, velocity from -20 to $\sim$0 km s^{-1}).

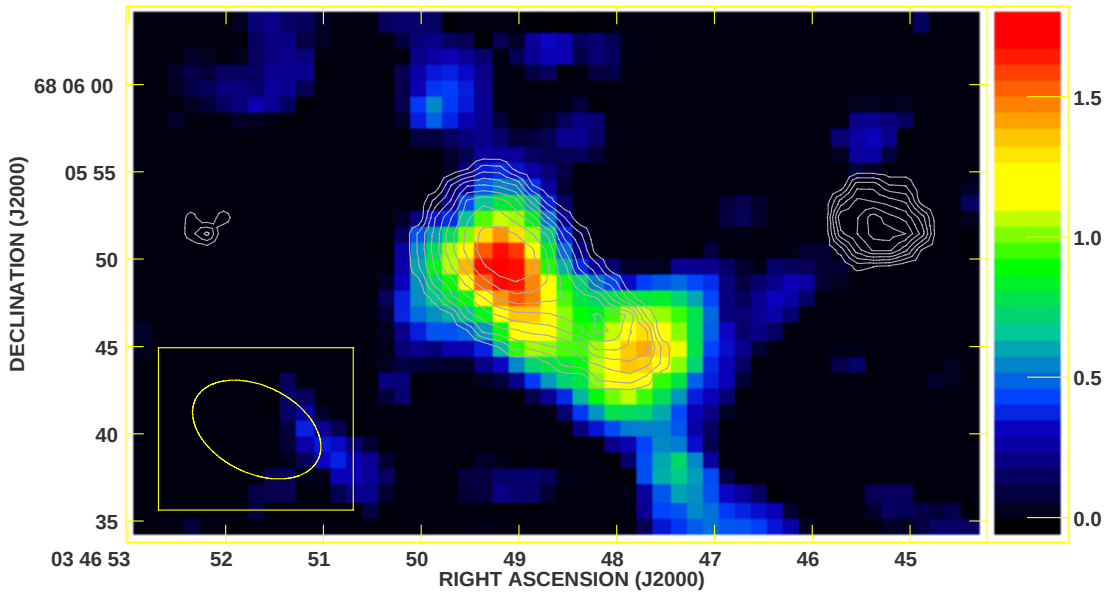

Figure 3.4: NH_3(6,6) integrated intensity in contours. HC_3N(10-9) integrated intensity in false-color scale. Contour levels are as in figure 3.1. The false-color scale is in mJy beam^{-1} km s^{-1} (Meier & Turner, 2005).

to keep the full resolution of each map. However, most of the maps we use for comparison in fact have a very similar angular resolution to our data. We use the latest HNC(1-0), HC_3N(10-9) and N_2H^+(1-0) results from Meier & Turner (2005). These three molecular lines have been measured using the Owens Valley Radio Observatory (OVRO) and have an angular resolution of 5-6" with a positional accuracy of $\sim 1''$. The CO(2-1) map by Schinnerer et al. (2003) was also made using OVRO, but the angular resolution is $1.2''$ with a positional uncertainty of less than $0.1''$. Matching the angular resolution of CO(2-1) to our NH_3 data was not useful because the detected structures would be smoothed away. CO(1-0) has been measured using the Berkeley-Illinois-Maryland Array (BIMA) together with the 12m NRAO antenna (Helfer et al., 2003). The angular resolution of $5.6''$ is similar to the resolution of our VLA data. The CO(1-0) data have a positional accuracy of $\sim 0.4''$. Only the CO(1-0) data include short spacing information, and are thus sensitive to large-scale structure. Therefore, the flux associated with the other molecular tracers must be assumed to be a lower limit. The lack of short spacings does not appear to be as important for NH_3(6,6) as there is no missing flux as compared to single-dish measurements. Nevertheless, some caution must be applied to detailed comparisons between molecules.

In order to understand the significance of the *west peak*, which is not detected in any of the other molecular lines, we also compare our results to a 6 cm continuum map from the VLA (Tsai et al., 2006) (figure 3.9). The 6 cm continuum peak appears

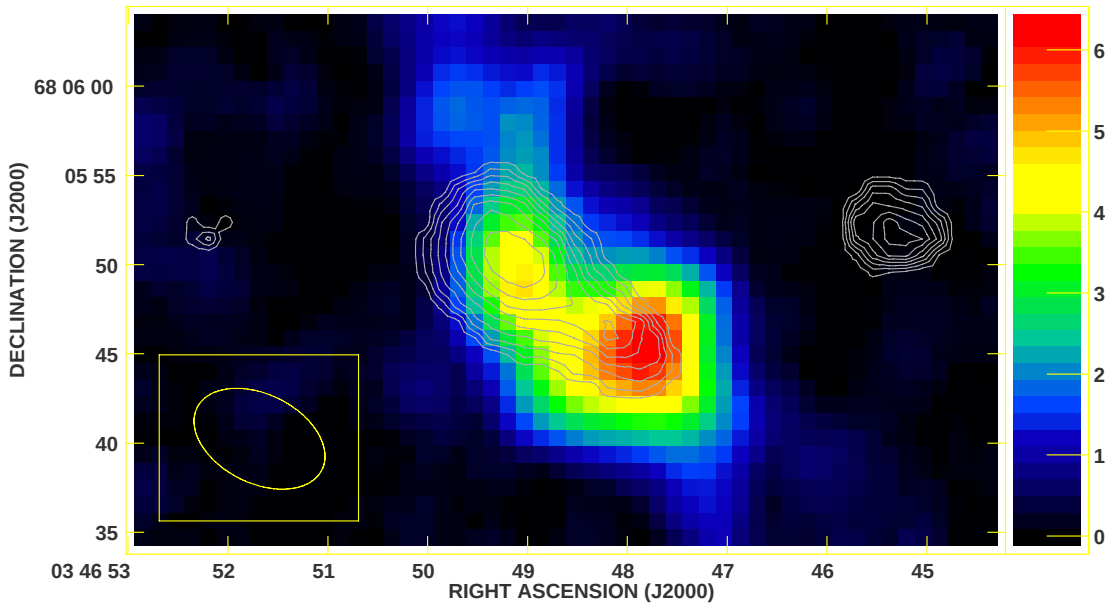

Figure 3.5: $NH_3(6,6)$ integrated intensity in contours. HNC(1-0) integrated intensity in false-color scale. Contour levels are as in figure 3.1. The false-color scale is in mJy beam^{-1} km s−1 (Meier & Turner, 2005).

spatially coincident with our 1.3 cm continuum map (figure 3.10). Therefore, we are confident that the features we observe in $NH_3(6,6)$ are well placed in comparison with the 6 cm map, i.e. the positional accuracy is reliable.

Finally, it would be very useful to compare the $NH_3(6,6)$ emission to emission from other metastable transitions of NH_3. Comparing our $NH_3(6,6)$ map with the $NH_3(1,1)$ and (2,2) maps by Ho et al. (1990) we find that, in general, the detected features on the three maps are remarkably different. Since the lower excitation lines are sensitive to colder gas, the $NH_3(1,1)$ and (2,2) maps appear to trace the more extended emission, such as the minispiral, and GMC D. However, the emission in these lower lines seems to "avoid" the position where the *continuum peak* is located, whereas the $NH_3(6,6)$ emission is very strong in that location. Ho et al. (1990) associated the weakness of $NH_3(1,1)$ and (2,2) toward the continuum source either with photoionization or high temperatures present in the nuclear region. Because of the detection of $NH_3(6,6)$, which is at 412 K above ground, the second scenario is indeed the most plausible explanation. More recent results in $NH_3(1,1)$ and (2,2) are consistent with the earlier results (M. Lebrón, private communication).

Below, we discuss the three $NH_3(6,6)$ peaks in turn.

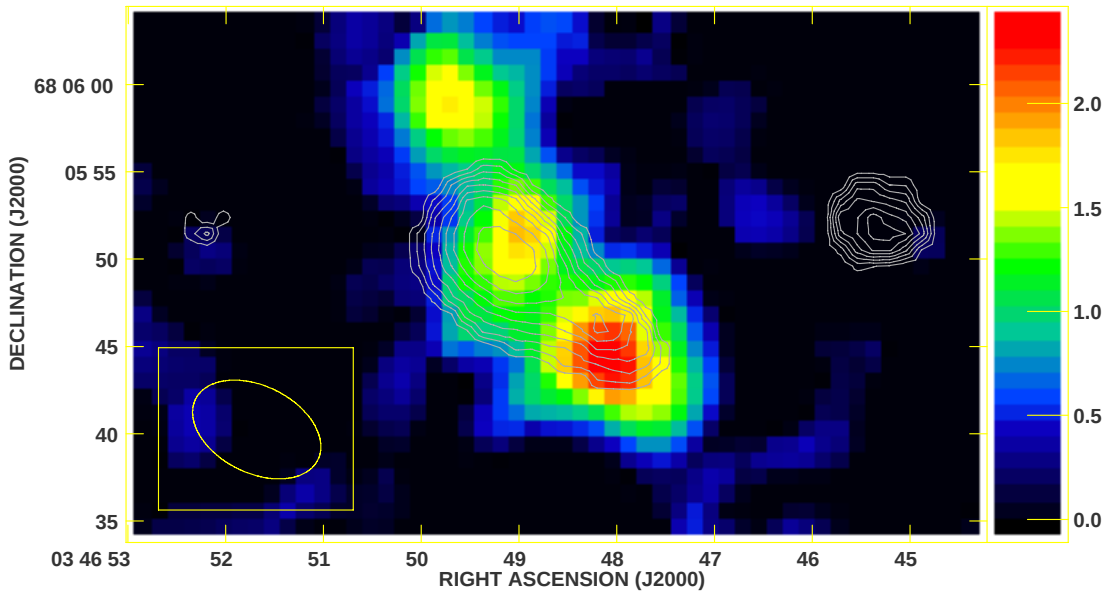

Figure 3.6: NH_3(6,6) integrated intensity in contours. N_2H^+(1-0) integrated intensity in false-color scale. Contour levels are as in figure 3.1. The false-color scale is in mJy beam^{-1} km s^{-1} (Meier & Turner, 2005).

3.4.1 (6,6) peak

When comparing the NH_3(6,6) map with the positions of the GMCs, we notice that the *(6,6) peak* is remarkably close to GMC C (figure 3.2). The two positions are in fact coincident to within the absolute positional uncertainties of the NH_3 map. We conclude that the *(6,6) peak* and GMC C are likely the same structure. Previous studies have demonstrated that the strongest star formation areas in the central region of IC 342 are GMCs B and C, which are both located where the arms meet the ring. Therefore, NH_3(6,6) traces areas where the star formation activity has been enhanced.

The HC_3N(10-9) emission from Meier & Turner (2005) has a structure similar to that of the NH_3(6,6) emission (figure 3.4). In both maps, the strongest line emission is found at the position of the *(6,6) peak*. We compare the line profiles detected in HC_3N(10-9) by Meier & Turner (2005) with that in NH_3(6,6) at the position of the GMC that is closer to our detected peak (GMC C) and we find that they have very similar velocities. Thus HC_3N(10-9) and NH_3(6,6) appear to trace the same high-density, high-temperature material.

When comparing the NH_3(6,6) results with those from the HNC(1-0) map by Meier & Turner (2005) we find that the emission of the GMC close to the position of the *(6,6) peak* (GMC C) is weaker than the emission arising from another region

of the map (figure 3.5). The different behavior might indicate that HNC(1-0) is a density tracer while NH_3(6,6) is a better temperature tracer. In fact, Meier & Turner (2005) note that HNC is more strongly detected in areas of high volume density, not only high column density.

The distribution of N_2H^+(1-0) is very similar to that of HNC(1-0) (figure 3.6), although the N_2H^+(1-0) emission is slightly more extended towards the north, tracing the northern arm of the minispiral. The N_2H^+(1-0) emission peaks at the location of GMC N, which is not close to the *(6,6) peak* (see figure 3.2). N_2H^+ is believed to trace dense quiescent gas (Womack et al., 1992). The lack of coincidence between the N_2H^+(1-0) and the NH_3(6,6) maps indicates that the ion is tracing the areas where the star formation seems to be less intense or non-existent, while the NH_3(6,6) is present in active star formation regions.

The *(6,6) peak* coincides with the CO(2-1) peak measured by Schinnerer et al. (2003) (figure 3.7). The CO(2-1) traces the eastern and western parts of the two molecular spiral arms where they form the molecular ring. The NH_3(6,6) appears to extend outside of the eastern arm, but the spatial coincidence is excellent when the different angular resolutions of the two data-sets are considered. This coincidence of NH_3(6,6) and CO(2-1) suggests that the gaseous material flowing inwards along the northern arm of the "minispiral" is interacting with the inner ring, heating GMC C, and therefore producing the CO(2-1) emission. This interaction may also be triggering a burst of star formation at the same location.

Like in the CO(2-1) map, the NH_3 *(6,6) peak* appears to be offset by $1''$ to the SE as compared to the CO(1-0) map by Helfer et al. (2003) (figure 3.8). In this case, the angular resolutions of the two maps are similar. The slight offset may not be significant given the absolute positional error of about $1''$. The CO(1-0) traces the more extended and colder gas that forms the S-shaped bar, whereas the NH_3(6,6) is more compact and detects the warmer material accumulated in the regions where the inflow from the bar meets the inner ring. However, the NH_3(6,6) and the CO(1-0) maps do seem to be well correlated, since both main peaks are detected.

When comparing the NH_3(6,6) map with the 6 cm continuum map, we find that the *(6,6) peak* appears at the edge of the 6 cm continuum emission (figure 3.9). The 6 cm emission seems to have a "tail" that ends at the position of the *(6,6) peak*. However, there is no evidence for a diffuse continuum component in this area. Becklin et al. (1980) and Turner & Ho (1983) found that the 6 cm continuum map of the center of IC 342 was mainly dominated by free-free thermal emission. However, in the northern part of the CND where the *(6,6) peak* is located, the emission was mostly from synchrotron origin. Thus, there is synchrotron emission associated with the *(6,6) peak*, but not with its surrondings. A possible explanation for these observations could be that the *(6,6) peak* is located in the position of a very concentrated burst of star formation that has developed some supernovae, but

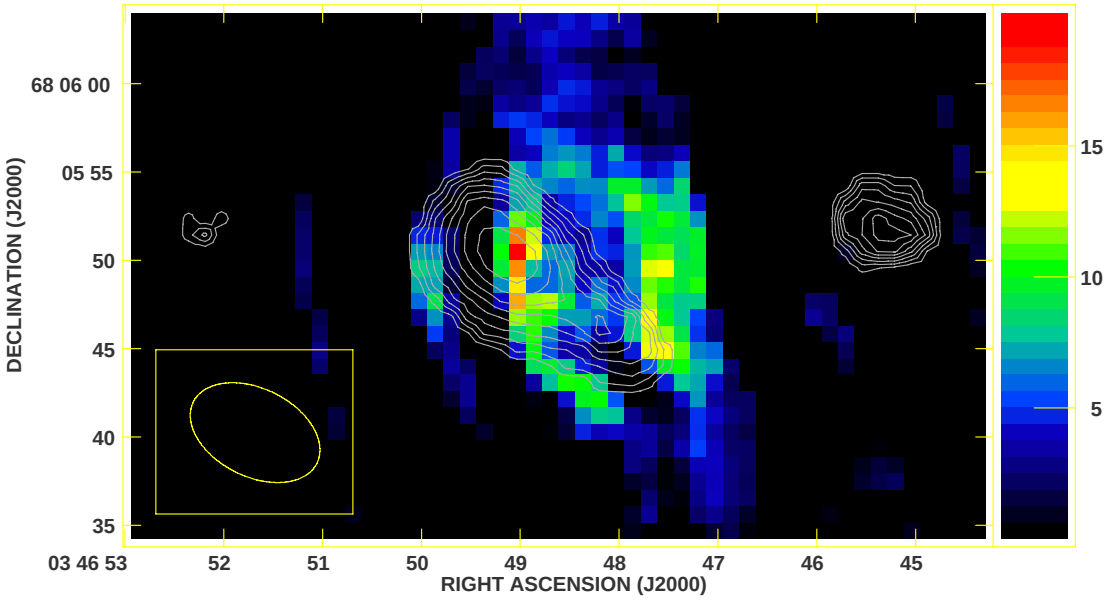

Figure 3.7: $NH_3(6,6)$ integrated intensity in contours. CO(2-1) integrated intensity is in false-color scale and traces the eastern and western parts of the molecular ring. Contour levels are as in figure 3.1. The false-color scale is in mJy beam^{-1} km s^{-1} (Schinnerer et al., 2003).

no such activity has taken place outside of this position.

In summary, the presence of a strong star formation region where the (6,6) peak is located, and a comparison of the $NH_3(6,6)$ distribution with other molecular lines, suggest that the *(6,6) peak* has the characteristics of a column density and temperature peak.

3.4.2 Continuum peak

The $NH_3(6,6)$ *continuum peak* is offset by 2″-3″ from GMCs B, A and N, which trace an arc around it (figure 3.2). This offset appears significant, especially since the $NH_3(6,6)$ *continuum peak* coincides well with the 6 cm continuum peak (figure 3.9). When comparing GMC B and the *continuum peak* spectra, we notice that even though the *continuum peak* spectrum is stronger, the integrated intensity is very similar. As remarked before, GMC B is a very strong star formation area. On the other hand, no trace of star formation has been detected towards GMC A to date. The lack of a strong $NH_3(6,6)$ detection at the position of GMC A supports the theory that there is no current star formation in this region. GMC A has a

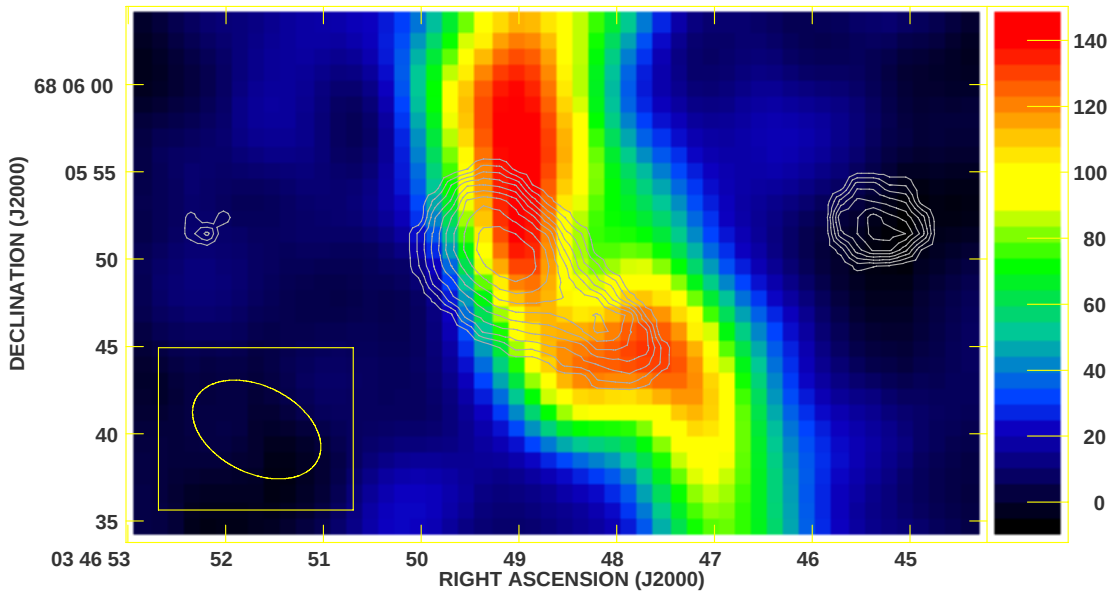

Figure 3.8: NH_3(6,6) integrated intensity in contours. CO(1-0) integrated intensity is shown in false-color scale, and traces the minispiral. Contour levels are as in figure 3.1. The false-color scale is in mJy beam^{-1} km s^{-1} (Helfer et al., 2003).

NH_3(6,6) spectrum only slightly more intense than the background emission-free positions (figure 3.3). We do not find a differentiated feature in the integrated intensity map where GMC N should be. However, the spectrum at this position is clearly above noise level.

The HC_3N(10-9) map from Meier & Turner (2005) shows a peak near the *continuum peak* (figure 3.4). As in the NH_3(6,6) map, the *continuum peak* seems weaker than the *(6,6) peak*. Since GMC B, which seems to be the GMC closer to the *continuum peak*, is the warmest region of the nucleus of IC 342, the fact that NH_3(6,6) and HC_3N(10-9) are weaker at this point may suggest that the total column density is not a maximum at this position.

The *continuum peak* is offset by 2″ north of the secondary peak in HC_3N(10-9) and the primary peak detected in HNC(1-0) by Meier & Turner (2005) (figure 3.5). This offset appears to be significant. A similar offset between NH_3(6,6) and N_2H^+(1-0) is also observed. These results suggest that neither HC_3N(10-9) nor HNC(1-0) nor N_2H^+(1-0) are tracing a temperature peak, which is in fact better traced by NH_3(6,6).

The *continuum peak* is a very weak feature in the CO(2-1) map (Schinnerer et al., 2003). Unlike NH_3(6,6), CO(2-1) does not detect the gas associated with the heating source located at the continuum peak, but instead traces the gas surrounding it (figure 3.7).

The *continuum peak* also appears offset by 3″ from the secondary peak detected in the CO(1-0) map by Helfer et al. (2003) (figure 3.8). As in the NH_3(6,6) map, this secondary peak is weaker than the one that coincides with the *(6,6) peak*, and although the kind of gas traced by the two molecules have different temperatures, the overall structure has some similarities.

Finally, as expected, the *continuum peak* is located close to the 6 cm continuum emission peak (figure 3.9). The 6 cm continuum emission seems to trace an arc structure around the NH_3(6,6) *continuum peak* rather than being concentrated at that same spot. In this case, the angular resolution is different by a factor of 10. With higher resolution, the NH_3(6,6) emission could be even better correlated with the 6 cm continuum structure. The good correspondence with the radio continuum peak, and the offset of a few arcseconds relative to other molecular peaks which sample lower temperature gas, suggests that the NH_3(6,6) emission could be tracing a hot molecular component near the nucleus. Israel & Baas (2003) suggest that the nucleus of IC 342 has two different molecular mass components, a cold and dense component, which represents about one third of the total molecular mass, and a less dense and hotter component. A similar situation has also been observed in the center of the Milky Way. By looking at six NH_3 metatestable inversion transitions (from (1,1) to (6,6)) in the Galactic center region (575 pc × 145 pc), Hüttemeister et al. (1993) find the distribution of the transition lines to differ from one another. While lower transition lines look similar, the higher transitions often look very different. In fact, Hüttemeister et al. (1993) find that molecular gas in the nuclear region of the Galaxy is best modeled as a mixture of hot ($\sim$ 200 K) and cold (25 K) gas, in which 75% of the gas is in the cold component. This "two-temperature" structure continues to hold even within 5 pc of the nucleus (Herrnstein & Ho, 2005). Furthermore, studies by Herrnstein & Ho (2002), with a similar velocity resolution to ours, find NH_3(6,6) to be clearly concentrated in the nucleus of the Milky Way. Obviously, the Galactic Center study refers to a much more concentrated and less massive material than the material detected in IC 342, given the different size-scales (2.7 kpc × 4.8 kpc for IC 342, 10 pc × 10 pc for the Galactic center). Therefore, the mechanism that drives the NH_3(6,6) in the nuclear region of IC 342, which is likely to be a star formation process, might be more extensive spatially than the mechanism that is working in the Galactic center. Nevertheless, given the similar behaviour we find in the nuclear regions of IC 342 and the Galactic center, this suggests that the *continuum peak* could be tracing the hot component present in the nucleus of IC 342, i.e. the *continuum peak* is a temperature peak.

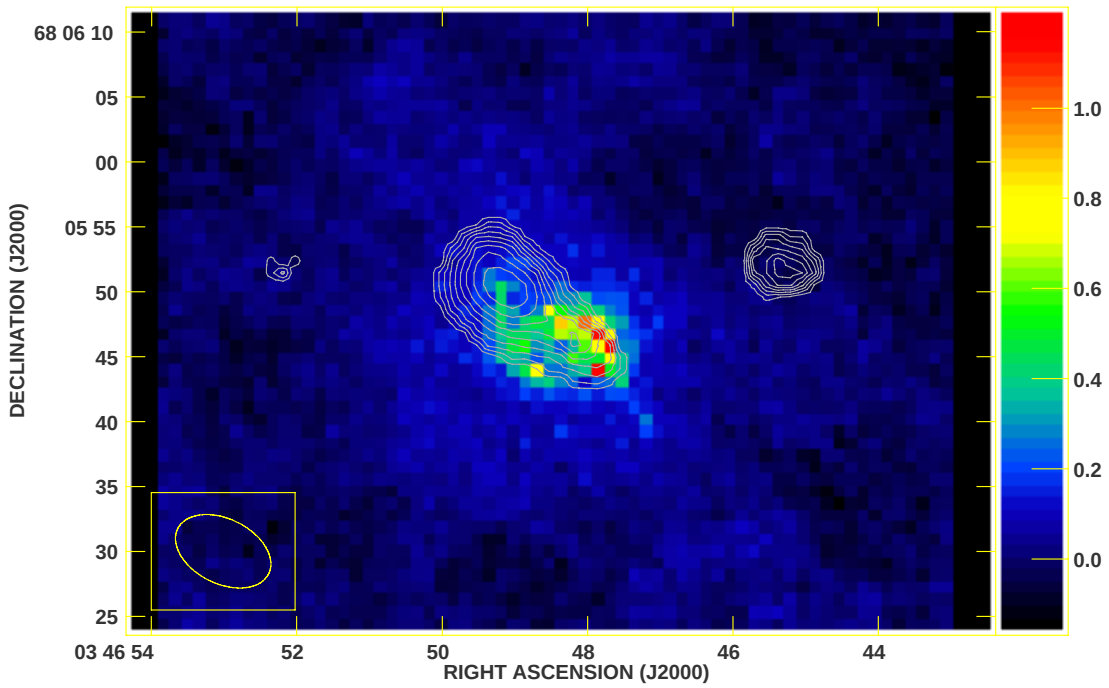

Figure 3.9: $NH_3(6,6)$ integrated intensity in contours. VLA 6 cm continuum integrated intensity in false-color scale. Contour levels are as in figure 3.1. The false-color scale is in mJy beam^{-1}.

3.4.3 West peak

The *west peak* has no counterpart in any other molecular line map that has been published to date. However, the careful reduction process that we have used gives us confidence to conclude that this structure is not a noise feature. In addition, the lack of a symmetric counterpart on the other side of the nucleus of IC 342 leads us to conclude that the *west peak* is unlikely a sidelobe effect. The *west peak* is not very strong, but it is a remarkable feature because it is detected over a wide velocity range. We compare the *west peak* spectrum to three randomly chosen noise-level spectra in figure 3.3. We find that, although weak, the overall flux level associated with the *west peak* is above the noise level.

The comparison of the $NH_3(6,6)$ emission map with the latest VLA 6 cm continuum emission map from Tsai et al. (2006) (A and C configurations combined) shows no evidence of radio continuum emission at this location (figure 3.9).

The presence of $NH_3(6,6)$ at positions where there have been no previous molecular detections has occurred elsewhere. In the Milky Way, $NH_3(6,6)$ has been detected within 2 pc of the Galactic center with no corresponding emission from other molecular tracers (Herrnstein & Ho, 2002). This molecular emission (termed the "high

line ratio cloud") is thought to be the result of absorption of low-energy transitions [in particular NH_3(1,1), (2,2) and (3,3)] by cool material along the line of sight (Herrnstein & Ho, 2005). Though the size scale of the Galactic center emission (< 2 pc) is much smaller than the size scales traced in our IC 342 data, it is possible that a similar geometrical effect could explain the lack of low-energy molecular emission associated with the IC 342 *west peak*.

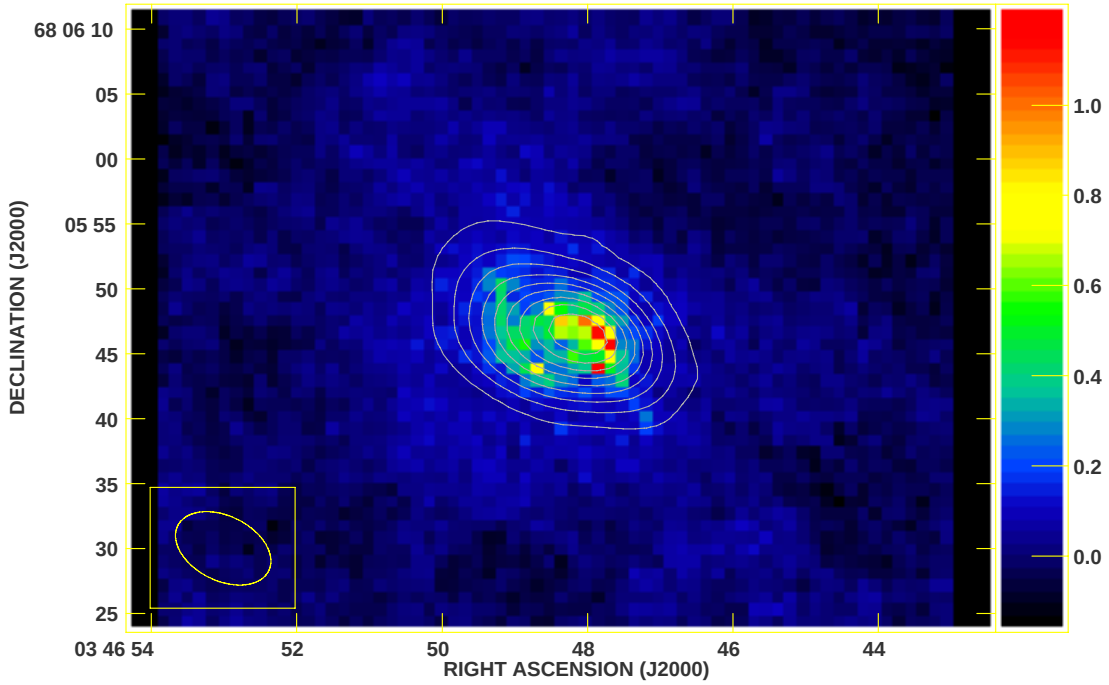

Figure 3.10: 1.3 cm continuum integrated intensity in contours. VLA 6 cm continuum integrated intensity in false-color scale. Contour levels are in steps of 10% of the continuum intensity peak, from 13 mJy beam^{-1} to 114 mJy beam^{-1}. The false-color scale is also in mJy beam^{-1}.

3.4.4 Mass estimates

Since we have detected three different peaks, we separate the NH_3(6,6) structure into three different areas and calculate the mass in each of them.

Because we have only measured one transition line, NH_3(6,6), we cannot directly calculate the excitation temperature of the gas. Theoretically, the NH_3(6,6) opacity could be measured using the hyperfine splitting of the NH_3(6,6) emission line. However, due to the weakness of the satellite lines (roughly 3% of the main hyperfine line for optically thin gas) and the large linewidths, this calculation is not possible

for our data. We therefore assume optically thin emission ($\tau \ll 1$) and also consider the source to fill the clean beam, giving

$$T_{ex}\tau \cong T_b\,. \tag{3.1}$$

We can obtain the T_b directly from the line profile, using

$$T_b \;=\; \frac{\lambda^2}{2k\Omega} S_\nu\,, \tag{3.2}$$

where λ is the wavelength, k is Boltzmann's constant, Ω the solid angle and S_ν is the peak flux density.

The column density is calculated using

$$N_{JK} \;=\; 4.1 \times 10^{-20}\, cm^{-2}\, \frac{\tau \nu^2\, T_{ex} \Delta v}{A_{10}\, k_{JK}}\,. \tag{3.3}$$

For NH_3(6,6), $k_{66} = 0.969$, $A_{10} = 3.38 \times 10^{-7}\,\mathrm{s}^{-1}$, and $\nu = 25.056\,\mathrm{GHz}$ (Herrnstein, 2003).

Once we know the value of the column density, we obtain the molecular mass through the following equation:

$$M_{H_2} \;=\; N_{66} \times Area \times \frac{1}{f_{66}} \times \left[\frac{N(H_2)}{N(NH_3)}\right] \times m_{H_2}\;, \tag{3.4}$$

where f_{66} is the fraction of NH_3 molecules in the (6,6) state, and is on the order of 0.1 for temperatures higher than 150 K. We use $\frac{N(H_2)}{N(NH_3)} = 10^{7.5}$ from Mauersberger et al. (2003), which is the relative abundance of H_2 to NH_3 in fairly warm environments ($T > 150\,\mathrm{K}$).

The resulting mass estimates for each NH_3(6,6) peak are given in Table 3.1.

We detect a total warm gas mass of 8.2×10^6 $M_\odot$, clearly much larger than the amount of warm gas mass detected in the interior of the Galactic center Circumnuclear Disk by Herrnstein & Ho (2002), 10^4 $M_\odot$ (inner 1.5 pc around Sgr A*). Rigopoulou et al. (2002) reported a warm mass of 5.0×10^6 $M_\odot$ measuring the quadrupole transition lines of H_2 using the *Infrared Space Observatory (ISO)*, assuming a distance of 3.6 Mpc and an area coverage of $14'' \times 27''$. If we assume the same distance and coverage (the *west peak* would be left outside), the warm gas

mass detected would be 9.4×10^6 $M_\odot$. Rigopoulou et al. (2002) estimate that the 2.5% of the gas in IC 342 is warm, using previous published data from Aalto et al. (1995) in various ^{12}CO, ^{13}CO and $C^{18}O$ transitions for the total molecular gas mass value, measured with a variety of telescopes. Using the same value for the total molecular gas mass (and correcting for the distance) we find that the percentage increases to 4.7%. Additionally, Mauersberger et al. (2003) report the 10% of the total molecular gas in IC 342 to be warm. Mauersberger et al. (2003) use the warm gas mass value reported by Rigopoulou et al. (2002) corrected for the assumed distance (1.8 Mpc), and compare it to the total molecular gas mass measured using $^{13}C^{16}O$ data taken with the Heinrich Hertz Telescope. Assuming the same distance (1.8 Mpc) and amount of total molecular gas mass than Mauersberger et al. (2003), and considering the three peaks, since the beam of Heinrich-Hertz-Telescope (34″) covers all three of them, the amount of warm gas mass would be 7.2×10^5 $M_\odot$, which represents the 5.5% of the total molecular gas mass. In summary, using two different values for the total molecular gas mass (from Rigopoulou et al. (2002) and Mauersberger et al. (2003)), and two different area coverages, we still find that the percentage of warm gas mass to total molecular gas mass is $\sim 5\%$.

Table 3.1: Calculated warm masses for the three detected peaks for a distance of 3.3 Mpc.

Peak	Line flux (10^{-3} Jy beam^{-1})	T_b (K)	Δv (km s^{-1})	N_{66} (10^{13} cm^{-2})	Area (10^4 pc^2)	M_{H_2} (10^6 $M_\odot$)
(6,6) peak	2.1	0.12	40	3.7	2.6	4.8
Continuum peak	1.4	0.08	50	3.1	1.2	1.8
West peak	1.1	0.06	80	4.0	0.8	1.6

3.5 Summary

We have imaged the nuclear region of IC 342 in NH_3(6,6) using the VLA. Three emission peaks are detected. The *(6,6) peak* corresponds well with GMC C and is probably a column density and temperature peak driven by a burst of star formation at the position where inflowing gas accumulates at a nuclear ring. The *continuum peak* is offset from GMCs B, N and A, but coincides with the 1.3 cm continuum peak. The 6 cm continuum peak is also very close, and due to the different resolution betweeen the two maps, we can not rule out that the two peaks could be in fact coincident. The *continuum peak* is likely a temperature peak corresponding to very hot gas similar to the hot gas seen in our own Galactic center around Sgr A*. The *west peak* is a tentative detection with not known molecular or continuum emission counterpart. The fact that the *west peak* remains undetected in lower transition

lines might be due to absorption along the line of sight, as is the case for the high line ratio cloud in the Galactic center. The presence of GMC N, as detected by Meier & Turner (2005), could not be positively confirmed in NH_3(6,6) emission. NH_3(6,6) emission above noise level is detected at the position where this GMC has been reported. However, we did not detect a distinctive feature at this location.

Chapter 4

Measuring the nuclear temperature in IC 342

4.1 Abstract

We present the first interferometric high-resolution detection of $NH_3(3,3)$ in the nucleus of the nearby galaxy IC 342, made with the Very Large Array (VLA). We obtain a $4.9'' \times 3.8''$ resolution that allow us to separate the different features in the nuclear region of IC 342. We detect extended emission tracing the S-shaped minispiral as well as the molecular ring. The strongest emission peaks are observed in the locations of three Giant Molecular Clouds (GMCs), two of them along the molecular ring, and the third located in the northern arm of the minispiral. Only in one of the GMCs detected in $NH_3(3,3)$ a star formation process has been detected. The comparison of the $NH_3(3,3)$ map with the $NH_3(6,6)$ map reported in chapter 3 shows that the hottest gas is at the dynamical center, while the colder gas is more widely spread out. The ratio of (6,6)/(3,3) is used to calculate the rotational temperature of the gas. The comparison of the nuclear region of IC 342 with the Galactic center proves that both sources have a lot of common characteristics, and that indeed IC 342 is an excellent candidate for the study of galactic nuclei.

4.2 Introduction

Numerous studies in nuclear regions of nearby galaxies have shown the presence of large quantities of molecular gas within a few parsecs of the dynamical center (Mauersberger & Henkel, 1991; Nguyen-Q-Rieu et al., 1992; Hüttemeister et al., 1995; Aalto et al., 1995; Jackson et al., 1993; Hüttemeister, Mauersberger & Henkel, 1997; Paglione, Jackson & Ishizuki, 1997; Sheth et al., 2002; Helfer et al., 2003; Mauersberger et al., 2003). The molecular gas is frequently found in the shape of large-scale bars, proved to be excellent tools to transport material towards the center (Matsuda & Nelson, 1977; Simkin, Su & Schwarz, 1980).

IC 342 is a prime candidate for studies of nuclear galactic regions because of its proximity to the Milky Way (3.3 Mpc Saha et al. (2002); Karachentsev (2005)) and its nearly face-on position. Due to its location close to the Galactic plane (only 10.6° from the Galactic equator, Downes et al. (1992)), extinction by Galactic gas and dust hinders the study of this galaxy. Fortunately, IC 342 is a rich source of molecular emission at radio wavelenghts, overcoming the dust absorption that hampers its study in the optical wavelength.

The inner 30″ of IC 342 are occupied by a nuclear stellar cluster (6-60 Myr, Böker et al. (1997)), surrounded by a molecular ring of dense gas of $\sim$ 80 pc radius. The ring interacts with two arms of incoming molecular gas towards the nucleus of IC 342, that form an S-shaped bar, a minispiral, first detected in CO(1-0) by Lo et al. (1984). The overall motion is from southwest to northeast (Schinnerer et al., 2003), following the kinematics of a bar potential. The two arms of the minispiral have different geometries, with the north-eastern arm much better defined than the south-western arm, suggesting that they are formed by two different structures (Schinnerer et al., 2003). Both the ring and the bar are composed of Giant Molecular Clouds (GMCs). Five of these GMCs were first defined by Downes et al. (1992) (GMCs A to E), as detected in HCN(1-0) using the IRAM interferometer. Two more GMCs were found by Meier & Turner (2005) (GMCs D' and N), located after a very exhaustive survey of molecular tracers in the central region of IC 342 with the Owens Valley Radio Observatory (OVRO). GMCs B and C are located in the regions where the molecular ring interacts with the southern and northern arms of the minispiral, respectively. At the locations of these two GMCs, strong star formation processes, as detected by NIR observations, are currently underway (Böker et al., 1997). GMC A is also located in the molecular ring, closer in projection to the dynamical center of IC 342 (Meier & Turner, 2005). GMC A does not seem to be undergoing a strong burst of star formation but it is very strongly detected in PDR tracers, such as C_2H and $C^{34}S$ (Meier & Turner, 2005). Because of its closeness to the nuclear stellar cluster and its brightness in terms of PDR detection (lacked by both GMCs B and C, but at the edges), Meier & Turner (2005) suggested that the nuclear stellar cluster is responsible for the ionization producing the PDRs, and not the

star formation regions close to GMCs B and C. Also, for GMC A to be much more affected, it is possible that this cloud is less dense that its companions, and more easily penetrated by UV radiation. GMC D is located along the northern arm of the minispiral, where large amounts of infalling material has been detected (Turner & Hurt, 1992). GMC D' was first described by Meier & Turner (2005) as a location where a number of different molecular lines were detected very strongly (HNC(1-0), $CH_3OH(2_k\text{-}1_k)$, $HNCO(4_{04}\text{-}3_{03})$ and $N_2H^+(1\text{-}0)$). It is located 5″ east of GMC D, towards the leading edge of the northern arm, due to the counterclockwise motion of the minispiral (Schinnerer et al., 2003), where the densities are higher (Wright et al., 1993; Meier & Turner, 2001). GMC N was detected in N-bearing molecules, such as N_2H^+ and HC_3N by Meier & Turner (2005). NIR observations have not detected star formation processes at the locations of GMCs D, D', E and N (Böker et al., 1997).

IC 342 has been studied in a broad selection of molecular tracers: HCN (Downes et al., 1992; Nguyen-Q-Rieu et al., 1992; Jackson et al., 1995; Paglione, Jackson & Ishizuki, 1997; Schulz et al., 2001), CO (Turner & Hurt, 1992; Wright et al., 1993; Turner et al., 1993; Meier et al., 2000; Schulz et al., 2001; Meier & Turner, 2001; Crosthwaite et al., 2001; Sheth et al., 2002; Israel & Baas, 2003; Helfer et al., 2003; Schinnerer et al., 2003), HCO^+ (Nguyen-Q-Rieu et al., 1992; Jackson et al., 1995), HNC (Hüttemeister et al., 1995; Meier & Turner, 2005), H_2CO (Hüttemeister, Mauersberger & Henkel, 1997), CH_3OH (Hüttemeister, Mauersberger & Henkel, 1997; Meier & Turner, 2005), C_2H, $C^{34}S$, N_2H^+, HNCO, HC_3N and SO (Meier & Turner, 2005) and SiO (Usero et al., 2006). Extremely remarkable results have been found from these thorough surveys, demonstrating that IC 342 is indeed a fertile source of information, and most importantly because of its similarities to the Milky Way.

In addition of all the molecular surveys previously mentioned, a number of NH_3 studies towards IC 342 have been carried out. As we explained in chapter 3, NH_3 is an excellent high-density tracer, due to its high dipole moment, requiring a density of $\sim 10^4\,\mathrm{cm}^{-3}$ to be excited. At the same time, the NH_3 inversion transitions trace a wide range of temperatures, from 23 K for (1,1) to 412 K for the (6,6) transition, all located around 1.3 cm, therefore mesurable with the same instrument. NH_3 is then a very important tool for the study of the dense and warm gas, expected to be found in the inner regions of galaxies.

Martin & Ho (1979) first detected $NH_3(1,1)$ in IC 342 using the 100 m Effelsberg telescope of the Max-Plank-Institut für Radioastronomie (first extragalactic NH_3 detection). Those observations were later reattempted with the 36.6 m telescope of the Haystack Observatory, together with $NH_3(2,2)$ (Ho, Martin, & Ruf, 1982) and the Very Large Array (VLA) (Ho & Martin, 1983). Extended emission along the minispiral and the molecular ring was found. Montero-Castaño, Herrnstein & Ho (2006) reported the detection of a high-excitation transition, $NH_3(6,6)$, in the

nuclear region of IC 342 (chapter 2).

NH_3(3,3) was first detected in IC 342 by Martin & Ho (1986), using the 100 m Effelsberg telescope of the Max-Plank-Institut für Radioastronomie. A few years later, Mauersberger et al. (2003) reported a new detection with the same telescope. However, no interferometric detection was attempted in this transition until now.

We have conducted the first high-resolution observations in NH_3(3,3) of the inner $1'$ of IC 342 using the VLA. For the first time in NH_3(3,3), we achieve enough resolution ($4.9'' \times 3.8''$) to elucidate the emission coming from the different condensations of molecular gas in the nuclear region of IC 342. Furthermore, due to our previous observations in NH_3(6,6), we can calculate the rotation temperature of the gas using the ratio of both transition lines and obtain an approximation to the kinetic temperature. Moreover, we can compare the different morphology of the molecular gas as traced by each transition, in order to better understand the processes taking place in the nuclear region of IC 342.

Also, because of the similarities between IC 342 and the Milky Way, and the previous observations of the later source both in NH_3(3,3) and (6,6) (McGary et al., 2001; Herrnstein & Ho, 2002, 2005), we can conduct a comparative study of both sources in terms of the distribution of high-density, high-temperature gas in the nuclear regions of spiral galaxies.

4.3 Observations

Observations of the NH_3(3,3) transition ($\nu = 23.870$ GHz) were made with the Very Large Array (VLA) in the D configuration on 2007 April 20. Only 24 antennas were available during the observation, 7 of them newly retrofitted as EVLA antennas. The pointing was centered on $\alpha_{J2000.0} = 03^h46^m48.7s$, $\delta_{J2000.0} = 68°05'46.7''$. We used a 25 MHz bandwidth divided into 31 spectral channels, obtaining a velocity resolution of 9.8 km s^{-1}. The velocity coverage was from -112 to 192 km s^{-1}, centered on $v_{LSR} = 40$ km s^{-1}.

The data were calibrated using the NRAO Astronomical Imaging Processing System (AIPS). Because of the presence of EVLA antennas, the data calibration was especially complicated and we followed the latest recommendations by the NRAO experts. The total on-source integration time was $\sim$ 9h30min. The flux calibrator was 0137+331 (3C 84) with an assumed flux of 1.05 Jy at 1.3 cm. The phase calibrators were 0228+673 at the beginning of the track and 0449+635 at the end, with measured fluxes of 0.72$\pm$0.02 Jy and 0.87$\pm$0.02 Jy, respectively. We performed

phase-only self-calibration on the broad-band continuum data and the results were subsequently applied to the line data. Continuum subtraction was performed in the uv data, using channels on both sides of the line (velocity ranges -73 to -53 km s^{-1} and 104 to 143 km s^{-1} were considered free of line emission). The final rms noise per channel is 0.3 mJy $beam^{-1}$, and the overall achieved rms is 2.9 mJy $beam^{-1}$ km s^{-1}. The deconvolution was performed using the task IMAGR in AIPS. Natural weighting of the uv data produced an image with a synthesized beam of $4.9'' \times 3.8''$ with a position angle of -78.7°. The integrated intensity map was produced using the task MOMNT, with a minimum flux cutoff of 0.24 mJy, chosen based on the noise threshold.

4.4 Results

We detect extended NH_3(3,3) emission in the central part of IC 342. The extended structure shows three line emission peaks, all three of them embedded in the same large structure (figure 4.1). From now on we will refer to the peaks as *northern peak*, *central peak* and *southern peak*. We observe that the *central peak* is much stronger than both the *northern* and *southern peaks*, which seem to be equally distant from their central companion.

We overlay the positions of the seven GMCs on our NH_3(3,3) emission map (figure 4.2) and we draw the spectra at the positions of each of the detected peaks as well as the GMCs. The positions of the GMCs were taken from Meier & Turner (2001), except for GMC D' and N, whose locations were described by Meier & Turner (2005). We observe that the *northern peak* coincides with GMC D', which is located in the northern arm of the minispiral. As we mentioned in the introduction, GMC D' has been found to be much stronger than GMC D in some molecular tracers, like N_2H^+. We can confirm that the same situation is found in NH_3(3,3). GMC D' is barely $5''$ east of GMC D, but the difference in NH_3(3,3) emission is remarkable. Given the counterclockwise motion of the minispiral (Schinnerer et al., 2003), GMC D' would be in the leading side of the arm, ahead of GMC D. GMC D' has also been strongly detected in SiO, as well as CH_3CO and HNCO, all of them shock tracers (Meier & Turner, 2005; Usero et al., 2006). Therefore, it appears that the environment where GMC D' is located is a turbulent one. At the same time, no star formation process has been detected at that location by NIR observations (Böker et al., 1997). Furthermore, Usero et al. (2006) reported that a star formation process is not expected to take place at the location of GMC D' because of the shear suffered by the spiral arm, which would inhibit the star formation process. Therefore, the presence of high-density and high-temperature gas, as indicated by the detection of NH_3(3,3), does not imply that the GMC is undergoing a burst of star formation.

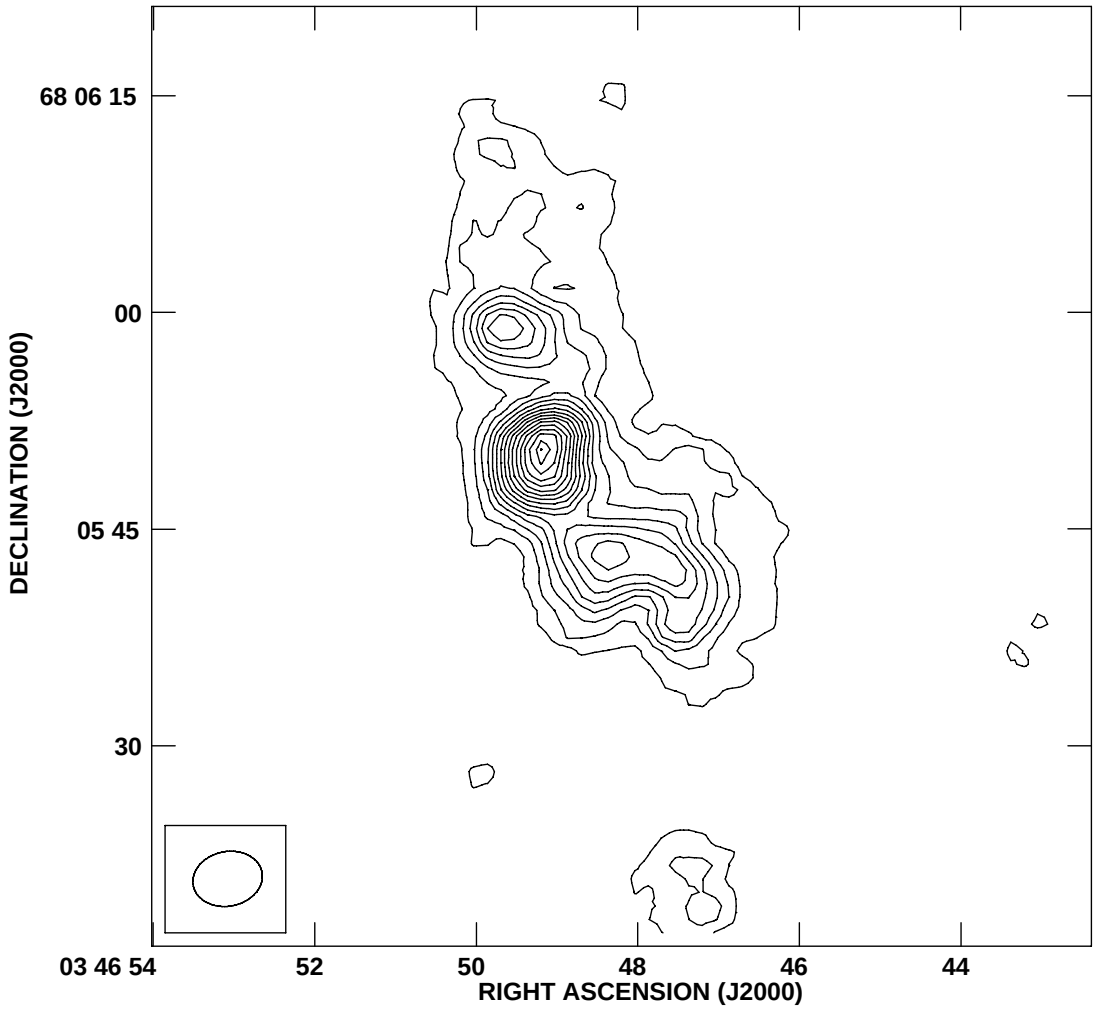

Figure 4.1: $NH_3(3,3)$ integrated intensity map. Contour levels are in steps of 6σ, from 3σ to 87σ, except for the highest contour level, at 91σ (8.7 to 26.5 $\times$ 10^1 mJy beam^{-1} km s^{-1}).

The *central peak* is located at the same position as GMC C, while the *southern peak* and GMC A are coincident. The fact that the strongest detected peak in $NH_3(3,3)$ coincides with a star formation region (as detected by NIR observations, Böker et al. (1997)), suggests the possibility of using this ammonia transition to trace star formation. However, we do not detect strong emission at the position of GMC B, another location of star formation. In fact, GMC A, where star formation, as indicated by NIR emission, has not been detected, is much stronger in $NH_3(3,3)$. As Meier & Turner (2005) stated, GMC A is a PDR cloud, probably much less dense than its companions along the molecular ring (GMCs B and C), allowing the nuclear stellar cluster radiation to penetrate (thus, the PDR explanation), and maybe even being torn apart by the tidal forces. The fact that GMC A is strong in $NH_3(3,3)$, a high-density tracer, could suggest that the cloud has a dense and warm

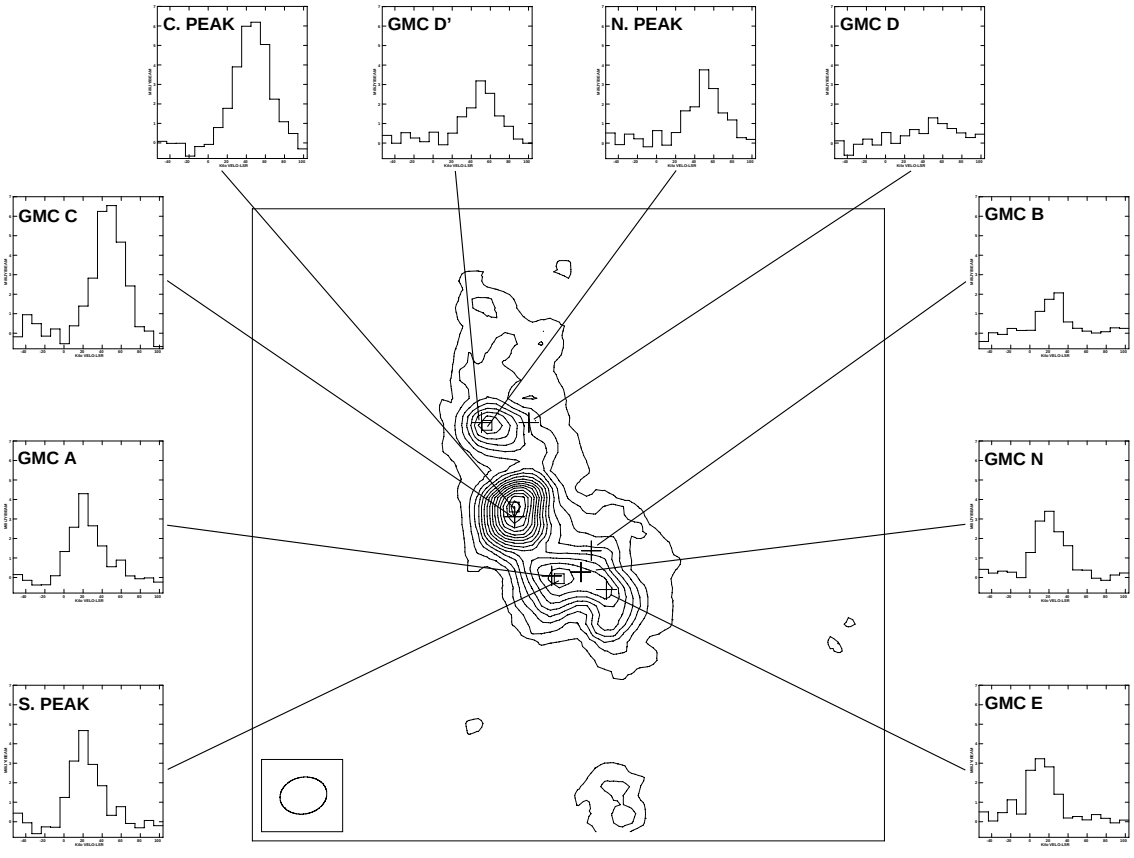

Figure 4.2: Spectra of the three peaks and the six GMCs. The squares represent the peaks detected in the $NH_3(3,3)$ emission and the crosses the GMCs as described by Downes et al. (1992), Meier & Turner (2001) and Meier & Turner (2005). Contour levels as in figure 4.1.

clumpy structure (too small to be seen as independent structures) where the more diffuse inter-clump material is allowing the UV radiation to penetrate. This result would be consistent with the hypothesis reported by Meier & Turner (2001), who stated that the GMCs are composed of small and dense clouds. Since GMC A is the closest GMC in projection to the nuclear stellar cluster (Meier & Turner, 2005), the radiation from the nearby stars is more likely to affect it. Both GMC N and E do not show a remarkable profile, nonetheless, the emission at those location is stronger than in GMC B and not at all negligible. Thus, the intensity of $NH_3(3,3)$ emission is not by itself a good measurement of star formation activity.

We compare the line emission map with the continuum emission map at 1.3 cm (figure 4.3). We observe that the continuum emission peak does not coincide with any of the line emission peaks. In fact, the *central* and the *southern peaks* seem to form an arc around the continuum peak. Therefore, unlike in the case of $NH_3(6,6)$

(chapter 3), we can not find a clear relationship between the continuum and the line emission. As we reported in chapter 3, the continuum peak is likely a temperature peak since it is clearly detected in $NH_3(6,6)$, tracing material at $\sim$ 412K, but not in lower-excitation (and therefore, tracers of colder material) transitions.

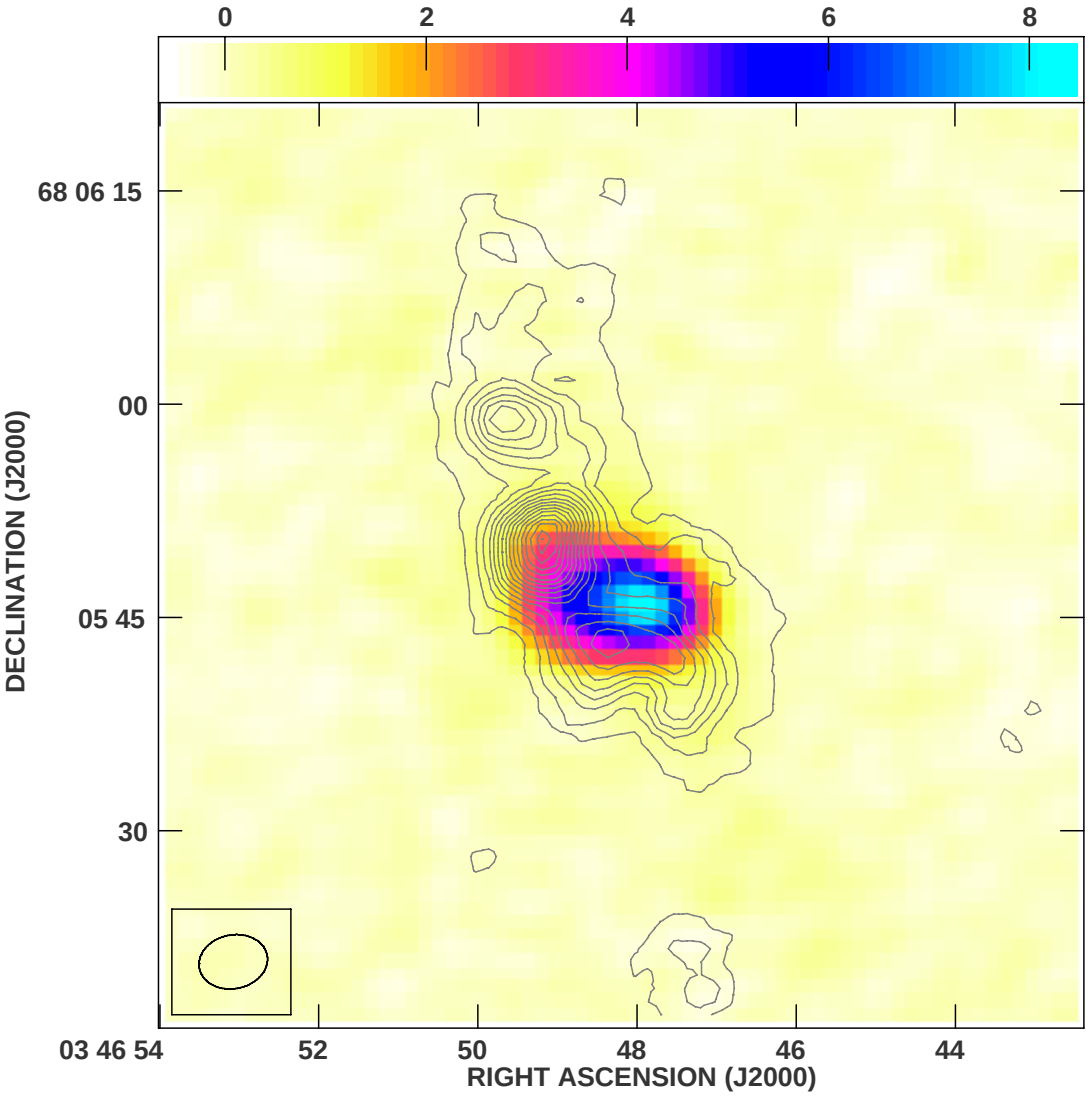

Figure 4.3: $NH_3(3,3)$ integrated intensity in contours. 1.3 cm continuum integrated intensity in false color-scale. Contour levels are as in figure 4.1. The false color-scale is in mJy beam^{-1}.

When comparing the $NH_3(3,3)$ emission map with the $NH_3(6,6)$ emission map from chapter 3 (figure 4.4, $NH_3(3,3)$ smoothed to the same resolution as $NH_3(6,6)$), we observe that the *central peak* coincides with what we called *line peak* in $NH_3(6,6)$ (chapter 3), whereas the other two peaks (even though the *southern peak* was smoothed away we can roughly guess its position) have no counterpart in the

(6,6) emission map. Both NH_3(1,1) and (2,2) appear to have a similar behavior to NH_3(3,3) (Ho et al., 1990). Due to the fact that NH_3(3,3) traces gas at $\sim$ 125 K and NH_3(6,6) at $\sim$ 412 K, this result seems to support the idea that the lack of emission in the continuum peak of low-temperature molecular lines is due to higher temperatures in the nucleus, not higher densities (Ho et al., 1990). To further investigate this assumption, we calculate the ratio of the NH_3(6,6) and (3,3) (figure 4.5). We can observe that the largest values of the ratio are reached in the inner part of the emission region, all around the two NH_3(6,6) central peaks (*line peak* and *continuum peak*). The largest ratios are located (apart from the *west peak*, not detected at all in NH_3(3,3)) in the location of the *continuum peak* and also north of the *northern peak*. This result suggests that the warmer gas is very centrally located in the nuclear part of IC 342, while the level of excitation and the temperature drops towards the minispiral. As expected, the concentration of higher-excitation gas is more remarkable in the position of the *continuum peak*, which coincides with the dynamical center of IC 342. This result is similar to what has been found in the Galactic center. We will discuss this further in the next section.

The rotational temperature can be calculated using the ratio of two NH_3 inversion lines. Because of the different orientations of the hydrogen spins in the NH_3 molecule, there are two spin states, "ortho" (K=3, all spins parallel) and "para" (K=3, all spins not parallel). The transitions between "ortho" and "para" states are very rare (Cheung et al., 1969). Therefore, calculating the rotational temperature using a mix of "ortho" and "para" species can produce a result that does not reflect the current conditions, but earlier ones, a problem solved using two species in the same spin state, like (3,3) and (6,6) (Ho & Townes, 1983).

When a system is in Local Thermodynamic Equilibrium (LTE), the relationship between two molecular transitions can be expressed by the Boltzmann equation:

$$\frac{n_1}{n_2} = \frac{g_1}{g_2} exp^{\frac{-\Delta E_{12}}{T_{ex}}} \tag{4.1}$$

where n_1, n_2 are the populations in levels 1 and 2, respectively, g_1 and g_2 are their statistical weights, T_{ex} is the excitation temperature and ΔE_{12} is the energy difference between the two transitions (in K).

The excitation temperature is then defined as:

$$T_{ex} = \frac{-\Delta E_{12}}{ln[\frac{n_1/g_1}{n_2/g_2}]} \tag{4.2}$$

.

For two rotation inversion transitions, such as in the case of the NH_3 molecule,

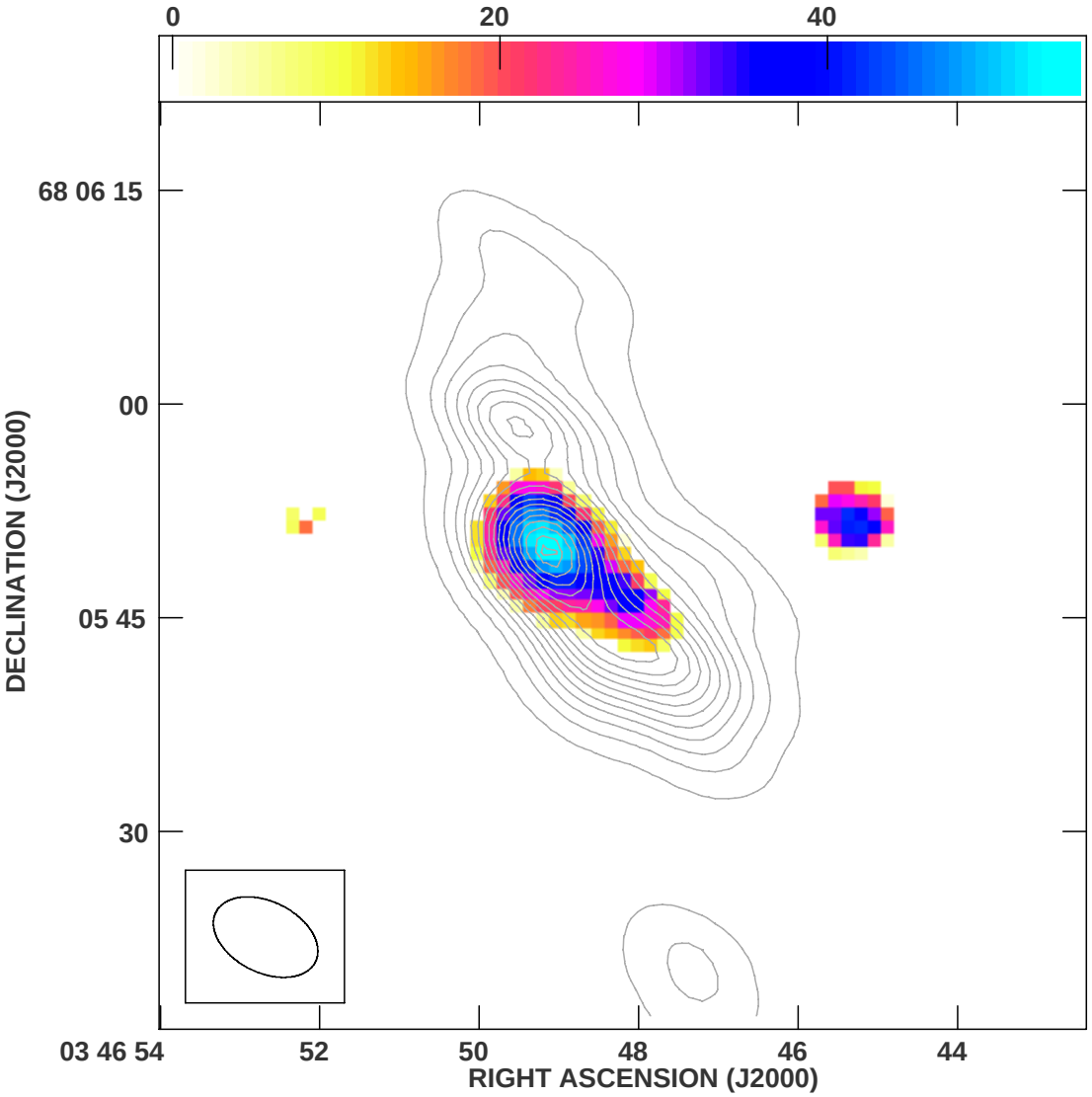

Figure 4.4: $NH_3(3,3)$ integrated intensity in contours. $NH_3(6,6)$ integrated intensity in false color-scale. Contour levels are in steps of 6σ, from 3σ to 93σ, except for the highest contour level, at 96σ (1.1×10^1 to 34.1×10^1 mJy beam^{-1} km s^{-1}). The false color-scale is in mJy beam^{-1} km s^{-1}.

the excitation temperature is the equivalent to the rotational temperature, therefore:

$$T_{rot} = \frac{-\Delta E_{12}}{ln[\frac{n_1/g_1}{n_2/g_2}]}. \tag{4.3}$$

The ratio of n_1/n_2 can be approximated to the ratio of the column densities N_1/N_2 if the emission from both transitions comes from the same region of the

cloud. The rotational temperature is then:

$$T_{rot} = \frac{-\Delta E_{12}}{ln[\frac{N_1/N_2}{g_1/g_2}]}. \tag{4.4}$$

The column density for the NH_3 is defined as:

$$N_{JK} = 4.1 \times 10^{-20}\, cm^{-2} \frac{\tau \nu^2\, T_{ex} \Delta v}{A_{10} k_{JK}}, \tag{4.5}$$

where k_{JK} is the fraction of molecules in the main line for the JK transition, A_{10} the Einstein coefficient in s^{-1}, ν the frequency in Hz, τ the opacity and Δv the linewidth in cm s^{-1}.

Because of the broad linewidths detected (figure 4.2), we can not separate the hyperfine components, therefore, we can not calculate the opacity. However, if we consider the line to be optically thin ($\tau \ll 1$) and the source to fill the beam, we can approximate:

$$T_{ex}\tau \cong T_b\,, \tag{4.6}$$

where T_b is the brightness temperature.

Applying equation 4.6 to equation 4.5, we obtain:

$$N_{JK} = 4.1 \times 10^{-20}\, cm^{-2} \frac{T_b \nu^2 \Delta v}{A_{10} k_{JK}}. \tag{4.7}$$

At the same time, the brightness temperature can be defined as:

$$T_b \;=\; \frac{\lambda^2}{2k\Omega} S_\nu\,, \tag{4.8}$$

where λ is the wavelength, k is Boltzmann's constant, Ω is the solid angle and S_ν the peak flux density.

If we apply equation 4.8 to equation 4.7 (assuming that both transitions have the same linewidth) and the result to equation 4.4, we can approximate the rotational temperature to (Estalella & Anglada, 1996):

$$T_{rot} = \frac{-\Delta E_{12}}{ln[\frac{g_2 A_{10_2} k_{22} S_{\nu_1}}{g_1 A_{10_1} k_{11} S_{\nu_2}}]}. \tag{4.9}$$

To calculate the rotational temperature for NH_3(6,6) and (3,3), we substitute: $\Delta E_{63} = 287$ K, $g_3 = 14$, $g_6 = 26$, $A_{10_3} = 2.56 \times 10^{-7}$ s^{-1}, $A_{10_6} = 3.38 \times 10^{-7}$ s^{-1}, $k_{33} = 0.894$ and $k_{66} = 0.969$.

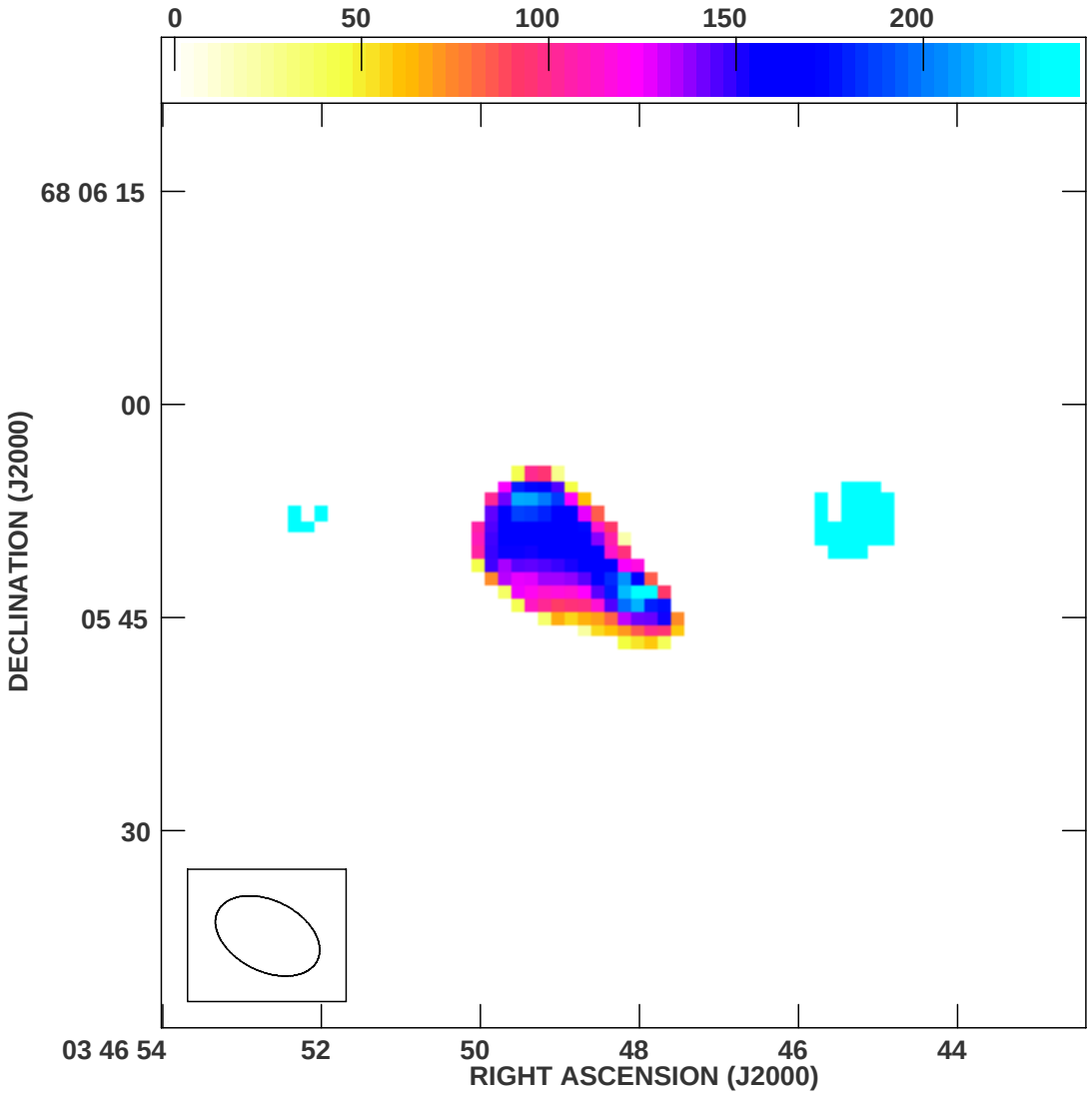

Figure 4.5: Ratio of NH_3(6,6) and NH_3(3,3) integrated intensity in IC 342. The range of values in the wedge is in terms of 10^{-3}.

In addition to the above difficulties, the calculation of the rotational temperature is hampered by the different spatial distribution of both transitions, therefore only

in a few places we can actually calculate the T_{rot}. Considering then that the gas is in LTE and is optically thin, we calculate a value of $T_{rot} \sim 120$ K at the location of the maximum ratio, i.e. the position of the *continuum peak*. Mauersberger et al. (2003) reported two different T_{rot} values in the nuclear region of IC 342. Transitions NH_3(1,1) to (3,3) adjusted to a 53 K value, while higher-excitation transitions, (5,5) to (9,9), required a much higher T_{rot}, 443 K. Martin & Ho (1986) found as well a lower value for the T_{rot}, 50 K. In order to obtain a more accurate value we need to be able to calculate the opacity of the line. However, the relative population of the hyperfine satellite lines compared to the main line for the NH_3(3,3) is only 0.008 (Townes et Schawlow, 1975), therefore, even in the case where the line-broadening is not so severe, measuring the emission from the satellite lines is a strenous task, since it is likely that they would not be above the rms noise level.

Because the transitions between metastable levels (J=K) can only occur due to collisions, the rotational temperature can also be a good approximation to the kinetic temperature, T_k (Ho, Martin & Barrett, 1981; Walmsley & Ungerechts, 1983). Ho, Martin & Barrett (1981) calculated, based on NH_3(1,1) and (2,2) observations, that the rotational temperature was 70% of the kinetic temperature for T_k = 30-100 K. Applying this approximation to our data, regardless the higher T_{rot} value, we obtain a value for the kinetic temperature of $\sim$ 170 K. Fittingly, the relationship between the obtained values of T_k and T_{rot} agrees with that calculated by Danby et al. (1988) for interstellar molecular clouds.

4.4.1 Comparison with the Galactic center

In the Galactic center, as well as in IC 342, the most highly-excited transitions of NH_3 are concentrated in the innermost part of the galaxy. Even though, because of the different distances to both sources (8 kpc to the Galactic center, Reid (1993)) we can not compare in terms of size of the nuclear regions, we can certainly draw similarities between the two sources.

As Herrnstein & Ho (2002, 2005) have demonstrated in the case of the Galactic center, NH_3(6,6) is concentrated close to the dynamical center of the Milky way, while the (3,3) transition is much more extended and is located further out from the supermassive black hole in the center. We observe a similar spatial distribution in IC 342 (figure 4.4). NH_3(3,3) is extended towards the minispiral, while NH_3(6,6) is much more compact and shows strong emission towards the dynamical center of IC 342, marked by the *continuum peak* (figures 3.1 and 4.3). Also, regarding the ratio, the points where S_ν(6,6) > S_ν(3,3) in the Galactic center are confined to the inner 2 pc, which represent the region inside the Circumnuclear Disk (CND), the molecular ring-like structure surrounding the nuclear stellar cluster and the super-

massive black hole in the Galactic center. In the case of IC 342, as we mentioned in the previous section, the points with the highest ratio are concentrated towards the dynamical center of IC 342, which agrees with the Galactic center results. However, we do not detect extremely large ratios, since the maximum is 0.24, while Herrnstein & Ho (2002) detected ratios up to 3.4, even though those were considered to be abnormally high due to line of sight absorption of the colder gas, NH_3(3,3). This lower (6,6)/(3,3) ratio in IC 342 is likely due to differential beam dilution effects, with the (6,6) having a smaller emitting area as compared to the (3,3).

Hüttemeister et al. (1993) suggested that the Galactic center ($4^\circ \times 1^\circ$) has a two-temperature gas composition, with $\sim 75\%$ of the molecular gas at ~ 25 K and the other 25% at ~ 200 K. The presence of multiple temperature components is consistent with the results of Herrnstein & Ho (2005) on the much smaller scale of the central 5 pc of the Milky Way. As we have seen in the previous section, the different temperature models for IC 342 seem to agree with a two-temperature component as well. Israel & Baas (2003) fitted the CO model to a gas composed in one third by cold, dense gas, while the rest of the molecular gas was hot and more diffuse, whereas Mauersberger et al. (2003) reported two different temperatures to explain the detections of the different NH_3 transitions in IC 342.

In summary, we can conclude that in the nuclear regions of both IC 342 and the Milky Way the molecular gas is centrally concentrated with multiple GMCs. We find that by comparing the HN_3(3,3) and (6,6) spatial distributions, heating is also concentrated towards the dynamical center of the galaxy.

4.5 Summary

We have successfully detected NH_3(3,3) emission in the nuclear region of IC 342 using the VLA. This is the first high-resolution detection of this ammonia transition in this nearby galaxy. We detect extended emission along the molecular ring and the minispiral. All seven GMCs as described by Downes et al. (1992) and Meier & Turner (2005) show a certain degree of emission, with GMC D, along the northern arm of the minispiral, the weakest of all. GMC C presents the strongest emission, coincident with NH_3(6,6) (chapter 3). In this location, a strong burst of star formation has been found, and therefore we can assume that the *central peak* is a column density and temperature peak. GMC A also shows strong emission in NH_3(3,3), but at the same time seems to be more susceptible to UV radiation penetration (Meier & Turner, 2005). This suggests that GMC A may be clumpy, dense and warm, where the radiation can penetrate to the inter-clump gas. We find GMC D' to be much stronger than GMC D, as it has been previously reported in other molecular tracers

such as N_2H^+ and shock tracers (Meier & Turner, 2005; Usero et al., 2006). GMC D' is located in a violent environment, where shock tracers are detected but no star formation has been detected in NIR observations. The molecular gas composing GMC D', although warm and dense, as expressed by the presence of NH_3(3,3), might be too exposed to the bar potential shear to be able to start a star formation process.

We find that the NH_3(3,3) line emission is not well correlated with the continuum emission at 1.3 cm. Because the continuum peak coincides with the dynamical center of IC 342, the result indicates that only the warmest gas, as traced by NH_3(6,6) (chapter 3), is spatially close to the supermassive black hole suggested to be in the center of IC 342 (Böker et al., 1999), as it is the case in the Galactic center (Herrnstein & Ho, 2002, 2005).

Comparing the NH_3(3,3) and the (6,6) data from chapter 3 we observe a different distribution of the two transitions, with the one tracing warmer gas, (6,6), being more concentrated towards the dynamical center than the one tracing colder gas, (3,3). We have not detected any correlation between the NH_3(3,3) emission and the (6,6) emission in the *west peak*. As we remarked in chapter 3, the *west peak* could be the location of very warm gas that can not be detected by lower temperature transitions due to line of sight absorption. We have also calculated the T_{rot} of the molecular gas, obtaining a 120 K value. This result is larger than the results obtained in previous single-dish observations. However, different models (Mauersberger et al., 2003; Israel & Baas, 2003) suggest that the molecular gas in the nuclear region of IC 342 might be composed by gas at two different temperatures, and we could have detected the higher temperature component.

The comparison between the different characteristics found in our study of the nuclear region of IC 342 and the Galactic center, suggests that both sources have indeed a lot of common trends. The distribution of high-density, high-temperature molecular gas with respect to lower temperature, but equally high-density gas in the central regions is similar in both sources. Moreover, the two-temperature component that best describes the behavior of the gas in the innermost regions is a common characterictic as well. Therefore, IC 342 has proved to be an invaluable instrument for the study of nuclear regions of spiral galaxies not only by itself, but also because of the implications of this research can have on our understanding of the Galactic center.

Chapter 5

Summary, Conclusions and Future Work

5.1 Summary

Two different but related studies have been undertaken in this work. The common goal has been the comprehension of the geometry, kinematics and excitation conditions of galactic nuclei. This study has been carried out through the observation of highly-excited transitions of high-density molecular tracers because of the well-known characteristics of the ISM present in nuclear environments, dense, warm and turbulent. In order to achieve the required high-resolution for this systematic study, we have made use of two interferometers, the Submillimeter Array (SMA) and the Very Large Array (VLA). This study could not have been conducted before because of the lack of proper instrumentation.

In the first place, we have studied the Galactic center and the interactions taking place between the different structures present in the inner 2 pc and the supermassive black hole located in the dynamical center of the Milky Way. This project has been carried out observing HCN(4-3) and CS(7-6) in the central region of our Galaxy using the SMA. In the second place, in order to further investigate the processes

taking place in a galactic nucleus, we have expanded the research to a nearby face-on galaxy, IC 342, proved to be strikingly similar to the Milky Way in terms of gas distribution, IR luminosity and presence of a nuclear star cluster. Although the dimensions we work with are different, previous studies have found IC 342 to be a likely comparison companion to the Milky Way where the nuclear features located in the Galactic center are found in a larger scale. This study has been conducted through the observation of two different inversion transitions of NH_3 using the VLA, equipped with newly retrofitted antennas during part of our study, and with upgraded K-band receivers all along.

The study of the Galactic center has shown the presence of very dense and clumpy gas in the inner region of the Milky Way, mostly concentrated along the circumnuclear disk (CND). However, the neutral gas in the CND has not homogeneous characteristics along the ring-like structure, but it shows changes in density, temperature and excitation conditions. The common rotation pattern around the supermassive black hole seems to link all the molecular gas detected in the CND, but the individual clumps are experiencing different processes. The inner part of the CND is being excited by the nuclear stellar cluster located in the cavity it is surrounding, while the outer part of the CND remains mostly unaffected. At the same time, the ionized gas composing the minispiral, that seems to be accreting towards Sgr A*, is interacting with the CND in some regions, even filling a gap found in the northern part of the CND. Comparisons with other molecular tracers have shown that the gas forming the CND is denser but colder than the gas detected inside the cavity. Also, because of the individual nature of the clumps, we have found that the CND itself is colder and less dense towards the north than towards the south. A possible connection between the outside GMCs, the CND and the inner molecular gas should be studied with great care, since the molecular neutral gas inside the cavity seems to be approaching Sgr A*, without an apparent connection to the minispiral. The clumpy nature of the CND has raised the question of whether the structure is transient or long-lived. Our calculations have confirmed the stability of the CND, since the individual clumps have proved to be dense enough to withstand the gravitational pull produced by the supermassive black hole. Furthermore, the amount of time needed, for even a few percent of the mass composing the CND, to be accreted by Sgr A* (based on the amount of material composing the CND and the infalling rate towards Sgr A*) is much longer than the rotational period of the CND, therefore, the clumps can circle the black hole without being completely stripped out in the meantime. In summary, the CND, while formed by material concentrated in individual clumps, is a stable structure rotating around Sgr A*.

To expand the study of galactic nuclei, we have observed NH_3(3,3) and (6,6) in the nuclear region of IC 342 (inner $\sim$ 800pc). NH_3 is a high-temperature molecular tracer. The nuclear region of IC 342 has proved to possess similar characteristics to the Galactic center, where previous studies of both transitions have provided

inestimable results. The extent of the warmer molecular gas (as traced by NH_3(6,6)) is much more reduced than the gas distribution detected with the lower transition, (3,3). While (6,6) is mostly concentrated towards the dynamical center of the galaxy and the molecular ring, (3,3) is more spread out, even showing strong detection towards the arms of the minispiral. NH_3(3,3) is not detected towards the dynamical center of IC 342, prompting the connection to the Galactic center results, where the warmer gas is located closer to the center than the colder gas, as we could see in the first part of this work. At the same time, the strong detection of both transitions at locations where NIR studies have not shown any star formation activity, indicates that NH_3 is a valuable tracer of high-temperature and high-density gas, but not of star formation per se. However, by detecting two inversion transitions, we have been able to calculate the rotational temperature of the gas in the nucleus of IC 342. The result we have obtained, $T_{rot} = 120$ K, and the comparison with previous studies, have suggested that the nuclear gas distribution in IC 342 is better explained by the presence of two gas components, each defined by a different temperature, with our results showing the warmer component. Studies in the Galactic center have confirmed a similar situation. Finally, we have detected emission from warm gas at a location separated from the center of IC 342, visible only in NH_3(6,6). The lack of detection in other molecular tracers, and even in the lower transition, (3,3), suggests a case of absorption along the line of sight by cool foreground clouds.

In summary, the detection of three high-density, high-temperature molecular tracers in different highly-excited transitions, both in the Galactic center and IC 342, has firstly confirmed the presence of very dense gas in the inner regions of both galaxies. Moreover, the warmer and dense molecular gas is located closer to the dynamical center in both cases, more so than the colder gas, which is rotating around the very center. In the case of the Milky Way, this colder and denser gas, which has formed a long-term structure, in spite of the gravitational pull of the supermassive black hole, could be interacting with the warmer gas which seems to be approaching Sgr A*. Obviously, we can not make such a statement for IC 342, since the larger distance to the source prevents us from obtaining a sharper image of the inner parsecs. However, the similar density and temperature-related molecular gas distributions in both galaxies, and the two-temperature gas component model that best describe them, clearly show that both sources are intimately related and together can provide a deeper understanding of galactic nuclei.

5.2 Conclusions

In the following sections, a summary of the conclusions already expressed in the previous chapters is presented. The conclusions are separated into two groups, attending to the source in consideration. However, as we have already mentioned, the results are complementary, since both sources are closely connected.

5.2.1 Galactic center

- ⋆ Highly-excited transitions from two high-density tracers, HCN(4-3) and CS(7-6), have been successfully detected within 2 pc of the supermassive black located in the dynamical center of the Milky Way using the SMA.
- ⋆ Both molecular tracers, HCN(4-3) and CS(7-6), are strongly detected in the southern part of the CND, and more scarcely in the northern part, especially CS(7-6).
- ⋆ The molecular distribution along the CND suggests a different excitation level in the northern and southern parts of the CND, with the northern part less dense and colder than the southern part.
- ⋆ The southeastern part of the CND, the *southern extension*, is the densest region in the CND, whereas the *southwest lobe* appears warmer but more diffuse. The *southern extension* could be spiraling inwards towards the central supermassive black hole, becoming more diffuse in the process.
- ⋆ The inner side of the CND is more highly excited than the outer side, most likely because of radiation from the nuclear stellar cluster.
- ⋆ There seems to be an interaction between the CND and the minispiral. Line-broadening is observed in the regions where the CND and the minispiral spatially coincide. Furthermore, there is a "gap" in the northern region of the CND that is filled by the northern arm of the minispiral.
- ⋆ The CND has a clumpy morphology, composed by clumps of varying sizes, from $3''$ to $13''$.
- ⋆ The clumps are dense enough to overcome the tidal shear from the central supermassive black hole ($n_{H_2} > 1.4 \times 10^7\,\mathrm{cm}^{-3}$). At the same time, the rotation time of the CND is much shorter than the time needed for the material composing the CND to infall towards Sgr A* (8×10^4 yr vs. 9×10^6 yr, infalling rate 1.5×10^{-2} $\mathrm{M}_\odot$ yr^{-1}). Therefore, the CND would be a long-term structure.

⋆ The results suffer from lack of short-spacings, especially towards the southern part of the CND. However, the missing extended emission does not greatly influence the final outlook of the CND, therefore, the emission is dominated by the clumps.

5.2.2 IC 342

⋆ Two transitions of a high-density and high-temperature tracer, NH_3, have been detected in the nuclear region of the nearby galaxy IC 342.

⋆ The higher-excitation transition, $NH_3(6,6)$, has been found mostly concentrated towards the dynamical center of IC 342. Three strong emission peaks have been detected in $NH_3(6,6)$: the *(6,6) peak*, the *continuum peak* and the *west peak*.

⋆ The *continuum peak* coincides with the 1.3 continuum emission peak and it is close enough to the 6 cm continuum emission peak to consider it correlated. This emission peak does not coincide with any of the GMCs previously described in various molecular tracers and no star formation process has been detected. The *continuum peak* is considered a temperature peak and the lack of correlation with other lower-temperature tracers suggests that the vicinity of the dynamical center is occupied by very hot gas.

⋆ The *(6,6) peak* is located at the position of a star formation GMC, GMC C. GMC C is found in the region where the molecular ring surrounding the nuclear region of IC 342 meets the arms of the minispiral, which are composed by material flowing inwards. The *(6,6) peak* is considered a column density and temperature peak.

⋆ The *west peak* is located in a region further west from the dynamical center, isolated. No previous detection of this peak have been reported neither in lower temperature tracers nor in continuum observations. Therefore, the peak could be composed by high-temperature gas and absorption along the line of sight might be responsible of the lack of detection in other tracers, a situation also found in the Galactic center.

⋆ $NH_3(3,3)$, tracing gas at $\sim$ 125 K, has been found in a more extended area than $NH_3(6,6)$. Three emission peaks have been detected: the *northern peak*, the *central peak* and the *southern peak*.

⋆ The *central peak* is the strongest peak in $NH_3(3,3)$ and has been detected at the location of GMC C. The peak position coincides with that of the strongest

peak in NH_3(6,6). This detection further supports the idea of the *central peak* being a temperature and column density peak.

- ⋆ The *northern peak* is located in the northern arm of the S-shaped large scale stellar bar of IC 342 and coincides with the position of GMC D'. GMC D' is located in a turbulent environment, along the leading edge of the northern arm of the bar, and although formed by warm and dense material, it seems not to be undergoing star formation as a result of the tidal shear from the bar potential.

- ⋆ The *southern peak* coincides with the location of GMC A, and it is not experiencing a burst of star formation. GMC A seems to be especially clumpy, formed by dense and warm clumps of material, with the inter-clump gas diffuse enough for the UV radiation from the nuclear stellar cluster to penetrate.

- ⋆ The lack of emission in NH_3(3,3) in the dynamical center of IC 342 suggests that the material in the inner region is very warm, but not necessarily denser than in other areas, as it has been proved in the Galactic center.

- ⋆ The *west peak* detected in NH_3(6,6) has no counterpart in (3,3), probably because of absorption along the line of sight by cool foreground clouds.

- ⋆ The rotation temperature calculated using both ortho transitions is $\sim$ 120 K. The value of the kinetic temperature can be deduced from the rotational temperature to be $\sim$ 170 K. The gas distribution in the nuclear region of IC 342 seems best fitted by a two-temperature gas component model.

The comparison between the characteristics of the Galactic center and those of the nuclear region of IC 342 prove that both sources have several similarities and can be combined to provide a more comprehensive understanding of the geometry, dynamics and excitation conditions of galactic nuclei.

5.3 Future Work

Many questions remain unanswered regarding the morphology, dynamics and kinematics of galactic nuclei. In the first place, we still do not know how exactly the material reaches the inner parsecs of the galaxies, although large-scale stellar bars seem to be effective instruments to carry material towards the center. However, only in the case of the Milky Way we are able to observe the very center of a galaxy, down to the innermost parsecs. The gas present in this central region might be

undergoing an accretion process towards the supermassive black hole. Nonetheless, the intricacies of the process, whether the gas is directly dragged inwards or circles Sgr A* before actually falling inside, how long that circling process takes, can stable orbits form around the supermassive black and many other questions are still being discussed. For this reason it is important to continue the study of the Galactic center with the help of a number of molecular tracers, especially highly-excited high-density molecular tracers since, as it has been proved, the characteristics of the nuclear ISM are favorable to the presence of this kind of material. At the same time, the advent of high resolution instruments in the latter years, such as the SMA, CARMA (as well as the newly retrofitted VLA) and, in the near future, ALMA, have greatly improved our understanding of galactic nuclei and will continue to do so. Molecular species that were previously detected by single-dish observations, can now be resolved, providing a comprehensive image of the morphology of the central regions of galaxies and, by extension, of their kinematics and dynamics.

An interesting project to undertake would be the quest for molecular gas inside the inner cavity of the Milky Way. This would help to better understand the physical characteristics of the molecular gas located in close proximity to a supermassive black hole. At the same time, the potential detection of molecular gas in the innermost parsecs would redefine the accretion models and drive a reconsideration of the "feeding" process undergone by the black hole, since not only the ionized gas from the minispiral would account for the accreted mass.

The detection of ionized molecular species in the Galactic center, further away from the nuclear stellar cluster, would be the next step. The presence of ionized gas in the CND could better explain its mass distribution, since if the radiation is able to penetrate, the density of the region should be low enough for the absorption by the dust to be negligible. Identifying the regions where the density is at its lowest, and their relationship with the inner minispiral, could provide some understanding of the interactions taking place in the CND, whether the mass is being accreted into the black hole. Precise steps have already been taken in this direction, as it is reported in appendix A.

Furthermore, the study should be expanded outwards, to include the molecular structures already detected in $NH_3(3,3)$ in the inner 10 pc. The possible interaction between these structures and the CND is still questionable. The combination of those data with the mass distribution results from the previous potential study could explain if the regions of the CND where the mass density is higher are related to the external GMCs and if so, whether the material is accumulating because the GMCs are acting as reservoirs.

In the case of IC 342, a similar study to the one developed for the Galactic center, combining the results from high-temperature tracers as compared to those provided by high-density tracers, and the implications of this relationship should be the next

logical step to follow. A better comprehension of the chemical differentiation of the gas distribution, whether it is driven by the dynamics of the inner parsecs, which could be the explanation for the warmer gas located closer to the dynamical center, or the consequence of an intrinsic different composition, or both, can contribute to the understanding of the processes implied in the gas dragging towards the center and the ultimate end of this material. At the same time, the comparison of the results with those for the Galactic center can provide, once more, a more complete picture of the interactions happening in nuclear environments.

Appendix A

Mapping the CND

A.1 Abstract

We report the first interferometric detection of HCN(3-2) and HCO^+(3-2) within 2 pc of Sgr A*, made with the compact configuration of the SubMillimeter Array (SMA). Because of the not so good quality of the data, we show these results as an appendix, since it is still a work in progress. We aim to continue this study with new data that will improve the uv coverage, and therefore the resolution. Only one track has been obtained so far and, as can be seen because of the excellent results shown in chapter 2, more integration time is needed, as well as the addition of a subcompact configuration observation.

A.2 Observations

Observations of HCN(3-2) ($\nu = 265.886180$ GHz) and HCO^+(3-2) ($\nu = 267.557625$ GHz) were made with the Submillimeter Array (SMA) in the compact configuration on 2006 July 29. We produced a 16-pointing mosaic (figure A.1), covering a $\sim 2' \times 2'$ area around Sgr A*. The minispiral and the CND were well within the region. The

pointings were placed at half-beam spacings (the primary beam for these frequencies is 47″). The data consisted of two 2 GHz bandwidths, upper sideband (USB) and lower sideband (LSB), divided into 24 spectral windows, each of them composed by 128 channels with a velocity resolution of 0.92 km s^{-1}. Due to the proximity of the two molecular lines in the bandwidth, they were both observed in the lower sideband (LSB). The velocity coverage was from -1996 km s^{-1} to 239 km s^{-1}, centered on the HCN(3-2) line at $v_{LSR} = 0$ km s^{-1}. We averaged every 5 km s^{-1} because of the broad nature of molecular lines in close proximity to Sgr A*. The continuum subtraction was performed in the uv plane, using channels on both sides of the molecular lines. The total integration time per pointing varied from 5 to 10 minutes. However, due to the half-beam spacing distribution, the total integration time for the central 1′ was in fact 25 minutes. The flux calibrator was Callisto and the phase calibrator was 1924-292, with a flux value of 2.59 Jy.

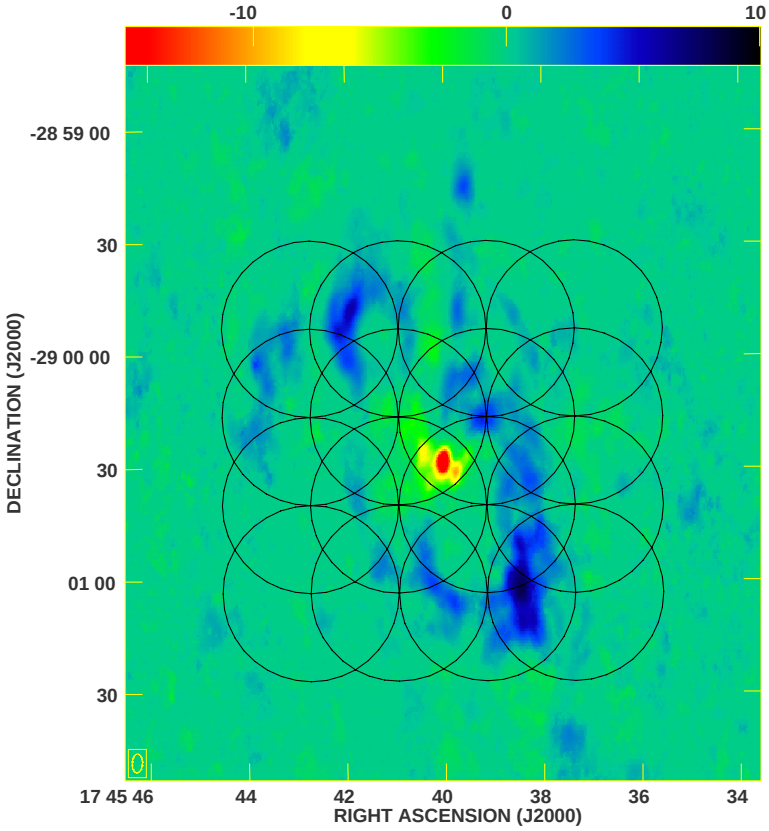

Figure A.1: 16-pointing mosaic. The background image is HCN(1-0) from Christopher et al. (2005). Sgr A* is seen in absorption.

The data were calibrated using the MIR software package, and the imaging process was done using both the Multichannel Image Reconstruction Image Analysis and Display (MIRIAD) and the NRAO Astronomical Imaging Processing System (AIPS). The reduction and imaging processes were extensively described in

chapter 2, therefore we do not repeat the explanation here, only the dissimilarities. The integrated intensity maps were produced using a minimum flux cutoff of 1.2 Jy beam^{-1}for HCN(3-2) and 1.1 Jy beam^{-1}for HCO$^+$(3-2). Natural weighting of the uv data produced an image with a synthesized beam of $6.9'' \times 2.6''$ and a position angle of 41.1°.

The final RMS per channel is 0.3 Jy beam^{-1}and the overall achieved RMS sensitivity is 6.0 Jy beam^{-1}kms^{-1} for HCN(3-2) and 0.2 Jy beam^{-1}and 1.4 Jy beam^{-1}kms^{-1} for HCO$^+$(3-2).

A.3 HCN(3-2)

We detect HCN(3-2) within 2 pc of Sgr A* (figure A.2). The emission is very strong towards the south, and barely noticeable towards the north. This result is not surprising considering previous reports on emission in the Galactic center. Both previous observations of HCN(3-2) (Jackson et al., 1993; Marshall et al., 1995) and other transitions, HCN(1-0) (Güsten et al., 1987; Wright et al., 2001; Christopher et al., 2005) and HCN(4-3) (Marshall et al. (1995) and chapter 2), suggest the southern part of the CND to have stronger emission than the northern part. The emission is very clumpy all along the CND, formed by a group of small structures, clumps, connected between each other in the southern part and more scattered towards the north.

We observe strong emission towards the south of the CND main structure (we will name it *southern arc*). This structure has not been detected before neither in HCN(1-0) nor in HCN(4-3) (in both cases the map coverage was similar to the HCN(3-2) coverage). Previous HCN(3-2) single-dish observations barely cover that south of the CND, therefore we have not counterpart to compare our data with, and certainly not with similar angular resolution. Concerned that this detection could be an artifact, we plotted the spectra at the "troubled" locations (spectra I and J) and observed very strong peaks, especially in spectra J (figure A.3). We can also observe other characteristics from the spectra at the different clumps. First, we can see that the rotation pattern is clearly detected, with spectrum B and G at opposite sides of the velocity range. Next, we observe that the *southern extension* (using the same nomenclature that Christopher et al. (2005)) harbors the strongest peak, but unlike what we detected in HCN(4-3) (chapter 2), the *southwest lobe* is much weaker than the *southern extension*. We can also clearly see that the "70 km s^{-1} cloud" is detected in HCN(3-2) (spectrum E), easily spotted because of the narrow spectrum. Spectrum A is very narrow as well, but unlike spectrum E, it is taken at a greater distance from Sgr A*, in what we have called the *northeast arm* (chapter 2), where,

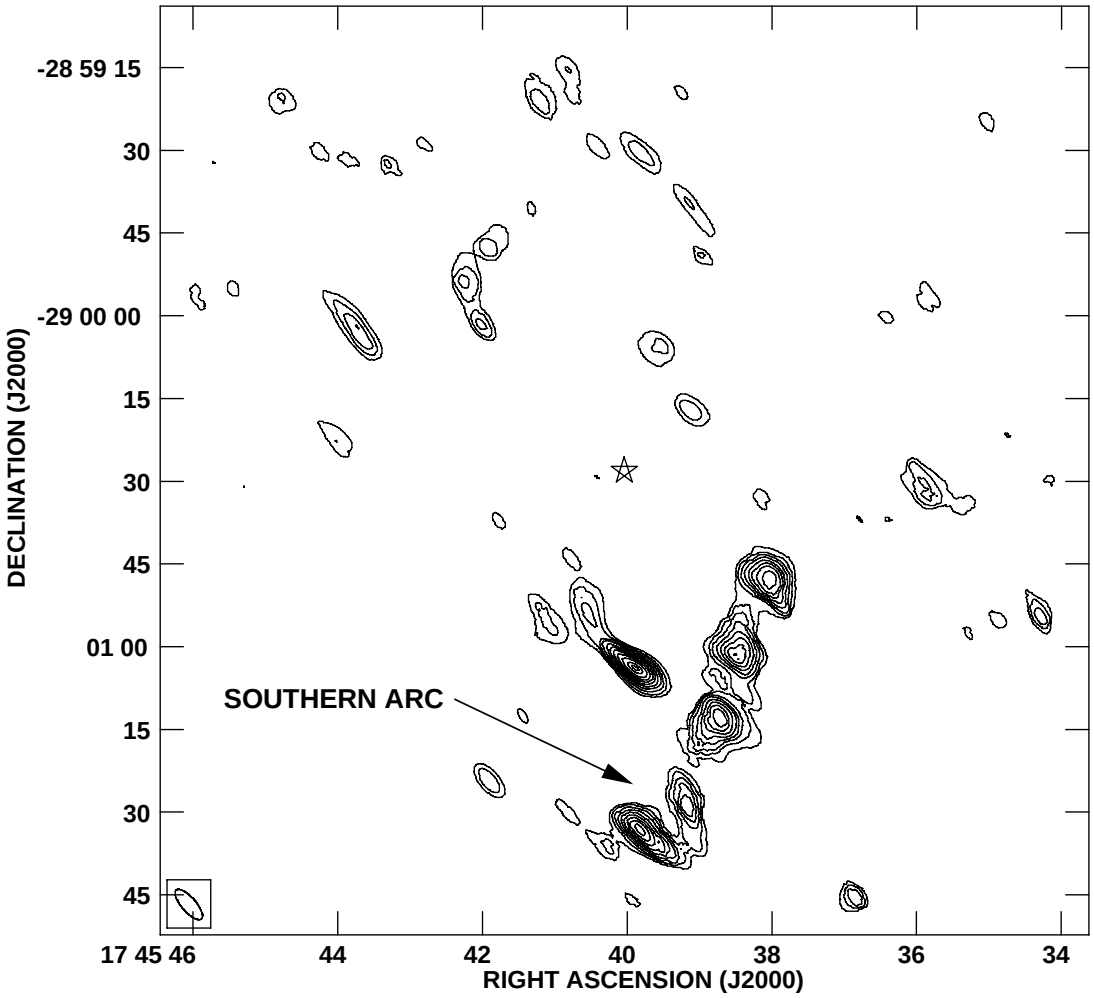

Figure A.2: HCN(3-2) integrated intensity in contours. Contour levels are in steps of 3σ, from 3σ to 42σ (1.9×10^1 to 25.3×10^1 Jy beam^{-1} km s^{-1}). Sgr A* is marked with a star.

as we observed in HCN(4-3), the material seems to be less exposed to the gravitational pull of the supermassive black hole, therefore presenting narrower features in the spectrum because of the weaker interaction. Both spectra F and H show a remarkable similarity, with an absorption feature around $\sim$0 km s^{-1}. As Güsten et al. (1987) noticed, there is a foreground cloud around that velocity, producing narrow absorption features. That absorption is really noticeable in HCN(1-0) data, but not as worrisome in higher-excitation lines, as Jackson et al. (1993) and Marshall et al. (1995) have previously remarked. The fact that both spectra F and H are so similar might indicate that they are sidelobes of spectrum G, however, we know from other molecular tracers (HCN(4-3) and CS(7-6), chapter 2) that there is strong emission in the location of clump F.

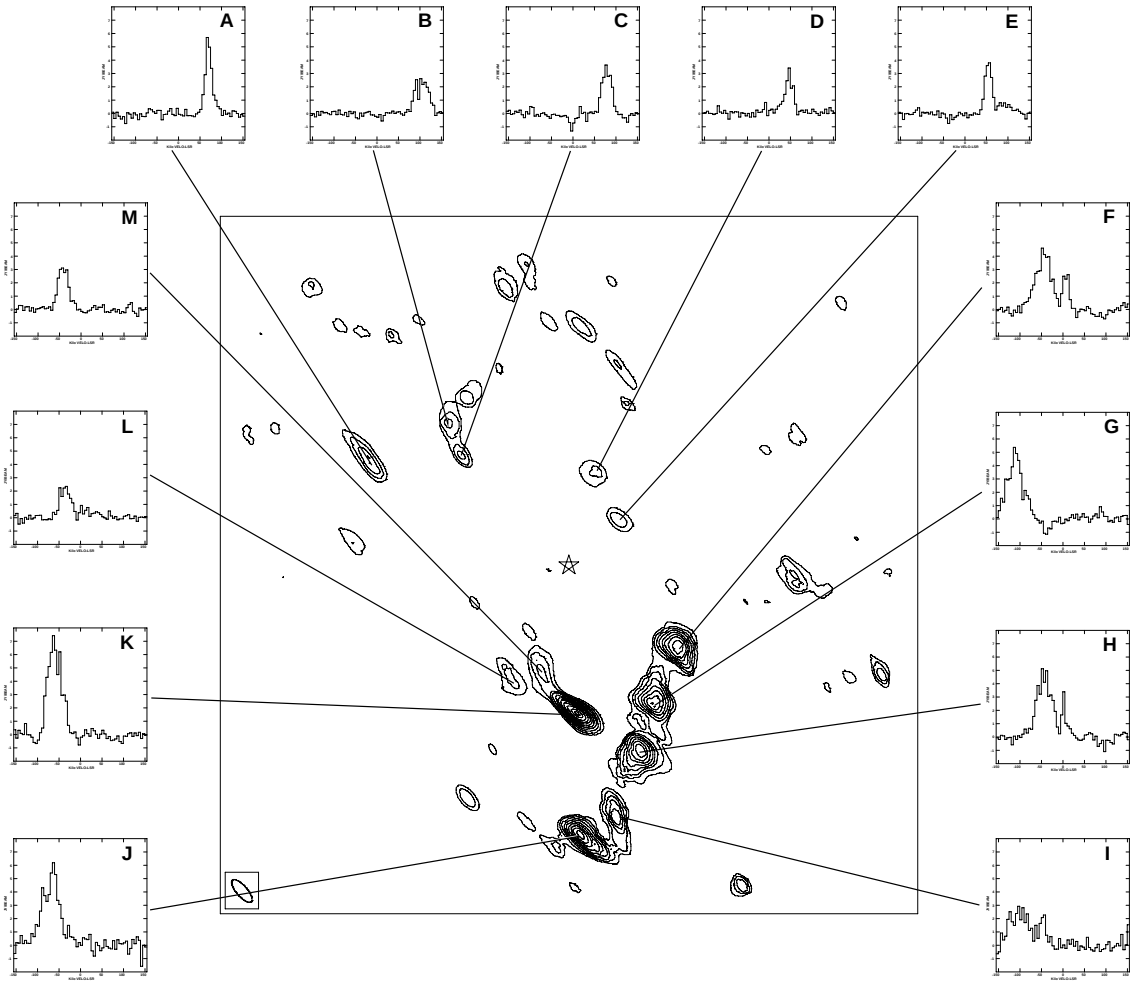

Figure A.3: HCN(3-2) spectra measured at the positions of the different clumps. Sgr A* is marked with a star.

Comparing our data with HCN(1-0) from Christopher et al. (2005) (after smoothing both maps to the same resolution), we observe that both transitions correlate very well, even towards the north of the CND, where HCN(3-2) is very faint (figure A.4). We see a good correlation along the *southwest lobe*, the *southern extension*, the *northeast lobe* and the *northeast arm* (see figure 2.2 for the different features). The fact that the higher-excitation transition is stronger along the southern part of the CND was already observed when using an even higher transition, HCN(4-3) (Marshall et al. (1995) and chapter 2). However, HCN(1-0) is not detected in the *southern arc*. One possible answer to this lack of detection could be that the gas towards the southern part of the CND is warmer and the material is mostly more excited, but not enough for HCN(4-3) to be detected. In order to check that possibility we compare the HCN(3-2) with NH_3(3,3) from McGary et al. (2001) (figure A.5). NH_3(3,3) traces gas at $\sim$ 125 K and it is mostly concentrated towards the south of the CND. There is strong NH_3(3,3) emission in the *southwest lobe* and also

the *northeast arm*, but the vast majority of the emission comes from the *southern streamer*, that connects the CND to the "20 km s^{-1} cloud". The *southern arc* does not coincide with the *southern streamer*, although it looks like both features could interact, but this could simply be a projection effect. When we compare the spectrum at the *southern streamer* (figure 8, spectrum K in McGary et al. (2001)) and at the *southern arc* (spectrum J) they are indeed different, therefore they seem to be tracing completely unrelated material. However, low-resolution data from Jackson et al. (1993) seemed to detect emission connecting to the *southern streamer*. A more detailed study of the southern region of the CND is surely a good follow-up to our results.

The comparison of HCN(3-2) and HCN(4-3) shows good correlation between the two maps (figure A.6, both maps smoothed to the same resolution). The emission peaks coincide in the *southwest lobe* and the *southern extension* and even in the *northeast lobe*, with a similar relationship between the strength of the peaks in the southern and the northern parts of the CND. As mentioned before, the *southern arc* has not been detected in HCN(4-3), as it is apparent in the figure. However, HCN(4-3) seems to show some faint emission towards that direction, although not nearly as southern-extended. The nature of the *southern arc* remains uncertain for now.

A.4 HCO^+(3-2)

HCO^+(3-2) is observed mainly along the southern part of the CND (figure A.7), mostly concentrated in the *southern extension*, and much weaker in the *southwest lobe* than HCN(3-2) (figure A.2) and HCN(4-3) (figure 2.2). Because of the distribution of both HCN(3-2) and HCO^+(3-2) in the LSB, HCO^+(3-2) could only be observed at the very edge of the bandwidth. Therefore, the velocity range was not as wide as for the HCN(3-2) line, covering only from -103 to 150 km s^{-1}, which can be observed in the spectra in figure A.8. For this reason, the emission detected in peak F is much weaker than expected. Observing spectrum E and comparing it with the profiles at that same position in HCN(3-2) (figure A.3) and HCN(4-3) (figure 2.4) we notice that the location of peak E is the most blueshifted, with a peak around $\sim$ -105 - 110 km s^{-1}, a range of velocities out of reach in our HCO^+(3-2) data. It is important to keep this circumstance in mind when studying our results.

We can observe in figure A.7 that the "70 km s^{-1} cloud" is not detected in HCO^+(3-2), unlike HCN(3-2), HCN(4-3) and CS(7-6) (see chapter 2). Marr et al. (1993) and Wright et al. (2001) had previously reported that the "70 km s^{-1} cloud" was detected in HCN(1-0), but not in HCO^+(1-0). We can confirm that in a even

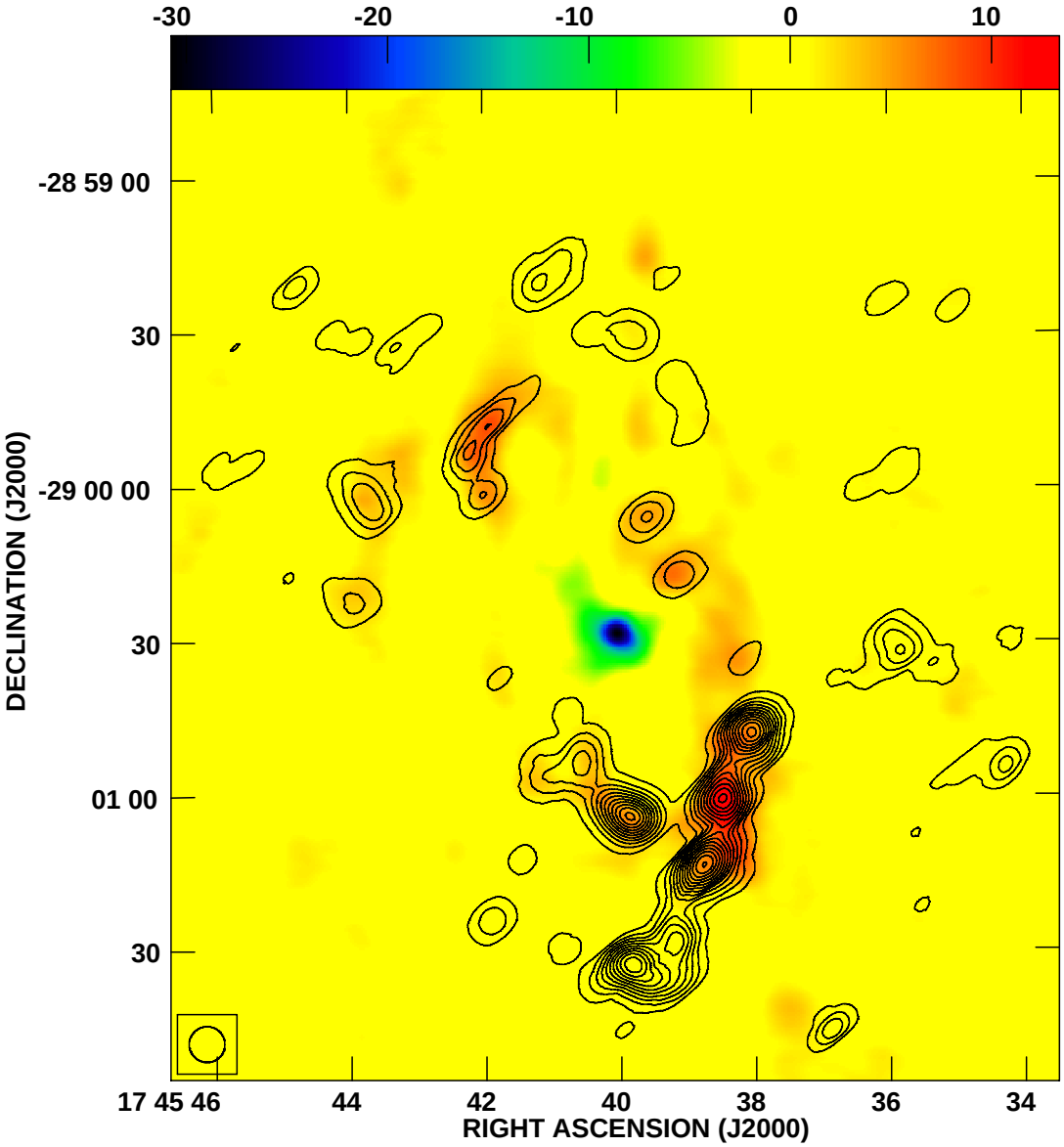

Figure A.4: HCN(3-2) integrated intensity in contours. HCN(1-0) integrated intensity in false-color scale from Christopher et al. (2005). Contour levels are in steps of 6σ from 3σ to 75σ (1.7×10^1 to 41.8×10^1 Jy beam^{-1} km s^{-1}). The false color-scale is in Jy beam^{-1} km s^{-1}. Sgr A* is seen in absorption in HCN(1-0).

higher-excitation transition line, the "70 km s^{-1} cloud" is not detected. However, we do detect a different feature outside of the main CND body, clump C, with a very narrow profile. Clump C coincides with the position of the *linear filament* (using Christopher et al. (2005) nomenclature, figure 2.2), which was not detected in HCN(3-2), but it was in HCN(4-3). The *linear filament* is situated in the same location that what has been described as the northernmost connection between the

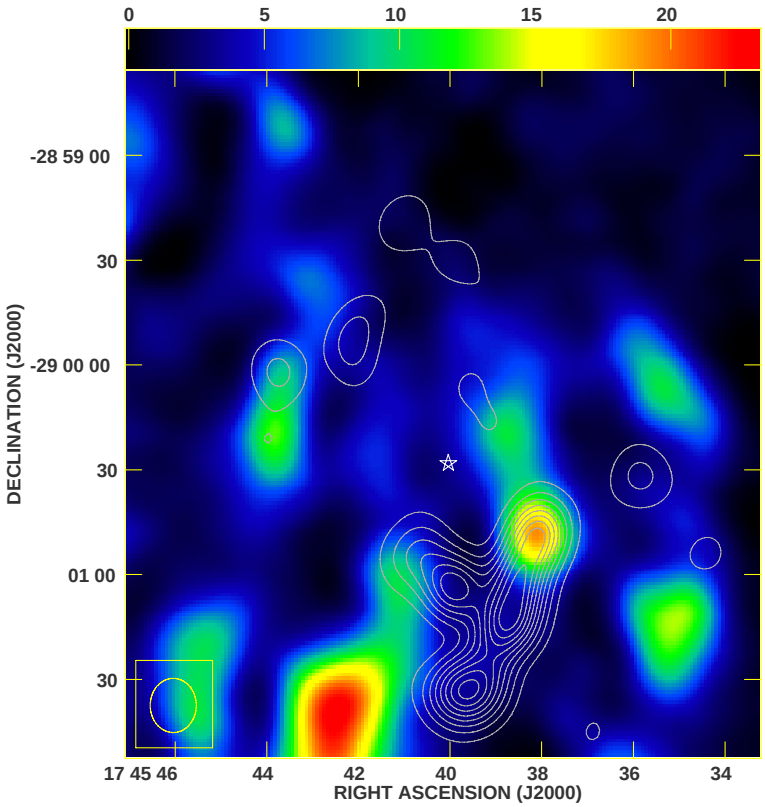

Figure A.5: HCN(3-2) integrated intensity in contours. NH_3(3,3) integrated intensity in false color-scale from McGary et al. (2001). Contour levels are in steps of 10% of the intensity peak, from 6.7×10^1 to 61.8×10^1 Jy beam^{-1} km s^{-1}. The false color-scale is in Jy beam^{-1} km s^{-1}. Sgr A* is marked with a star.

CND and the *western streamer* (McGary et al., 2001), a long south-north feature detected in NH_3(3,3). However, position-velocity diagrams in NH_3(3,3) could not find an obvious connection between the CND and the *western streamer* (McGary et al., 2001). Christopher et al. (2005) observed the *linear filament* in HCN(1-0), but remained undetected in HCO^+(1-0). We can also detect emission in what we have called the *northeast arm*. Very narrow profiles are detected in both clumps A and J, probably due to their larger distance from Sgr A*. (figure A.8).

The strongest emission comes from the *southern extension* (clump I, figure A.8), but, as mentioned before, we are losing part of the emission from the *southwest lobe*. Therefore, it is impossible to judge whether the HCO^+(3-2) could have been stronger there or not. Also, we detect the same problem than in HCN(3-2), spectra D and F are very similar, maybe sidelobes?

When comparing HCO^+(3-2) and HCO^+(1-0) (figure A.9, HCO^+(3-2) and HCO^+(1-0) smoothed to the same resolution) we observe the good correlation between both

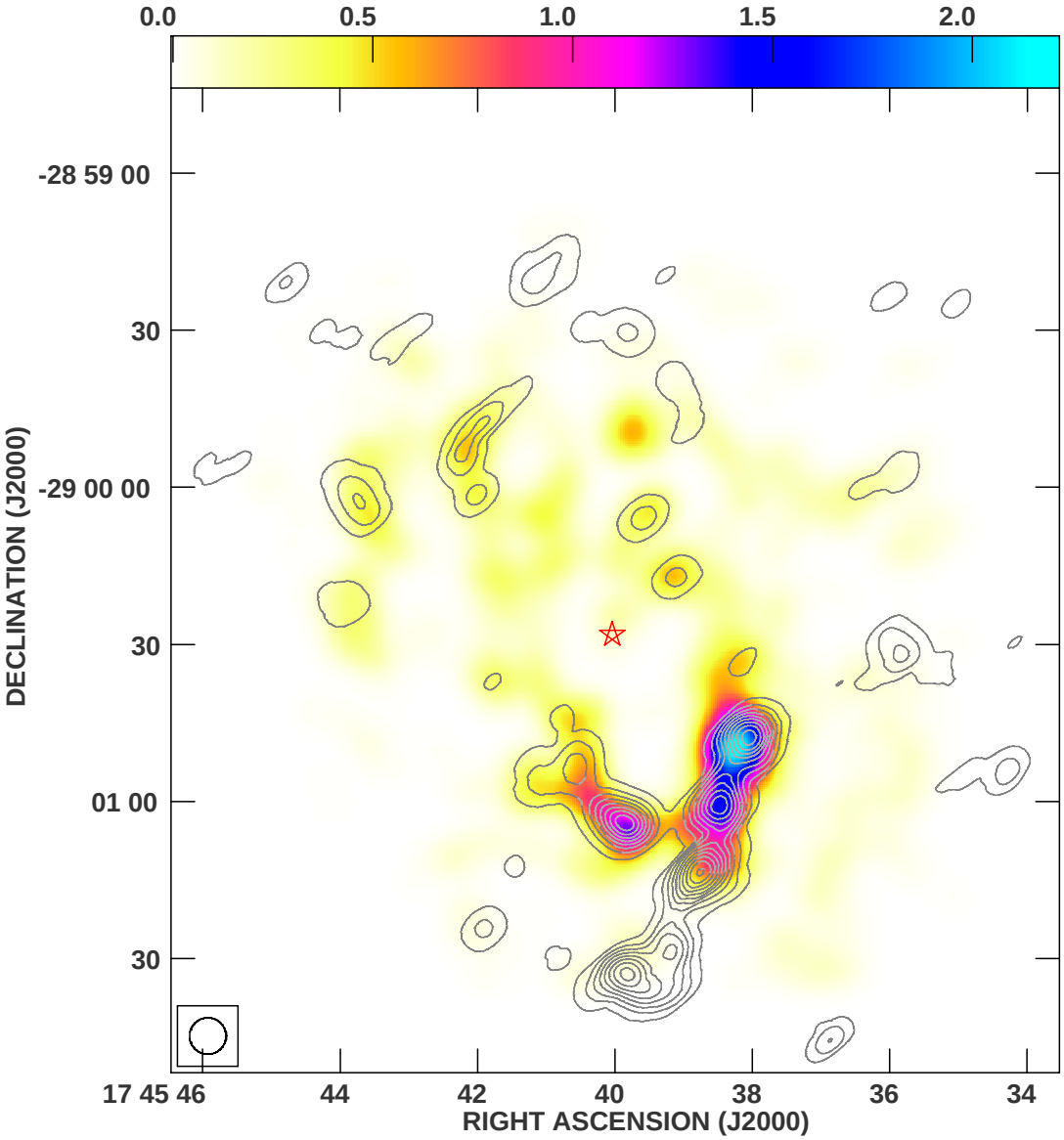

Figure A.6: HCN(3-2) integrated intensity in contours. HCN(4-3) integrated intensity in false-color scale. Contour levels are in steps of 6σ from 3σ to 57σ (2.2×10^1 to 41.5×10^1 Jy beam^{-1} km s^{-1}). The false-color scale is in kJy beam^{-1} km s^{-1}. Sgr A* is marked with a star.

transitions in the southern part of the CND, except for the *southern arc*, not detected in HCO$^+$(1-0). The northern and western parts of the CND are much better traced by HCO$^+$(1-0), since we do not observe traces of HCO$^+$(3-2) in those regions. As mentioned before, the *linear filament* has been detected in HCO$^+$(3-2), but we can clearly see that the same case does not apply to the (1-0) transition. This result suggests that the material forming the *linear filament* is at higher temperature than

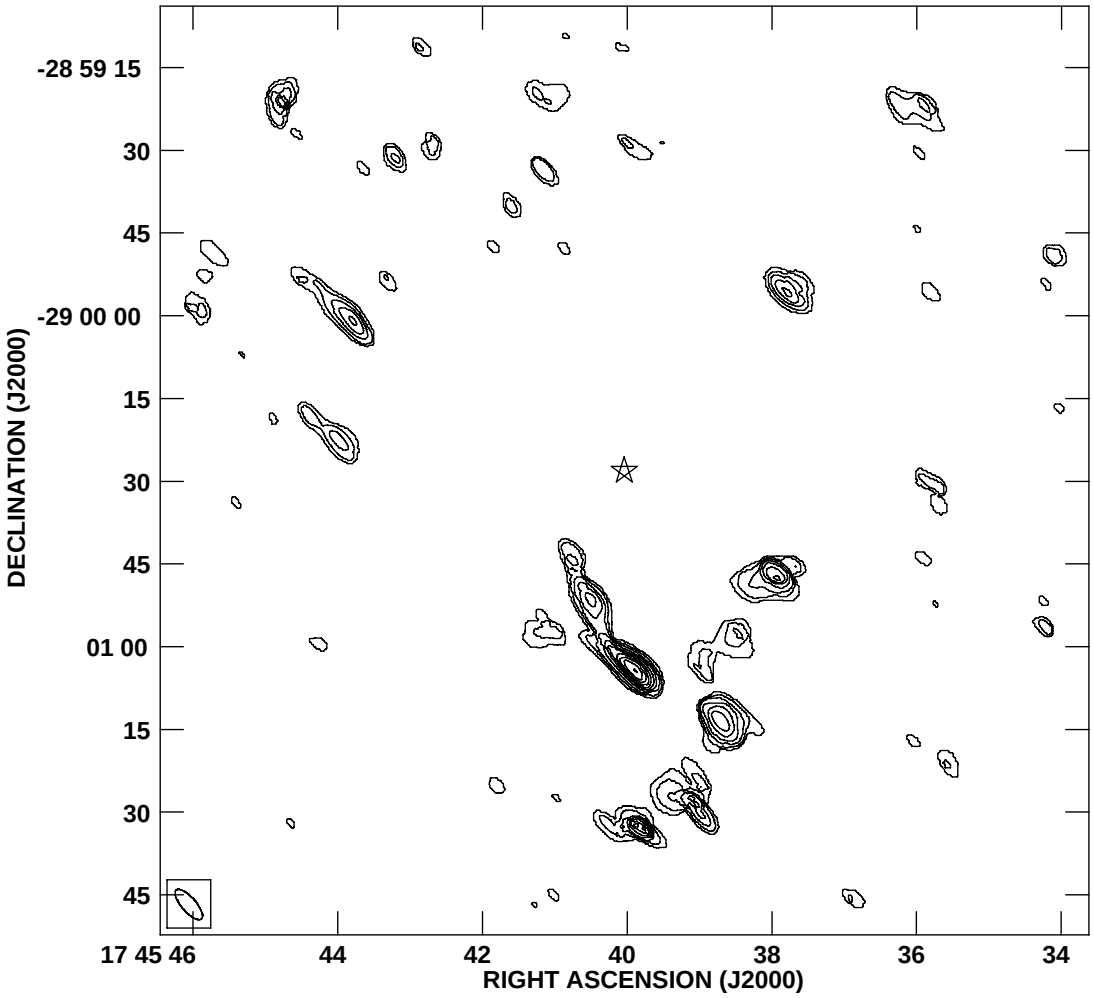

Figure A.7: HCO^+(3-2) integrated intensity in contours. Contour levels are in steps of 3σ, from 3σ to 24σ, except for the highest contour level, at 26σ (1.4×10^1 to 12.1×10^2 Jy beam^{-1} km s^{-1}). Sgr A* is marked with a star.

the western part of the CND, seen in the lower transition, but not in the higher one.

An important comparison to make is between HCO^+(3-2) and HCN(3-2) (figure A.10). Wright et al. (2001) reported that HCN(1-0) and HCO^+(1-0) traced the same material, but HCO^+(1-0) was altogether weaker. We observe that HCN(3-2) and HCO^+(3-2) nicely correlate all along the southern part of the CND and also the *southern arc* and the *northeast arm*. Unlike HCN(3-2), HCO^+(3-2) is not present neither in the *northeast lobe* nor in the "70 km s^{-1} cloud", as discused above. On the other hand, the *linear filament* is only detected in HCO^+(3-2).

Marr et al. (1993) calculated the ratio of HCO^+(1-0)/HCN(1-0) and discovered an over-abundance of HCN(1-0) in the CND, with ratio values from 0.06 to 0.2,

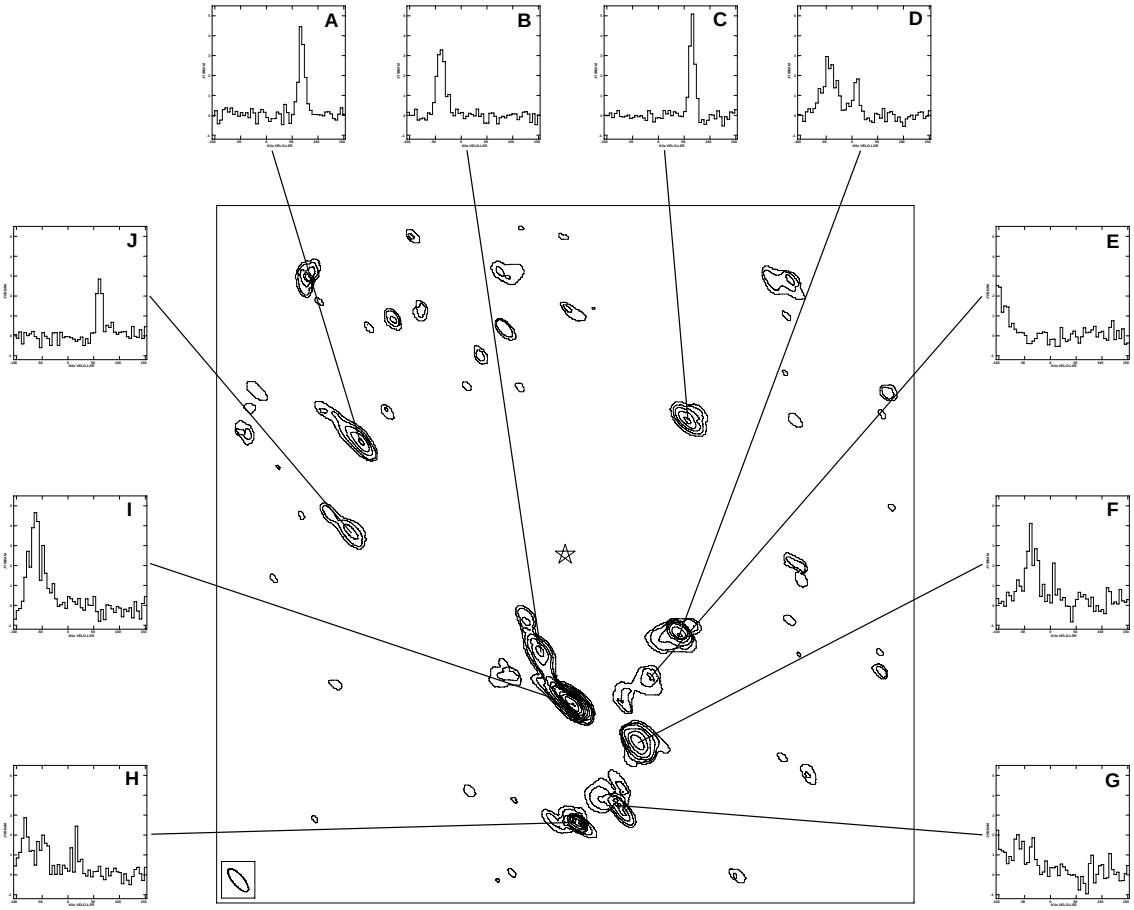

Figure A.8: HCO^+(3-2) spectra measured at the positions of the different clumps. Sgr A* is marked with a star.

whereas the ratio is close to unity for the quiescent molecular clouds in the Galactic disk (Nyman, 1983; Vogel & Welch, 1983; Blake et al., 1987). Christopher et al. (2005) reported a typical channel HCO^+(1-0)/HCN(1-0) ratio of 0.4. Also, Christopher et al. (2005) suggested that the high-mass regions of the CND harbored the lowest HCO^+(1-0)/HCN(1-0) ratios, while the highest ratios where found in lower-mass regions. We calculate the ratio of HCO^+(3-2) and HCN(3-2) using only the values with flux $\geq 3\sigma$ and find very high values in some regions, especially in the innermost part of the *southern extension* (figure A.11). However, an increase of ionization in the inner edge of the molecular ring is not expected because of the large optical depth of the clumps, which shields them from the radiation (Marr et al., 1993). This situation might have caused the lower abundance of HCO^+. Also, shocks or grain evaporation could help to the enhancement of HCN (Marr et al., 1993; Christopher et al., 2005). Christopher et al. (2005) found the lowest ratios in the *soutwest lobe* and the *northeast lobe*. We can see that in the (3-2) transi-

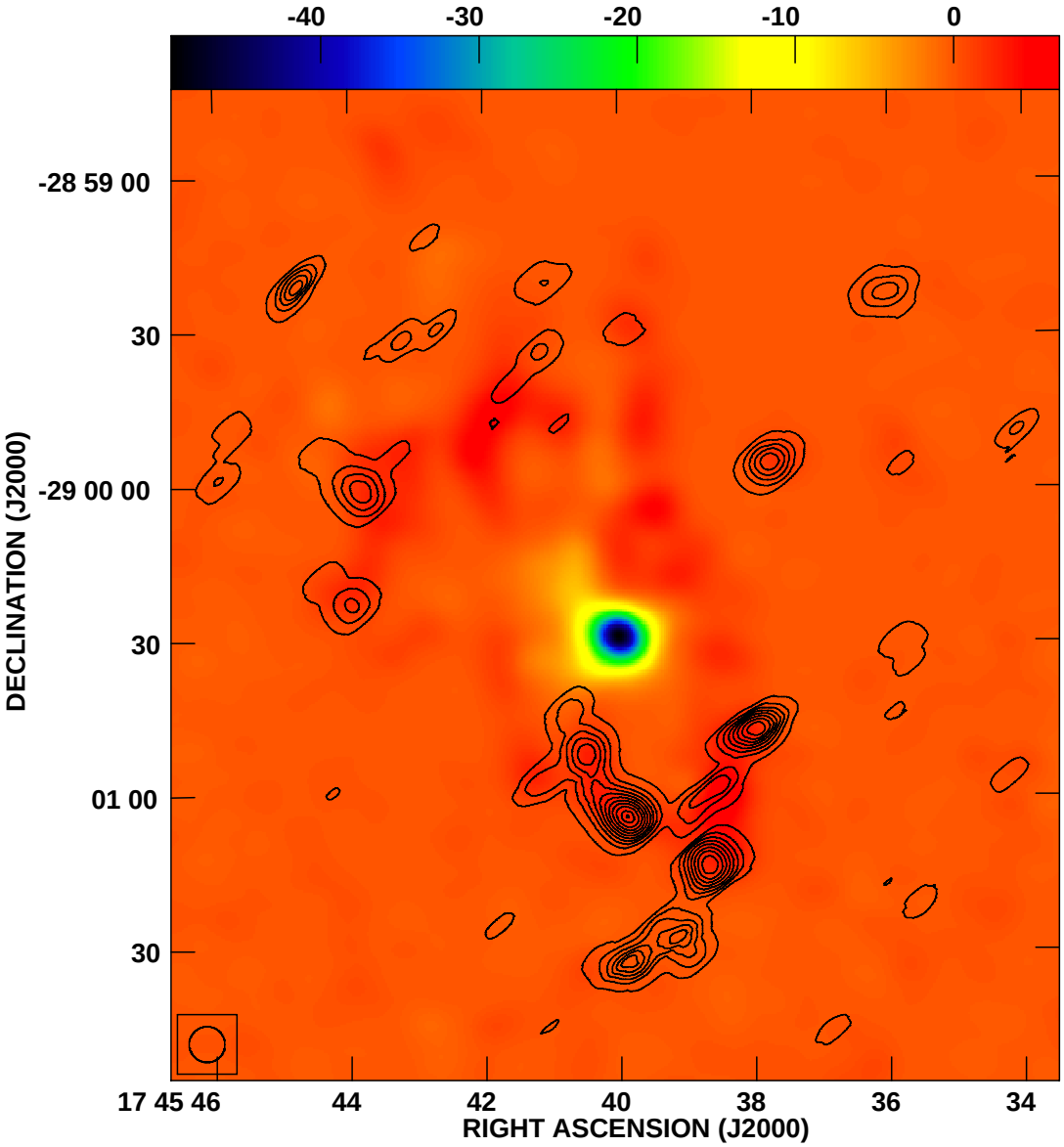

Figure A.9: HCO^+(3-2) integrated intensity in contours. HCO^+(1-0) integrated intensity in false color-scale. Contour levels are in steps of 20σ from 3σ to 123σ, except for the highest contour level, at 144σ (2.6 to 1.2 $\times$ 10^2 Jy beam^{-1} km s^{-1}). The false color-scale is in Jy beam^{-1} km s^{-1}. Sgr A* is seen in absorption in HCO^+(1-0).

tion we also find de lowest ratio in the *southwest lobe* and the *northeast lobe* is not even detected in HCO+(3-2). We can conclude that the behavior of the HCO^+(3-2)/HCN(3-2) ratio is similar to the lower transition ratio, and except for certain few positions in the CND, the value of the ratio is lower than 1, i.e. lower than in Galactic disk molecular clouds.

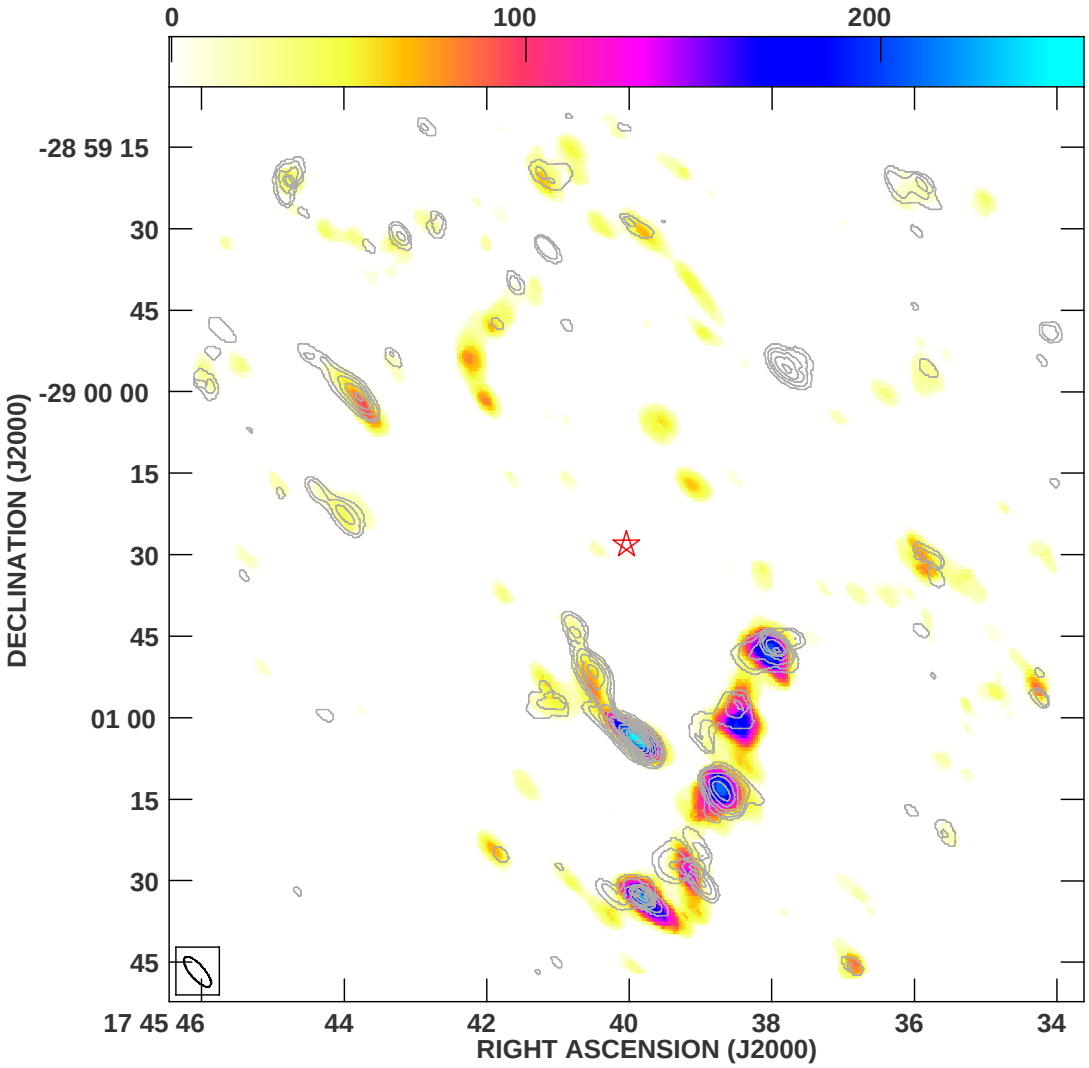

Figure A.10: HCO^+(3-2) integrated intensity in contours. HCN(3-2) integrated intensity in false color-scale. Contour levels are as in figure A.7. The false color-scale is in Jy beam^{-1} km s^{-1}. Sgr A* is marked with a star.

A.5 Summary

We have succesfully detected HCN(3-2) and HCO^+(3-2) in the Galactic Center region, within 2 pc of Sgr A*. Moreover, HCO^+(3-2) has never been reported before in this region. Both molecular lines trace the southern part of the CND, but are very much absent from the northern part. We also observe an over-abundance of HCN(3-2) with respect to HCO^+(3-2) in the CND, a result that was previously reported in the (1-0) transition. However, our results have a less than ideal coverage, with a very elongated synthesized beam. We have found an structure towards the south of

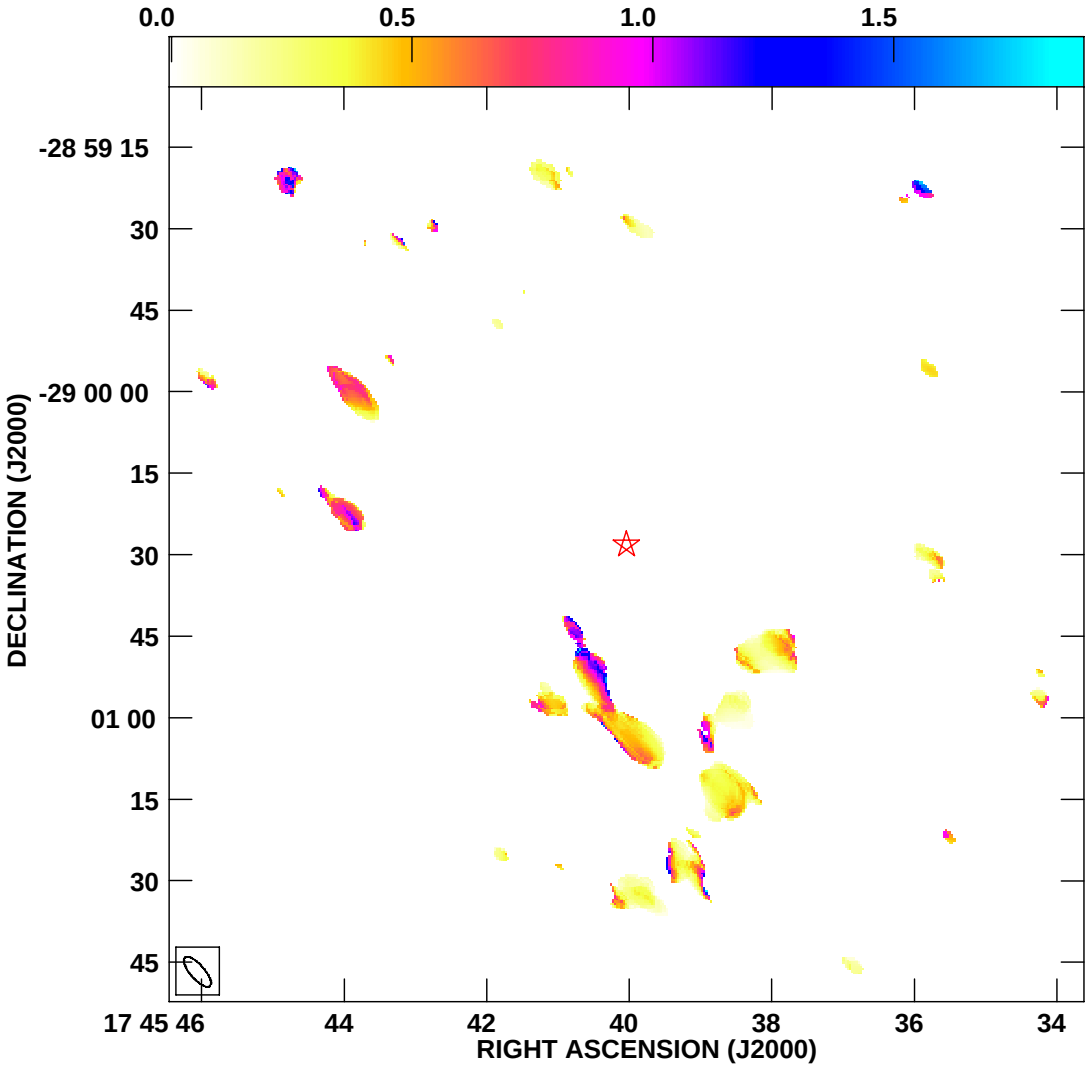

Figure A.11: Ratio of HCO^+(3-2) and HCN(3-2) integrated intensity in the Galactic center. Sgr A* is marked with a star.

the CND, the *southern arc* whose presence had not been reported before. Also, some sidelobe problems can be present. Therefore, we aim to repeat the observations in order to be able to provide a more conclusive evidence of our findings.

Bibliography

Aalto, S., Booth, R.S., Black, J.H. & Johansson, L.E.B. 1995, A&A, 300, 369

Armstrong, J.T. & Barrett, A.H. 1985, ApJS, 57, 535

Baganoff, F. K., Bautz, M. W., Brandt, W. N., Chartas, G., Feigelson, E. D., Garmire, G. P., Maeda, Y., Morris, M., Ricker, G. R., Townsley, L. K. & Walter, F. 2001, Nature, 413, 45

Balick, B. & Brown, R.L. 1974, ApJ, 194,265

Becklin, E.E., Gatley, I., Mathews, K., Neugebauer, G. Sellgren, K., Werner, M.W. & Wynn-Williams, C.G. 1980, ApJ, 236, 441

Becklin, E.E., Gatley, I. & Werner, M.W. 1982, ApJ, 258, 135

Beuther, H., Thorwirth, S., Zhang, Q., Hunter, T.R., Megeath, S.T., Walsh, A.J. & Menten, K.M. 2005, ApJ, 627, 834

Binney, J., Gerhard, O.E., Stark, A.A., Bally, J. & Uchida, K.I. 1991, MNRAS, 252, 210

Blake, G.A., sutton, E.C., Masson, C.R. & Phillips, T.G. 1987, ApJ, 315, 621

Böker, T., Föster-Schreiber, N.M. & Genzel, R. 1997, AJ, 114, 1883

Böker, T., van der Marel, R.P. & Vacca, W.D. 1999, ApJ, 118, 831

Boone, F., Baker, A. J., Schinnerer, E., Combes, F., García-Burillo, S., Neri, R., Hunt, L. K., Léon, S., Krips, M., Tacconi, L. J. & Eckart, A. 2007, A&A, 471, 113

Bradford, C.M., Stacey, G.J., Nikola, T., Bolatto, A.D., Jackson, J.M., Savage, M.L. & Davidson, J.A. 2005, ApJ, 623, 866

Cheung, A.C., Rank, D.M., Townes, C.H., Knowles, S.H. & Sullivan, W.T.III. 1969, ApJLetters, 157, L13

Choi, M., Evans II, N.J., Tafalla, M. & Bachiller, R. 2000, ApJ, 538, 738

Christopher, M.H. , Scoville, N.Z., Stolovy, S.R. & Yun, M.S. 2005, ApJ, 622, 346

Coil, A.L. & Ho, P.T.P. 1999, ApJ, 513, 752

Coil, A.L. & Ho, P.T.P. 2000, ApJ, 533, 245

Combes, F., García-Burillo, S., Boone, F., Hunt, L. K., Baker, A. J., Eckart, A., Englmaier, P., Léon, S., Neri, R., Schinnerer, E. & Tacconi, L. J. 2004, A&A, 414, 857

Crosthwaite, L.P., Turner, J.L., Hurt, R.L., Levine, D.A., Martin, R.N. & Ho, P.T.P. 2001, ApJ, 122, 797

Danby, G., Flower, D.R., Valiron, P., Schilke, P. & Walmsley, C.M. 1988, MNRAS, 235, 229

Dent, W.R.F., Matthews, H.E., Wade, R. & Duncan, W.D. 1993, ApJ, 419, 650

Downes, D., Radford, S.J.E., Guilloteau, S., Guélin, M., Greve, A. & Morris, D. 1992, A&A, 262, 424

Englmaier, P. & Shlosman, I. 2000, ApJ, 528, 677

Estalella, R. & Anglada, G. 1996, Introducción a la física del medio interestelar, First Edition, Ed. Universitat de Barcelona

Fux, R. 1999, A&A, 345, 787

Gatley, I., Jones, T.J., Hyland, A.R., Beattie, D.H. & Lee, T.J. 1984, MNRAS, 210, 565

Genzel, R., Watson, D.M., Crawford, M.K. & Townes, C.H. 1985, ApJ, 297, 766

Ghez, A.M., Salim, S., Hornstein, S.D., Tanner, A., Lu, J.R., Morris, M., Becklin, E.E. & Duchêne, G. 2005, ApJ, 620, 744

Gürkin, M.A. & Rasio, F.A. 2005, ApJ, 628, 236

Güsten, R., Genzel, R., Wright, M.C.H., Jaffe, D.T., Stutzki, J. & Harris, A.I. 1987, ApJ, 318, 124

Harju, J., Lehtinen, K., Booth, R.S. & Zinchenko, I. 1998, A&AS, 132, 211

Harris, A.I., Jaffe, D.T., Silber, M. & Genzel, R. 1985, ApJ, 294, L93

Helfer, T.T. & Blitz, L. 1993, ApJ, 419, 86

Helfer, T.T., Thornley, M.D., Regan, M.W., Wong, T., Sheth, K., Vogel, S.N., Blitz, L. & Bock, D.C.-J. 2003, ApJS, 145, 259

Henkel, C., Mauersberger, R., Peck, A.B., Falcke, H. & Hagiwara, Y. 2000, A&A, 361, L45

Herrnstein, R.M. & Ho, P.T.P. 2002, ApJ, 579, L83

Herrnstein, R.M. 2003, Ph.D Thesis, Harvard University

Herrnstein, R.M. & Ho, P.T.P. 2005, ApJ, 620, 287

Ho, P.T.P., Martin, R.N. & Barrett, A.H. 1981, ApJ, 246, 761

Ho, P. T. P., Martin, R. N., & Ruf, K. 1982, A&A, 113, 155

Ho, P.T.P. & Martin, R.N. 1983, ApJ, 272, 484

Ho, P.T.P. & Townes, C.H. 1983, ARA&A, 21, 239

Ho, P.T.P., Turner, J.L. & Martin, R.N. 1987, ApJ, 322, L67

Ho, P.T.P., Martin, R.N., Turner, J.L. & Jackson, J.M. 1990, ApJ, 355, L19

Ho, P.T.P., Ho, L.C., Szczepanski, J.C., Jackson, J.M., Armstrong, J.T. & Barrett, A.H. 1991, Nature, 350, 309

Ho, P.T.P., Moran, J.M. & Lo, K.Y. 2004, ApJ, 616, L1

Hüttemeister, S., Wilson, T.L., Bania, T.M. & Martín-Pintado, J. 1993, A&A, 280, 255

Hüttemeister, S., Henkel, C., Mauersberger, R., Brouillet, N., Wiklind, T. & Millar, T. J. 1995, A&A, 295, 571

Hüttemeister, S., Mauersberger, R. & Henkel, C. 1997, A&A, 326, 59

Hüttemeister, S., Dahmen, G., Mauersberger, R., Henkel, C., Wilson, T.L. & Martín-Pintado, J. 1998, A&A, 334, 646

Ishizuki, S., Kawabe, R., Ishiguro, M., Okumura, S.K., Morita, K.I., Chikada, Y.& Kasuga, T. 1990, Nature, 344, 224

Israel, F.P. & Baas, F. 2003, A&A, 404, 495

Jackson, J.M., Geis, N., Genzel, R., Harris, A.I., Madden, S., Poglitsch, A., Stacey, G.J. & Townes, C.H. 1993, ApJ, 402, 173

Jackson, J.M., Paglione, T.A.D., Carlstrom, J.E. & Rieu, N.-Q. 1995, ApJ, 438, 695

Jackson, J.M., Heyer, M., Paglione, T.A.D. & Bolatto, A.D. 1996, ApJ, 456, L91

Karachentsev, I.D. 2005, ApJ, 129, 178

Krabbe, A., Genzel, R., Drapatz, S. & Rotaciuc, V. 1991, ApJ, 382, L19

Krips, M., Eckart, A., Neri, R., Pott, J. U., Léon, S., Combes, F., García-Burillo, S., Hunt, L. K., Baker, A. J., Tacconi, L. J., Englmaier, P., Schinnerer, E. & Boone, F. 2005, A&A, 442, 479

Krips, M., Neri, R., García-Burillo, S., Combes, F., Schinnerer, E., Baker, A. J., Eckart, A., Boone, F., Hunt, L., Léon, S. & Tacconi, L. J. 2007, A&A, 468, 63

Lapinov, A.V., Schilke, P., Juvela, M. & Zinchenko, I.I. 1998, A&A, 336, 1007

Lo, K.Y., Berge, G.L., Claussen, M.J., Heiligman, G.M., Leighton, R.B., Masson, C.R., Moffet, A.T., Phillips, T.G., Sargent, A.I., Scott, S.L., Wannier, P.G. & Woody, D.P. 1984, ApJ, 282, L59

Lugten, J.B., Genzel, R., Crawford, M.K. & Townes, C.H. 1986, ApJ, 306, 691

Marr, J.M., Wright, M.C.H. & Backer, D.C. 1993, ApJ, 411, 667

Marrone, D.P., Moran, J.M., Zhao, J.-H. & Rao, R. 2007, ApJ, 654, 57

Marshall, J., Lasenby, A.N. & Harris, A.I. 1995, MNRAS, 277, 594

Martin, R.N. & Ho, P.T.P. 1979, A&A, 74, L7

Martin, R.N. & Ho, P.T.P. 1986, ApJ, 308, L7

Matsuda, T. & Nelson, A.H. 1977, Nature, 266, 608

Mauersberger, R. & Henkel, C. 1991, A&A, 245, 457

Mauersberger, R., Henkel, C., Weiß, A., Peck, A.B. & Hagiwara, Y. 2003, A&A, 403, 561

McGary, R.S., Coil, A.L. & Ho, P.T.P. 2001, ApJ, 559, 326

Meier, D.S., Turner, J.L. & Hurt, R.L. 2000, ApJ, 531, 200

Meier, D.S. & Turner, J.L. 2001, ApJ, 551, 687

Meier, D.S. & Turner, J.L. 2005, ApJ, 618, 259

Mezger, P.G., Zylka, R., Salter, C.J., Wink, J.E., Chini, R., Kreysa, E. & Tuffs, R. 1989, A&A, 209, 337

Mezger, P.G., Duschl, W.J. & Zylka, R. 1996, A&AReview, 7, 289

Montero-Castaño, M., Herrnstein, R.M. & Ho, P.T.P. 2006, ApJ, 646, 919

Morris, M. & Serabyn, E. 1996, ARA&A, 34, 645

Nguyen-Q-Rieu, Jackson, J.M., Henkel, C., Bach, T. & Mauersberger, R. 1992, ApJ, 399, 521

Nyman, L.-A. 1983, A&A, 120, 307

Ott, J., Weiss, A., Henkel, C. & Walter, F. 2005, ApJ, 629, 767

Paglione, T.A.D., Jackson, J.M. & Ishizuki, S. 1997, ApJ, 484, 656

Paumard, T., Genzel, R., Martins, F., Nayakshin, S., Beloborodov, A.M., Levin, Y., Trippe, S., Eisenhauer, F., Ott, T., Gillesen, S., Abuter, R., Cuadra, J., Alexander, T. & Sternberg, A. 2006, ApJ, 643, 1011

Quataert, E. 2003, in Astron. Nachr., Vol. 324, No. S1, Special Supplement "The central 300 parsecs of the Milky Way", Eds. A.Cotera, H. Falcke, T.R. Geballe & S. Markoff., Vol. 324, No.1, 435

Reid, M.J. 1993, ARA&A, 31, 345

Rigopoulou, D., Kunze, D., Lutz, D., Genzel, R. & Moorwood, A.F.M. 2002, A&A, 389, 374

Roberts, D.A. & Goss, W.M. 1993, ApJS, 86, 133

Rodríguez-Fernández, N.J., Combes, F., Martín-Pintado, J., Wilson, T.L. & Apponi, A. 2006, A&A, 455, 963

Rohlfs, K. & Wilson, T.L. 2000, Tools of Radio Astronomy, Fourth Edition, Springer-Verlag

Saha, A., Claver, J. & Hoessel, J.G. 2002, AJ, 124, 839

Sakamoto, K., Okumura, S.K., Ishizuki, S. & Scoville, N.Z. 1999, ApJ, 525, 691

Sanders, R.H. 1998, MNRAS, 294, 35

Schinnerer, E., Böker, T. & Meier, D.S. 2003, ApJ, 591, L115

Schödel, R. & Eckart, A. 2005, Memorie della Società Astronomica Italiana, 76, 65

Schulz, A., Gürsten, R., Köster, B. & Krause, D. 2001, A&A, 371, 25

Scoville, N.Z., Stolovy, S.R., Rieke, M., Christopher, M.H. & Yusef-Zadeh, F. 2003, ApJ, 594, 294

Serabyn, E. & Lacy, J.H. 1985, ApJ, 293, 445

Serabyn, E & Güsten, R. 1986, A&A, 161, 334

Serabyn, E., Güsten, R., Walmsley, C.M., Wink, J.E. & Zylka, R. 1986, A&A, 169, 85

Serabyn, E., Güsten, R. & Evans, N.J. 1989, in IAU Symp. 136, "The Center of the Galaxy", Ed. M. Morris (Dordrecht: Kluwer), 417

Serabyn, E., Lacy, J.H. & Achterman, J.M. 1992, ApJ, 395, 166

Sheth, K., Vogel, S.N., Regan, M.W., Teuben, P.T., Harris, A.I. & Thornley, M.D. 2002, AJ, 124, 2581

Shukla, H., Yun, M.S. & Scoville, N.Z. 2004, ApJ, 616, 231

Simkin, S.M., Su, H.J. & Schwarz, M.P. 1980, ApJ, 237, 404

Takakuwa, S., Ohashi, N., Bourke, T.L., Hirano, N., Ho, P.T.P., Jørgensen, J., Kuan, Y.-J., Wilner, D.J. & Yeh, S.C.C. 2007, ApJ, 662, 431

Takano, S., Nakai, N. & Kawaguchi, K. 2002, PASJ, 54, 195

Telesco, C.M., Dressel, L.L. & Wolstencroft, R.D. 1993, ApJ, 414, 120

Townes, C.H. & Schawlow, A.L. 1975, Microwave Spectroscopy, Dover

Tsai, C.-W., Turner, J.L., Beck, S.C., Crosthwaite, L.P., Ho, P.T.P. & Meier, D.S. 2006, AJ, 132, 2383

Turner, J.L. & Ho, P.T.P. 1983, ApJ, 268, L79

Turner, J. L., & Hurt, R. L. 1992, ApJ, 384, 72

Turner, J.L., Hurt, R.L. & Hudson, D.Y. 1993, ApJ, 413, L19

Usero, A., García-Burillo, S., Martín-Pintado, J., Fuente, A. & Neri, R. 2006, A&A, 448, 457

Vogel, S.N. & Welch, W.J. 1983, ApJ, 269, 568

Vollmer, B. & Duschl, W.J. 2000, NewA, 4, 581

Walmsley, C.M. & Ungerechts, H. 1983, A&A, 122, 164

Weiß, A., Neininger, N., Henkel, C., Stutzki, J. & Klein, U. 2001, ApJ, 554, L143

Womack, M., Ziurys, L.M. & Wyckoff, S. 1992, ApJ, 393, 188

Wright, M.C.H., Marr, J. & Backer, D.C. 1989, in IAU Symp. 136, "The Center of the Galaxy", Ed. M. Morris (Dordrecht: Kluwer), 143

Wright, M.C.H., Ishizuki, S., Turner, J.L., Ho, P.T.P. & Lo, K.Y. 1993, ApJ, 406, 470

Wright, M.C.H., Coil, A.L., McGary, R.S., Ho, P.T.P. & Harris, A.I. 2001, ApJ, 551, 254

Yusef-Zadeh, F. & Morris, M. 1987, ApJ, 320, 545